ABSTRACT

COOTE, TASHNI-ANN. Substituent Effects on Exchange Coupling: Controlling the Interactions between Unpaired Electrons. (Under the direction of Dr. David A. Shultz).

Design, synthesis, and characterization of novel high-spin species are critical for advancing the field of molecular magnetism, and subsequently creating new magnetic materials. As a means of grasping an understanding of how it is that one can control the electronic, hence magnetic interactions within a high-spin species, this study focuses on structure- property relationships in a series of bis(semiquinone) biradicals. The biradical moiety is the simplest of exchange-coupled systems. As electron-withdrawing, -donating and neutral substituents are placed on the coupler or spin carrier fragment of the biradicals under study, it is shown that there is a substituent effect operating within the series of ferromagnetically coupled *m*-phenylene bis(semiquinone) moieties.

SUBSTITUENT EFFECTS ON EXCHANGE COUPLING:

Controlling the Interactions between Unpaired Electrons

by

TASHNI-ANN COOTE

A dissertation submitted to the Graduate Faculty of
North Carolina State University
in partial fulfillment of the
requirements for the Degree of
Doctor of Philosophy

CHEMISTRY

Raleigh, NC

2006

APPROVED BY:

Dr. David Shultz Chair of Advisory Committee	Dr. Bruce Novak
Dr. Tatyana Smirnova	Dr. Chris Gorman

DEDICATION

"To live is Christ, to die is gain." The apostle Paul said it beautifully. Whether I live or die, the things that I do are all being done for my Savior, Jesus Christ.

My spirituality is responsible for my survival in this graduate program. My undulating laboratory results have many a times made the option of leaving grad school to attend pharmacy school seem much more attractive than laboring over a project, that at times, it seemed as if I would never complete. Then Sunday would roll around and my pastor, Dr. H.C. Miller, would preach a sermon on perseverance and I would return to the lab with uplifted spirits – ready to tackle my magnetic nemesis all over again!

Emerson and Greta Coote, my two beautiful parents, were responsible for "introducing" me to The Father at my christening. My parents took an active role in my educational, spiritual, and physical development. They constantly reminded me to aim for the stars, so that if I should fall, I would have fallen on a cloud. So, at this stage of my life, after being in school for 22 years, this thesis is the "interest" that has accrued on their investment.

Here's to you Mummy and Daddy! I am truly blessed to have parents like you.

With all my love,

Tash

BIOGRAPHY

Tashni-Ann Coote was born on September 1, 1980 in Manchester, Jamaica, to Emerson M^{c}Gregor and Greta-Faye Coote. She attended Glenmuir Preparatory School where she participated in theatre, dance and the national Spelling Bee competition. An avid reader, her dad accompanied her to the May Pen library every Saturday to borrow several children's books. Her dad often tells the story that the small town library could not keep up with the pace at which Tashni read the library's books. They often did not have new books on a weekly basis to feed her literary appetite. Her parents saw her talent and took an active role in her education at this early stage of her life.

She started out her high school years at Glenmuir High and finished up at Holy Childhood High Girls School with top honors, graduating at the age of 15. Her passes qualified her for entrance into the British Certified 'A'-level program at Wolmers High Girls School where she acquired the prestigious position of *Prefect* at that level.

Her studies took her to Brooklyn, New York, where she attended Kingsborough Community College. Here she maintained a 4.0 GPA and graduated *summa cum laude* as the valedictorian of the year 2000, after one and a half years of study. She went on to Shaw University in Raleigh, North Carolina, where she received her B.S. in Chemistry and graduated *summa cum laude* with a GPA of 3.9. Her interest in chemistry led her to North Carolina State University, and under the leadership of Dr. David Shultz, she earned her PhD in chemistry. She was offered and has accepted a position at BASF- The Chemical Company.

ACKNOWLEDGEMENTS

I must first thank Yahweh for giving me the strength to complete this graduate program. There were times when the end was not in sight and the ground on which I stood felt shaky, but by His grace, I have met the requirements for the Doctorate of Philosophy in Chemistry.

I would like to thank Mummy and Daddy for all of their words of encouragement and their love and support. My sister, Peta-Gaye Shaw has been instrumental in my survival in Raleigh. Her and her husband, Ian, have always opened their doors to me for Sunday evening dinners. Their child, my little pumpkin, Yanni-Taylor is my pride and joy. Chase, my roommate, thanks for splitting the rent! My entire family has been there to support me through their prayers and words of encouragement. Thanks family!

The Shultz group is hilarious! Candice, Linda, Rob, Chucky, Sofi, Nick, Jess, Joe B., Riz, kept me laughing day in and day out. Thanks for everything! My advisor, Professor David A. Shultz is one of the smartest men I know! He never failed to voice his belief that I would one day make a successful professor. Dave, your enthusiasm is contagious! Unfortunately, your genius is not, but I caught your enthusiasm for the fundamental science, and I am honored to have you as my P.I.

I would be amiss if I didn't mention some people who have been instrumental in my academic life. Dr. David Shafer is "the man"! He extended my very first internship opportunity to me when I was an undergraduate at Shaw University. He led me to meet Dr. Novak, one of NC State's finest professors, and fittingly, a member of my committee. I extend my gratitude to the rest of my committee members, Dr. Chris Gorman and Dr. Tatyana Smirnova, both of whom were firm, yet supportive during my prelim exams.

Phi Lambda Upsilon is an honor society that I am very proud to have been a member of. PLU gave me an opportunity to assume leadership responsibilities in my graduate career - a lesson well learned. I must acknowledge Dr. Damian "D.Y." Young – a seasoned PLU member and a very good friend. After meeting and speaking with him while I was in undergrad, I knew that NC State's chemistry department would be the perfect place for me, for if it produced students like Damian then it had to be doing something right. Ibrahim Bori – you are the hardest working man I know! Thanks for all of your suggestions on how to get my synthesis to work!

Michael D. Wallace. Very few people can understand the zones I get into when I start studying. When Michael and I met, I was focused on getting my Associates degree and he never once caused me to lose focus. Since then he has seen me through my Bachelors degree and was there to support me during my graduate classes and the long nights that I had to spend at the lab. Time has gone by, our season came and went, but I would still like to say thank you so much for being there for me when all the curtains were closed and the crowd had dissipated. D.J. Dubroy, you make me want to do better! Thanks for your love and support. Let's see if we can keep the flame burning for 72 years.

I can't complete my acknowledgements without mentioning my girlfriends. I have been blessed to have some of the most supportive friends a woman could ever hope for. Ms. Skeeta Mcfarlane, Dr. Tiffani Bailey, Ms. Courtney Hinson, Ms. Denise Nelson, Ms. Ramona Grant and Ms. Sophia Chin. You ladies constitute my inner circle! Love you lots! Now that my studies are over, can we all put on summer dresses and go to the mall?

Tashni-Ann Coote

TABLE OF CONTENTS

LIST OF TABLES

LIST OF FIGURES

LIST OF SCHEMES

Chapter 1. Exchange Coupling in Biradical Molecules

1.1. Magnetism in the Scheme of Organic Chemistry.

Many years after the advent of quantum mechanics came a surge of technological advances in the data storage and computer logic industries.[1] However, despite our technological leaps, the theory of magnetism has progressed more slowly. Our insatiable interest in magnetism is not without merit. The ramifications of this phenomenon are ubiquitous throughout our everyday lives. No longer is the concept of magnetism singularly associated with refrigerator magnets and compasses, but this era has marked the birth of magnetically levitated trains[2] and light modulated molecular switching devices.[3] Magnetism has given birth to neologisms such as spintronics[4,5] – an emerging technology that exploits the inherent spin of an electron in addition to its charge to yield devices that bear data storage capacities far beyond that of their traditional analogs.

Interactions between the intrinsic spin of two electrons gives rise to magnetism. This "communication" between the electrons, known as electron spin exchange coupling, is innately interesting and fittingly an important observable upon which the research presented herein is based. Nowhere are the effects of exchange coupling more important than in the field of magnetism – more specifically magnetochemistry. This field focuses on the relationship between the magnetic properties of a chemical entity and its electronic structure. The Shultz group tailors its research towards testing the limits of exchange coupling using organic biradicals as primary testing components. If one were able to control the electronic interactions between the unpaired electron centers within the biradical, then the basis for achieving high-spin ground states would have been set.

Toward this end, I have undertaken a project that is centered on designing, synthesizing and elucidating structure-property relationships in biradicals – the simplest exchange-coupled systems. Biradicals possess two unpaired electrons exchange coupled to each other via through-bond and/ or though-space pathways.[1] The biradicals under study are bis(semiquinone) complexes - the anion radicals of which have unpaired electrons and are potential building blocks of high spin molecules.[6-10]

The objective of this study is to investigate to what extent the electronic, hence magnetic interactions within a biradical moiety are affected as electron-withdrawing, -donating and neutral substituents are placed on the coupler or semiquinone spin carrier fragment of the biradical. Although the biradical system is electronically simple, it is a sufficient candidate for studying the interplay between π-topology, conformation and coulombic repulsions between electrons – properties that are probes of exchange coupling limits.

1.2. The fundamentals of Magnetism.

Magnetization is a property that describes the extent to which a material is affected by a magnetic field. The magnetization, M, of a sample is generally described by eq 1.1.[11] Here, the sample magnetization is related to an applied magnetic field, H, by a dimensionless constant, χ_{exp}, known as magnetic susceptibility.

$$M = \chi_{exp}H \qquad \textbf{eq. 1.1}$$

The magnetic susceptibility is comprised of several components namely, a diamagnetic, paramagnetic, and a Pauli susceptibility.[12]

$$\chi_{exp} = \chi_{dia} + \chi_{para} + \chi_{Pauli} \quad \textbf{eq. 1.2}$$

All molecules have a diamagnetic contribution, χ_{dia}, to the overall susceptibility. This value can be approximated by summing up the diamagnetic contributions of all the individual atoms and bonds in the molecule. Pascal tabulated the diamagnetic contributions of atoms and functional groups in the 1940s.[11] The diamagnetic susceptibility contribution to a molecule is about two orders of magnitude less than the paramagnetic contribution. Pauli susceptibility, χ_{Pauli}, is the magnetic susceptibility of the conducting electrons and does not apply to the molecules studied in the Shultz group; hence the χ_{Pauli} term can be omitted from eq. 1.2 for our purposes. The experimental susceptibility, χ_{exp}, is recorded via SQUID (Semi-Conducting Quantum Interference Device) magnetometry. Since the overall magnetic susceptibility is an experimentally observed quantity, and χ_{dia} can be calculated. Eq. 1.2 can therefore be rewritten as eq. 1.3

$$\chi_{para} = \chi_{exp} - \chi_{dia} \quad \textbf{eq. 1.3}$$

The most important magnetic property of a material is its susceptibility.[13] It provides both a quantitative and qualitative measure with which to compare magnetic materials. A negative value for χ indicates that a material is repelled by an applied magnetic field, while a positive value for χ indicates that a material is attracted to the applied field. The value of χ_{exp} falls within a certain range for each material. This allows for classification of magnetic materials into five main categories as shown in Table 1.1 below.

Table 1.1. Classification of materials according to their magnetic properties.

Class	Magnitude of χ_{exp} (emu•Kmol^{-1})	Structure on Atomic Scale	Examples
Diamagnetic	Approximately -10^{-6} to -10^{-5}	Atoms have no permanent dipole moment	Noble gases, water most diatomic gases
Paramagnetic	Approximately $+10^{-5}$ to $+10^{-3}$	Atoms have permanent dipole moments; Neighboring moments do not interact	Some metals, *e.g.*, Cr Some diatomic gases *e.g.*, O_2
Ferromagnetic	Large and positive	Atoms have permanent dipole moments.	Transition Metals *e.g.*, Fe
Antiferromagnetic	Small and positive	Atoms have permanent dipole moments.	Compounds of transition metals *e.g.*, MnO
Ferrimagnetic	Large and positive	Atoms have permanent dipole moments.	Fe_3O_4 (Magnetite) mixed oxides of Fe and other elements

At the atomic level, the orientation of magnetic moments accounts for the differences in response to an externally applied magnetic field and subsequently for the differences in the values for magnetic susceptibility. Figure 1.1 shows how the magnetic moments of individual atoms are aligned throughout a 3D bulk material.[12]

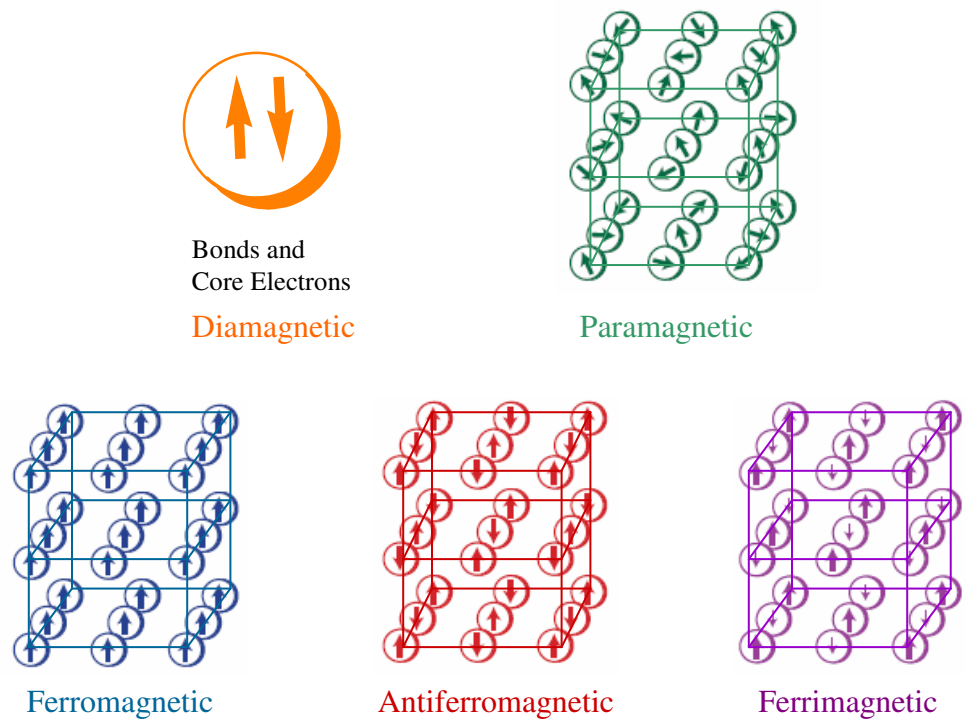

Fig. 1.1. The alignment of magnetic moments at absolute zero for the five main types of magnetism.

Diamagnetism arises from closed-shell core electrons. Because all the electrons are paired, when an external magnetic field is applied, an internal field is produced which opposes the externally applied field.[14] Diamagnetism is a weak effect, which is characterized by a negative temperature-independent magnetic susceptibility. Any substance that has one or more unpaired electrons in the atoms, molecules or ions that compose it is called paramagnetic. If a magnetic field is applied to such a material, the magnetic dipole moments align with the magnetic field. When the magnetic field is removed, the electrons resume their random thermal motion. This behavior results in a material that has no net magnetic moment because of cancellation of moments due to their random orientations. Because the dipoles try to align with the applied field, the susceptibilities of such materials are positive.

Pierre Curie investigated the temperature dependence of paramagnetic susceptibility, and found that the susceptibilities of paramagnetic materials follow the relationship;[12]

$$\chi_{para} = \frac{C}{T} \qquad \textbf{eq. 1.4}$$

where, C is a material specific Curie constant and T is temperature. The Curie law is limited to materials that show no interaction between neighboring spins. However, *ideal* paramagnetism is the exception rather than the rule. Most, if not all paramagnetic materials deviate from the Curie Law and obey the Curie-Weiss law:

$$\chi_{para} = \frac{C}{T - \theta} \qquad \textbf{eq 1.5}$$

where θ is the Weiss constant and has units of temperature.[12]

The Weiss constant is the molecular field correction for weak intermolecular interactions and is related to several parameters;[12]

$$\theta = \frac{zJ'S(S+1)}{3k_B} \qquad \textbf{eq 1.6}$$

where z is the number of nearest neighbors, J' is the energy gap between the ground state and the lowest excited state. S is the spin quantum number, and k_B is Boltzmann's constant. When θ is zero, the Curie Law is obeyed. When θ is non-zero, then there is an interaction between neighboring magnetic moments and the material is only paramagnetic above a certain transition temperature. If θ is positive, then the material is ferromagnetic below the transition temperature T_c (Curie temperature). If θ is negative, then the material is antiferromagnetic below the transition temperature T_N (Néel temperature).[15]

In a ferromagnetic substance, there is a preponderance of electrons with spins aligned in one direction. The individual magnetic fields of the atoms in a given region tend to align in the same direction, so that they reinforce one another. Such a region is called a domain. In an unmagnetized sample, the domains are of different sizes and have different orientations.[15,16] When an external magnetic field is applied, domains whose orientations are in the same general direction as the external field will grow at the expense of domains with other orientations. Because there is parallel alignment with the externally applied field, the susceptibilities of such materials are positive.

Antiferromagnetism is similar to ferromagnetism; however, the spins align in an antiparallel fashion throughout the 3-D bulk material. The behavior gives rise to no spontaneous magnetic moment. Ferrimagnetic behavior requires a material with at least two distinct species with different moments. These moments interact

antiferromagnetically, but are of different magnitudes; hence a net magnetic moment is realized.

1.3. A quantum mechanical description of electron spin exchange coupling

- Interaction of unpaired electrons in biradicals.

Consider the interaction of two electrons. Each electron can be either spin up (↑) or spin down (↓), and there are two ways for the two spins to interact: either parallel (↑↑), or antiparallel, (↑↓). If the spins are parallel, the total spin, S_{Tot}, is 1. On the other hand, if the spins are antiparallel, then S_{Tot} is 0. In terms of spin multiplicity, $(2S_{Tot} + 1)$, these correspond to the triplet and singlet states respectively.

Quantum Mechanics dictates that the wavefunction of a system of interacting identical particles must not distinguish amongst the particles. There are two possible cases for the wavefunction of a system of identical particles: those that are symmetric and those that are antisymmetric with respect to label interchange. According to the Pauli principle, the total wavefunction of a system of electrons must be antisymmetric with respect to the interchange of any two electrons.

A good approximation is to write the total electronic wavefunction as a product of two parts: *space* and *spin*.[1] In order for the overall wavefunction (eq 1.7) to be antisymmetric, one of the two components must be antisymmetric (A) and the other symmetric (S), giving two results, A_{space} x S_{spin} and S_{spin} x A_{space}.

$$\Psi_{Total} = \Psi_{space} \times \Psi_{spin} \qquad \textbf{eq 1.7}$$

To consider the orbital or spatial component of the wave function, a two-electron, two-orbital system is devised; $\Psi = \phi_A(1)\phi_B(2)$.[17] This wavefunction is unacceptable

because electron (1) can be distinguished from electron (2), i.e. $\phi_A(1)\phi_B(2) \neq \phi_A(2)\phi_B(1)$. Therefore, normalized linear combinations of the wavefunctions above are constructed:

$$\Psi_S = \frac{1}{\sqrt{2}} [\phi_A(1)\phi_B(2) + \phi_B(1)\phi_A(2)] \quad \textbf{eq 1.8}$$

$$\Psi_A = \frac{1}{\sqrt{2}} [\phi_A(1)\phi_B(2) - \phi_B(1)\phi_A(2)] \quad \textbf{eq 1.9}$$

Ψ_S and Ψ_A represent the symmetric and antisymmetric wavefunctions respectively. Using the permutation operator, P_{12} (a mathematical operator which exchanges two electrons), to act on the above two wavefunctions, Ψ_S and Ψ_A are shown to be acceptable:

$$P_{12}\Psi_S = \frac{1}{\sqrt{2}} [\phi_A(1)\phi_B(2) + \phi_B(1)\phi_A(2)] = \Psi_S \quad \textbf{eq 1.10}$$

$$P_{12}\Psi_A = \frac{1}{\sqrt{2}} [\phi_A(1)\phi_B(2) + \phi_B(1)\phi_A(2)] = -\Psi_A \quad \textbf{eq 1.11}$$

The other half of the total electronic wavefunction is comprised of the spin. For two electrons in two spin orbitals there exists four possible combinations: $\alpha(1)\alpha(2)$, $\beta(1)\beta(2)$, $\alpha(1)\beta(2)$, and $\beta(1)\alpha(2)$. The first two are symmetric with respect to exchange, but the latter two must be taken as linear combinations because they allow for distinction between the electrons. The resulting four spin functions and their symmetries with respect to exchange of electron labels are:

Symmetric spin functions	**Antisymmetric spin function**
$\alpha(1)\alpha(2)$, $\beta(1)\beta(2)$, $\frac{1}{\sqrt{2}}(\alpha(1)\beta(2)+\beta(1)\alpha(2))$	$\frac{1}{\sqrt{2}}(\alpha(1)\beta(2)-\beta(1)\alpha(2))$

Fig. 1.2. Symmetric and antisymmetric spin functions.

Since $\Psi_{Total} = \Psi_{space} \times \Psi_{spin}$ must be antisymmetric, we must multiply the symmetric space function by an antisymmetric spin function.

$$\Psi_{Total} = \frac{1}{\sqrt{2}} [\phi_A(1)\phi_B(2) + \phi_B(1)\phi_A(2)] \times \frac{1}{\sqrt{2}} [\alpha(1)\beta(2) - \beta(1)\alpha(2)] \quad \text{singlet state} \quad \textbf{eq 1.12}$$

The other spatial wavefunction is antisymmetric so it must be multiplied by a symmetric spin function. We can use any one of the three symmetric two-electron spin functions in order to maintain an overall antisymmetric wavefunction. This results in a triply degenerate state.

$$\left.\begin{aligned} \Psi_{Total} &= \frac{1}{\sqrt{2}} [\phi_A(1)\phi_B(2) - \phi_B(1)\phi_A(2)] \times \alpha(1)\alpha(2) && \textbf{eq 1.13} \\ \Psi_{Total} &= \frac{1}{\sqrt{2}} [\phi_A(1)\phi_B(2) - \phi_B(1)\phi_A(2)] \times \beta(1)\beta(2) && \textbf{eq 1.14} \\ \Psi_{Total} &= \frac{1}{\sqrt{2}} [\phi_A(1)\phi_B(2) - \phi_B(1)\phi_A(2)] \times \frac{1}{\sqrt{2}} [\alpha(1)\beta(2) + \beta(1)\alpha(2)] && \textbf{eq 1.15} \end{aligned}\right\} \text{triplet state}$$

A two-electron/two-orbital model can be used to demonstrate how preferences for ferromagnetic or antiferromagnetic states can arise. The different possible electron configurations discussed above, are shown below in Figure 1.3.

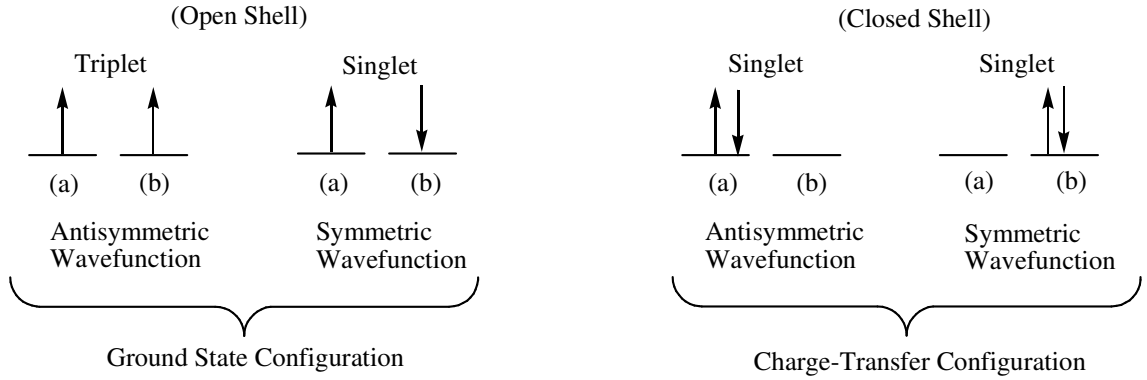

Fig. 1.3. Open shell (left) ground-configuration states and closed-shell (right) charge-transfer states of a two-electron/two-orbital system.

Equation 1.16 is the zero[th]-order Hamiltonian. It is a simple electrostatic energy operator used to calculate the energy of each state.

$$H^{(0)} = h(1) + h(2) \qquad \textbf{eq 1.16}$$

The spatial wavefunctions of the four states are as follows:

$$\Psi_{T,OS} = \frac{1}{\sqrt{2}} [\phi_A(1)\phi_B(2) - \phi_B(1)\phi_A(2)] \qquad \textbf{eq 1.17}$$

$$\Psi_{S,OS} = \frac{1}{\sqrt{2}} [\phi_A(1)\phi_B(2) + \phi_B(1)\phi_A(2)] \qquad \textbf{eq 1.18}$$

$$\Psi_{S+,CS} = \frac{1}{\sqrt{2}} [\phi_A(1)\phi_A(2) + \phi_B(1)\phi_B(2)] \qquad \textbf{eq 1.19}$$

$$\Psi_{S-,CS} = \frac{1}{\sqrt{2}} [\phi_A(1)\phi_A(2) - \phi_B(1)\phi_B(2)] \qquad \textbf{eq 1.20}$$

Energy of the triplet is:

$$E_{triplet,\,OS} = \frac{1}{2} \left\langle \phi_A(1)\phi_B(2) - \phi_B(1)\phi_A(2) \right| h(1) + h(2) \left| \phi_A(1)\phi_B(2) - \phi_B(1)\phi_A(2) \right\rangle$$

$$= \frac{1}{2} [\left\langle \phi_A(1)\phi_B(2) \right| h(1) + h(2) \left| \phi_A(1)\phi_B(2) \right\rangle -$$

$$\left\langle \phi_A(1)\phi_B(2) \right| h(1) + h(2) \left| \phi_B(1)\phi_A(2) \right\rangle -$$

$$\left\langle \phi_B(1)\phi_A(2) \right| h(1) + h(2) \left| \phi_A(1)\phi_B(2) \right\rangle +$$

$$\left\langle \phi_B(1)\phi_A(2) \right| h(1) + h(2) \left| \phi_B(1)\phi_A(2) \right\rangle]$$

$$= \frac{1}{2} [\left\langle \phi_B(2) \middle| \phi_B(2) \right\rangle \left\langle \phi_A(1) \right| h(1) \left| \phi_A(1) \right\rangle +$$

$$\left\langle \phi_A(1) \middle| \phi_A(1) \right\rangle \left\langle \phi_B(2) \right| h(2) \left| \phi_B(2) \right\rangle -$$

$$\left\langle \phi_B(2) \middle| \phi_A(2) \right\rangle \left\langle \phi_A(1) \right| h(1) \left| \phi_B(1) \right\rangle -$$

$$\left\langle \phi_A(1) \middle| \phi_B(1) \right\rangle \left\langle \phi_B(2) \right| h(2) \left| \phi_A(2) \right\rangle -$$

$$\left\langle \phi_A(2) \middle| \phi_B(2) \right\rangle \left\langle \phi_B(1) \right| h(1) \left| \phi_A(1) \right\rangle -$$

$$\left\langle \phi_B(1) \middle| \phi_A(1) \right\rangle \left\langle \phi_A(2) \right| h(2) \left| \phi_B(2) \right\rangle +$$

$$\left\langle \phi_A(2) \middle| \phi_A(2) \right\rangle \left\langle \phi_B(1) \right| h(1) \left| \phi_B(1) \right\rangle +$$

$$\left\langle \phi_B(1) \middle| \phi_B(1) \right\rangle \left\langle \phi_A(2) \right| h(2) \left| \phi_A(2) \right\rangle]$$

$$= \frac{1}{2}[\alpha + \alpha - 0 - 0 - 0 - 0 + \alpha + \alpha] = 2\alpha \qquad \textbf{eq.1.21}$$

where α is the coulomb integral, $\alpha = \langle\ \phi_A(1)\,|\,h(1)\,|\phi_A(1)\ \rangle = \langle\ \phi_B(2)\,|\,h(2)\,|\phi_B(2)\ \rangle$.

Energy of the open-shell singlet is:

$$E_{singlet,\,OS} = \frac{1}{2}\langle\ \phi_A(1)\phi_B(2) + \phi_B(1)\phi_A(2)\,|\,h(1) + h(2)\,|\phi_A(1)\phi_B(2) + \phi_B(1)\phi_A(2)\ \rangle$$

$$= \frac{1}{2}[\langle\ \phi_A(1)\phi_B(2)\,|\,h(1) + h(2)\,|\phi_A(1)\phi_B(2)\ \rangle +$$

$$\langle\ \phi_A(1)\phi_B(2)\,|\,h(1) + h(2)\,|\phi_B(1)\phi_A(2)\ \rangle +$$

$$\langle\ \phi_B(1)\phi_A(2)\,|\,h(1) + h(2)\,|\phi_A(1)\phi_B(2)\ \rangle +$$

$$\langle\ \phi_B(1)\phi_A(2)\,|\,h(1) + h(2)\,|\phi_B(1)\phi_A(2)\ \rangle]$$

$$= \frac{1}{2}[\langle\ \phi_B(2)\,|\phi_B(2)\ \rangle\langle\ \phi_A(1)\,|\,h(1)\,|\phi_A(1)\ \rangle +$$

$$\langle\ \phi_A(1)\,|\phi_A(1)\ \rangle\langle\ \phi_B(2)\,|\,h(2)\,|\phi_B(2)\ \rangle +$$

$$\langle\ \phi_B(2)\,|\phi_A(2)\ \rangle\langle\ \phi_A(1)\,|\,h(1)\,|\phi_B(1)\ \rangle +$$

$$\langle\ \phi_A(1)\,|\phi_B(1)\ \rangle\langle\ \phi_B(2)\,|\,h(2)\,|\phi_A(2)\ \rangle +$$

$$\langle\ \phi_A(2)\,|\phi_B(2)\ \rangle\langle\ \phi_B(1)\,|\,h(1)\,|\phi_A(1)\ \rangle +$$

$$\langle\ \phi_B(1)\,|\phi_A(1)\ \rangle\langle\ \phi_A(2)\,|\,h(2)\,|\phi_B(2)\ \rangle +$$

$$\langle\ \phi_A(2)\,|\phi_A(2)\ \rangle\langle\ \phi_B(1)\,|\,h(1)\,|\phi_B(1)\ \rangle +$$

$$\langle\ \phi_B(1)\,|\phi_B(1)\ \rangle\langle\ \phi_A(2)\,|\,h(2)\,|\phi_A(2)\ \rangle]$$

$$= \frac{1}{2}[\alpha + \alpha + 0 + 0 + 0 + 0 + \alpha + \alpha] = 2\alpha \qquad \textbf{eq.1.22}$$

Energy of the first closed-shell singlet is:

$$E_{singlet,\,CS} = \frac{1}{2}\langle\ \phi_A(1)\phi_B(2) + \phi_B(1)\phi_A(2)\,|\,h(1) + h(2)\,|\phi_A(1)\phi_B(2) + \phi_B(1)\phi_A(2)\ \rangle$$

$$= \frac{1}{2}[\langle\ \phi_A(1)\phi_B(2)\,|\,h(1) + h(2)\,|\phi_A(1)\phi_B(2)\ \rangle +$$

$$\langle\ \phi_A(1)\phi_B(2)\,|\,h(1) + h(2)\,|\phi_B(1)\phi_A(2)\ \rangle +$$

$$\langle\ \phi_B(1)\phi_A(2)\,|\,h(1) + h(2)\,|\phi_A(1)\phi_B(2)\ \rangle +$$

$$\langle\ \phi_B(1)\phi_A(2)\,|\,h(1)+h(2)\,|\,\phi_B(1)\phi_A(2)\ \rangle\ ]$$

$$= \frac{1}{2}[\langle\ \phi_B(2)\,|\,\phi_B(2)\ \rangle\langle\ \phi_A(1)\,|\,h(1)\,|\,\phi_A(1)\ \rangle +$$

$$\langle\ \phi_A(1)\,|\,\phi_A(1)\ \rangle\langle\ \phi_B(2)\,|\,h(2)\,|\,\phi_B(2)\ \rangle +$$

$$\langle\ \phi_B(2)\,|\,\phi_A(2)\ \rangle\langle\ \phi_A(1)\,|\,h(1)\,|\,\phi_B(1)\ \rangle +$$

$$\langle\ \phi_A(1)\,|\,\phi_B(1)\ \rangle\langle\ \phi_B(2)\,|\,h(2)\,|\,\phi_A(2)\ \rangle +$$

$$\langle\ \phi_A(2)\,|\,\phi_B(2)\ \rangle\langle\ \phi_B(1)\,|\,h(1)\,|\,\phi_A(1)\ \rangle +$$

$$\langle\ \phi_B(1)\,|\,\phi_A(1)\ \rangle\langle\ \phi_A(2)\,|\,h(2)\,|\,\phi_B(2)\ \rangle +$$

$$\langle\ \phi_A(2)\,|\,\phi_A(2)\ \rangle\langle\ \phi_B(1)\,|\,h(1)\,|\,\phi_B(1)\ \rangle +$$

$$\langle\ \phi_B(1)\,|\,\phi_B(1)\ \rangle\langle\ \phi_A(2)\,|\,h(2)\,|\,\phi_A(2)\ \rangle]$$

$$= \frac{1}{2}[\alpha + \alpha - 0 - 0 - 0 - 0 + \alpha + \alpha\ ] = 2\alpha \qquad \textbf{eq.1.23}$$

Energy of the second closed-shell singlet is:

$$E_{singlet,\,CS} = \frac{1}{2}\langle\ \phi_A(1)\phi_B(2) - \phi_B(1)\phi_A(2)\,|\,h(1)+h(2)\,|\,\phi_A(1)\phi_B(2) - \phi_B(1)\phi_A(2)\ \rangle$$

$$= \frac{1}{2}[\langle\ \phi_A(1)\phi_B(2)\,|\,h(1)+h(2)\,|\,\phi_A(1)\phi_B(2)\ \rangle -$$

$$\langle\ \phi_A(1)\phi_B(2)\,|\,h(1)+h(2)\,|\,\phi_B(1)\phi_A(2)\ \rangle -$$

$$\langle\ \phi_B(1)\phi_A(2)\,|\,h(1)+h(2)\,|\,\phi_A(1)\phi_B(2)\ \rangle +$$

$$\langle\ \phi_B(1)\phi_A(2)\,|\,h(1)+h(2)\,|\,\phi_B(1)\phi_A(2)\ \rangle\ ]$$

$$= \frac{1}{2}[\langle\ \phi_B(2)\,|\,\phi_B(2)\ \rangle\langle\ \phi_A(1)\,|\,h(1)\,|\,\phi_A(1)\ \rangle +$$

$$\langle\ \phi_A(1)\,|\,\phi_A(1)\ \rangle\langle\ \phi_B(2)\,|\,h(2)\,|\,\phi_B(2)\ \rangle -$$

$$\langle\ \phi_B(2)\,|\,\phi_A(2)\ \rangle\langle\ \phi_A(1)\,|\,h(1)\,|\,\phi_B(1)\ \rangle -$$

$$\langle\ \phi_A(1)\,|\,\phi_B(1)\ \rangle\langle\ \phi_B(2)\,|\,h(2)\,|\,\phi_A(2)\ \rangle -$$

$$\langle\ \phi_A(2)\,|\,\phi_B(2)\ \rangle\langle\ \phi_B(1)\,|\,h(1)\,|\,\phi_A(1)\ \rangle -$$

$$\langle\ \phi_B(1)\,|\,\phi_A(1)\ \rangle\langle\ \phi_A(2)\,|\,h(2)\,|\,\phi_B(2)\ \rangle +$$

$$\langle\ \phi_A(2)\,|\,\phi_A(2)\ \rangle\langle\ \phi_B(1)\,|\,h(1)\,|\,\phi_B(1)\ \rangle +$$

$$\langle\ \phi_B(1)\,|\,\phi_B(1)\ \rangle\langle\ \phi_A(2)\,|\,h(2)\,|\,\phi_A(2)\ \rangle]$$

$$= \frac{1}{2}[\alpha + \alpha - 0 - 0 - 0 - 0 + \alpha + \alpha\,] = 2\alpha \qquad \textbf{eq.1.24}$$

All of the energies calculated to zeroth order are equal to 2α, where α is the Hückel α value which is the energy of the electron found within a single orbital. Therefore, when calculated to zeroth order, if the two electrons occupy identical orbitals, their energies will be the same, regardless of their orientation. This is of course neglecting electron-electron repulsion. By using a first-order Hamiltonian, eq. 1.15, that accounts for electron-electron repulsion, we are able to calculate more accurate values for the energies of the four states. The energies of the open shell singlet and triplet states now become:

$$E_{triplet,OS} = \frac{1}{\sqrt{2}}\langle\ \phi_A(1)\phi_B(2) - \phi_B(1)\phi_A(2)\,|\,\frac{e^2}{r_{12}}\,|\,\phi_A(1)\phi_B(2) - \phi_B(1)\phi_A(2)\ \rangle$$

$$= \frac{1}{\sqrt{2}}\langle\ \phi_A(1)\phi_B(2)\,|\,\frac{e^2}{r_{12}}\,|\,\phi_A(1)\phi_B(2)\ \rangle - \langle\ \phi_A(1)\phi_B(2)\,|\,\frac{e^2}{r_{12}}\,|\,\phi_B(1)\phi_A(2)\ \rangle -$$
$$\langle\ \phi_B(1)\phi_A(2)\,|\,\frac{e^2}{r_{12}}\,|\,\phi_A(1)\phi_B(2)\ \rangle + \langle\ \phi_B(1)\phi_A(2)\,|\,\frac{e^2}{r_{12}}\,|\,\phi_B(1)\phi_A(2)\ \rangle]$$

$$= \frac{1}{\sqrt{2}}\langle\ \phi_A(1)\phi_A(1)\,|\,\frac{e^2}{r_{12}}\,|\,\phi_B(2)\phi_B(2)\ \rangle - \langle\ \phi_A(1)\phi_B(1)\,|\,\frac{e^2}{r_{12}}\,|\,\phi_A(2)\phi_B(2)\ \rangle -$$
$$\langle\ \phi_B(1)\phi_A(1)\,|\,\frac{e^2}{r_{12}}\,|\,\phi_A(2)\phi_B(2)\ \rangle + \langle\ \phi_B(1)\phi_B(1)\,|\,\frac{e^2}{r_{12}}\,|\,\phi_A(2)\phi_A(2)\ \rangle]$$

$$= \frac{1}{\sqrt{2}}[\,j^o - k - k + j^o\,]$$

$$= j^o - k \qquad \textbf{eq 1.25}$$

$$E_{singlet,\,OS} = \frac{1}{\sqrt{2}}\langle\ \phi_A(1)\phi_B(2) + \phi_B(1)\phi_A(2)\,|\,\frac{e^2}{r_{12}}\,|\,\phi_A(1)\phi_B(2) + \phi_B(1)\phi_A(2)\ \rangle$$

$$= \frac{1}{\sqrt{2}}\langle\ \phi_A(1)\phi_B(2)\,|\,\frac{e^2}{r_{12}}\,|\,\phi_A(1)\phi_B(2)\ \rangle + \langle\ \phi_A(1)\phi_B(2)\,|\,\frac{e^2}{r_{12}}\,|\,\phi_B(1)\phi_A(2)\ \rangle +$$
$$\langle\ \phi_B(1)\phi_A(2)\,|\,\frac{e^2}{r_{12}}\,|\,\phi_A(1)\phi_B(2)\ \rangle + \langle\ \phi_B(1)\phi_A(2)\,|\,\frac{e^2}{r_{12}}\,|\,\phi_B(1)\phi_A(2)\ \rangle\,]$$

$$= \frac{1}{\sqrt{2}} \left\langle \ \phi_A(1)\phi_A(1) \left| \frac{e^2}{r_{12}} \right| \phi_B(2)\phi_B(2) \ \right\rangle + \left\langle \ \phi_A(1)\phi_B(1) \left| \frac{e^2}{r_{12}} \right| \phi_A(2)\phi_B(2) \ \right\rangle +$$
$$\left\langle \ \phi_B(1)\phi_A(1) \left| \frac{e^2}{r_{12}} \right| \phi_A(2)\phi_B(2) \ \right\rangle + \left\langle \ \phi_B(1)\phi_B(1) \left| \frac{e^2}{r_{12}} \right| \phi_A(2)\phi_A(2) \ \right\rangle]$$
$$= \frac{1}{\sqrt{2}} [j^o + k + k + j^o]$$
$$= j^o + k \qquad \textbf{eq 1.26}$$

Energy of the first closed-shell singlet:

$$E_{singlet,\ CS} = \frac{1}{\sqrt{2}} \left\langle \ \phi_A(1)\phi_A(2) + \phi_B(1)\phi_B(2) \left| \frac{e^2}{r_{12}} \right| \phi_A(1)\phi_A(2) + \phi_B(1)\phi_B(2) \ \right\rangle$$
$$= \frac{1}{\sqrt{2}} \left\langle \ \phi_A(1)\phi_A(2) \left| \frac{e^2}{r_{12}} \right| \phi_A(1)\phi_A(2) \ \right\rangle + \left\langle \ \phi_A(1)\phi_A(2) \left| \frac{e^2}{r_{12}} \right| \phi_B(1)\phi_B(2) \ \right\rangle +$$
$$\left\langle \ \phi_B(1)\phi_B(2) \left| \frac{e^2}{r_{12}} \right| \phi_A(1)\phi_A(2) \ \right\rangle + \left\langle \ \phi_B(1)\phi_B(2) \left| \frac{e^2}{r_{12}} \right| \phi_B(1)\phi_A(2) \ \right\rangle]$$
$$= \frac{1}{\sqrt{2}} \left\langle \ \phi_A(1)\phi_A(1) \left| \frac{e^2}{r_{12}} \right| \phi_B(2)\phi_B(2) \ \right\rangle + \left\langle \ \phi_A(1)\phi_B(1) \left| \frac{e^2}{r_{12}} \right| \phi_A(2)\phi_B(2) \ \right\rangle +$$
$$\left\langle \ \phi_B(1)\phi_A(1) \left| \frac{e^2}{r_{12}} \right| \phi_A(2)\phi_B(2) \ \right\rangle + \left\langle \ \phi_B(1)\phi_B(1) \left| \frac{e^2}{r_{12}} \right| \phi_A(2)\phi_A(2) \ \right\rangle]$$
$$= \frac{1}{\sqrt{2}} [j^o + k + k + j^o]$$
$$= j^o + k \qquad \textbf{eq. 1.27}$$

Energy of the second closed-shell singlet:

$$E_{singlet,\ CS} = \frac{1}{\sqrt{2}} \left\langle \ \phi_A(1)\phi_A(2) - \phi_B(1)\phi_B(2) \left| \frac{e^2}{r_{12}} \right| \phi_A(1)\phi_A(2) - \phi_B(1)\phi_B(2) \ \right\rangle$$
$$= \frac{1}{\sqrt{2}} \left\langle \ \phi_A(1)\phi_A(2) \left| \frac{e^2}{r_{12}} \right| \phi_A(1)\phi_A(2) \ \right\rangle - \left\langle \ \phi_A(1)\phi_A(2) \left| \frac{e^2}{r_{12}} \right| \phi_B(1)\phi_B(2) \ \right\rangle -$$
$$\left\langle \ \phi_B(1)\phi_B(2) \left| \frac{e^2}{r_{12}} \right| \phi_A(1)\phi_A(2) \ \right\rangle - \left\langle \ \phi_B(1)\phi_B(2) \left| \frac{e^2}{r_{12}} \right| \phi_B(1)\phi_A(2) \ \right\rangle]$$
$$= \frac{1}{\sqrt{2}} \left\langle \ \phi_A(1)\phi_A(1) \left| \frac{e^2}{r_{12}} \right| \phi_B(2)\phi_B(2) \ \right\rangle - \left\langle \ \phi_A(1)\phi_B(1) \left| \frac{e^2}{r_{12}} \right| \phi_A(2)\phi_B(2) \ \right\rangle +$$
$$\left\langle \ \phi_B(1)\phi_A(1) \left| \frac{e^2}{r_{12}} \right| \phi_A(2)\phi_B(2) \ \right\rangle + \left\langle \ \phi_B(1)\phi_B(1) \left| \frac{e^2}{r_{12}} \right| \phi_A(2)\phi_A(2) \ \right\rangle]$$
$$= \frac{1}{\sqrt{2}} [j^o - k - k + j^o]$$
$$= j^o - k \qquad \textbf{eq. 1.28}$$

Within equations 1.25 through 1.28, $j = \left\langle \ \phi_B(1)\phi_A(1) \left| \frac{e^2}{r_{12}} \right| \phi_A(2)\phi_B(2) \ \right\rangle$ is a two-center *coulomb* integral, the electron-electron repulsion felt between two electrons in different

orbitals; $k = \left\langle \phi_A(1)\phi_B(1) \left| \frac{e^2}{r_{12}} \right| \phi_A(2)\phi_B(2) \right\rangle$ is a two-center *exchange* integral, the electron-electron repulsion felt between two electrons within the overlap region of two orbitals, and $j^o = \left\langle \phi_A(1)\phi_A(1) \left| \frac{e^2}{r_{12}} \right| \phi_B(2)\phi_B(2) \right\rangle$ is the one-center *coulomb* integral, electron-electron repulsion felt between two electrons in the same orbital. Usually, j^o is significantly larger than j.

So far, the energy of the states (equations 1.21-1.24) in terms of the energy of the electron in a single orbital (zero-order Hamiltonian, H_0) and the energy of the electron-electron repulsions in two orbitals (first-order Hamiltonian, H_1) have been described. Figure 1.4 is a pictorial representation of the energy of the states and the terms describing them. We should also notice that the lowest energy state is a triplet and that the energy gap between the triplet and the lowest-lying singlet is $\Delta E_{S\text{-}T} = 2\boldsymbol{J}_{Tot} = 2k$.

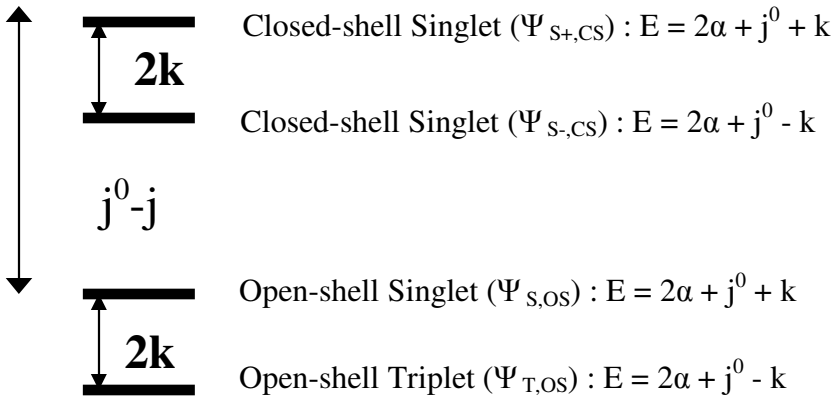

Fig. 1.4. Relative energy states of a two-electron/ two-orbital system, including the energy from the electron in a single orbital, (H_0), and electron-electron repulsions, (H_1). Notice that without second-order contributions (configuration interaction) the triplet state is lower in energy by 2*k* compared to that of the open-shell singlet.

1.4. Qualitative description of exchange coupling in biradicals.

1.4.1. Hund's rule in atomic carbon

The triplet state is lower than the singlet state in energy by $2k_{AB}$, where k_{AB} is the exchange integral. By examining the spatial wavefunctions, of the singlet and triplet states, this will become apparent.

$$\Psi_S = \frac{1}{\sqrt{2}} [\phi_A(1)\phi_B(2) + \phi_B(1)\,\phi_A(2)]$$

$$\Psi_T = \frac{1}{\sqrt{2}} [\phi_A(1)\phi_B(2) - \phi_B(1)\,\phi_A(2)]$$

The total wavefunction is comprised of spatial and spin wavefunctions. The total wavefunction must be antisymmetric with respect to electron label exchange.[18] If the spin wavefunction is symmetric, the spatial wavefunction must then be antisymmetric and vice versa. The allowable combinations therefore give an antisymmetric spatial wavefunction which describes the triplet, and a symmetric spatial wavefunction describing the singlet. Since the spatial wavefunctions are used to calculate the energies of the individual states, it should be apparent after examining equations 1.29 and 1.30 that the triplet state will be lower in energy.

$$E_{singlet} = \iint [\phi_A(1)\phi_A(1)\left|\frac{e^2}{r_{12}}\right|\phi_B(2)\phi_B(2)]d\tau 1\, d\tau 2 + \iint [\phi_A(1)\phi_B(1)\left|\frac{e^2}{r_{12}}\right|\phi_B(2)\phi_A(2)]d\tau 1\, d\tau 2 = j_{AB}+k_{AB} \quad \textbf{eq. 1.29}$$

$$E_{singlet} = \iint [\phi_A(1)\phi_A(1)\left|\frac{e^2}{r_{12}}\right|\phi_B(2)\phi_B(2)]d\tau 1\, d\tau 2 - \iint [\phi_A(1)\phi_B(1)\left|\frac{e^2}{r_{12}}\right|\phi_B(2)\phi_A(2)]d\tau 1\, d\tau 2 = j_{AB}-k_{AB} \quad \textbf{eq. 1.30}$$

The first term on the right of each equation describes the repulsion between two electrons when occupying different regions of space, and is known as the coulomb integral, j_{AB}. The second term on the right of each equation is the exchange integral, k_{AB}, and it describes the repulsion felt by two electrons occupying the same region of space. Figure 1.5 provides a graphical depiction of the difference between j_{AB} and k_{AB}.

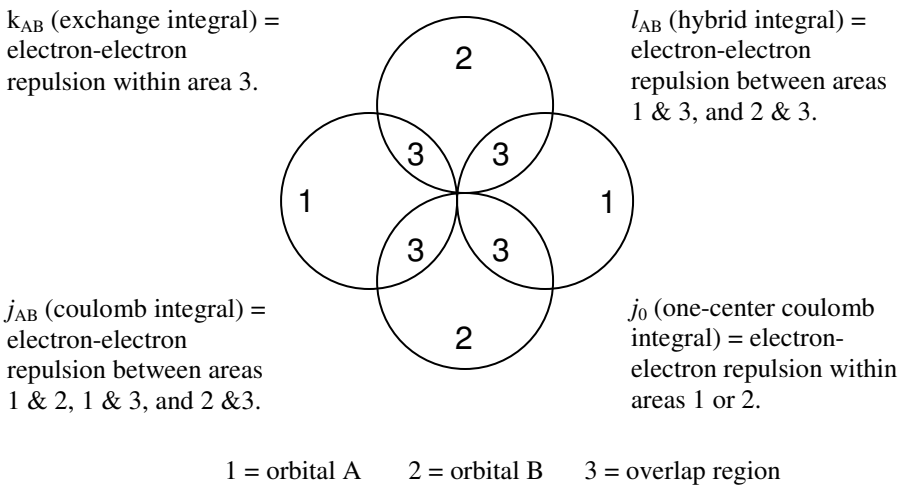

Fig. 1.5. Visual representation of equations 1.33 and 1.34.

From equation 1.29: $E_{singlet} = j_{AB} + k_{AB}$ **eq. 1.31**

From equation 1.30: $E_{triplet} = j_{AB} - k_{AB}$ **eq. 1.32**

$E_{singlet} - E_{triplet} = 2\,k_{AB}$

For a biradical to have a triplet lie below a singlet, two conditions must be met. The overlap integral, S, between the two singly-occupied molecular orbitals (SOMOs) must be zero, or nearly so.[18] If it is not, the bonding combination of orbitals will lie well below the anti-bonding, creating a large HOMO-LUMO gap and a strong preference for spin pairing into the lower orbital (a chemical bond). Second, the exchange integral between the two orbitals, *k*, must be large. We can illustrate the interplay of these two parameters by considering two degenerate orthogonal *p* orbitals, such as those in atomic carbon.

In atomic carbon, the ground state triplet results from high-spin coupling of two electrons in the singly-occupied orthogonal *p*-orbitals. This is a manifestation of Hund's rule, which states that in order to minimize electronic configuration energy, electrons align so as to maximize their spin.[19] From Figure 1.6, it is clear that S, the overlap integral is equal to zero, so the critical issue must be the exchange interaction, k.

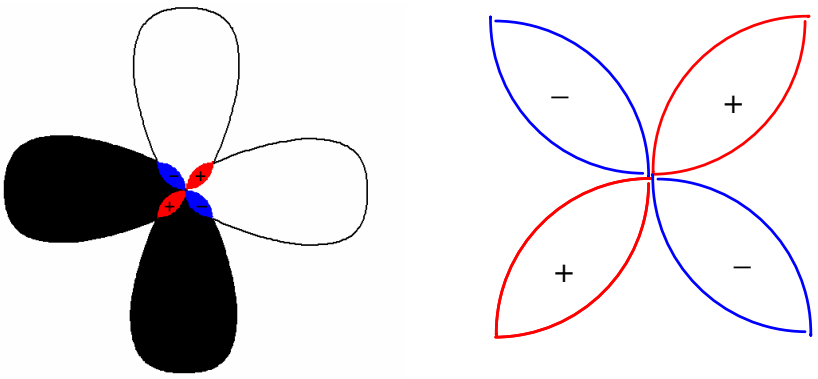

Fig. 1.6. Orthogonal *p* orbitals at an atomic center. The left figure illustrates the exact cancellation of regions of positive overlap by regions of negative overlap. The right figure is a magnification of the overlap region which shows that *k* is still substantial.

We can consider the overlap region as a region of space where two electrons may coexist but if they do, they will exhibit destabilizing coulombic repulsive forces between each other. The Pauli Exclusion Principle forbids electrons of parallel spin (triplet alignment) from occupying the same region of space; their motions are correlated so as to keep them apart. A singlet pair of electrons is not similarly correlated and so experiences greater electron-electron repulsion in the overlap region and is therefore destabilized.

The quantum mechanical basis for this is explained above. It is found that the triplet state is lower in energy than the singlet state by $2k_{AB}$, where k_{AB} is the exchange integral, $k = \left\langle \phi_A(1)\phi_B(1) \left| \frac{e^2}{r_{12}} \right| \phi_A(2)\,\phi_B(2) \right\rangle$. In other words, *k* is the energy that the electron *saves* by avoiding the overlap region between the two orbitals. The size of k_{AB} depends on the overlap density of the two orbitals. The greater the overlap region between the two orbitals, the larger k_{AB}, and consequently, the greater the preference for the triplet state.

1.4.2. Extending Hund's rule to molecules

Since the basis for a triplet ground state has been set, the question then becomes – can we extend Hund's rule to biradical molecules and conclude that the unpaired electrons within the degenerate SOMOs, that are analogous to the triply degenerate orbitals of atomic carbon, will align in a triplet fashion? Although Hund's rule describes triplet ground state preferences at a fundamental level of theory, it cannot be used as the sole determinant in predicting the ground state of biradicals. In molecules, in addition to in-phase orbital overlap, bond connectivity and the relative energies of the SOMOs are important in determining the spin preference of the biradical.

Two main theories predict the ground state in multi-spin molecules: valence bond (VB) theory,[20] and molecular orbital (MO) theory.[1] The VB approach, developed mainly by Ovchinikov, is able to predict the ground state in a biradical system, but cannot be used as a tool to determine the size of the singlet-triplet energy gap. The MO approach has the advantage of being able to give a qualitative estimate of the size of the singlet-triplet gap, but is sometimes unable to determine the ground state when the gap is very small.

We can use the trimethylenemethane (TMM), *m*- phenylene, and tetramethylenemethane (TME) biradicals shown in Figure 1.7 to best illustrate these theories. In the VB approach, one assumes that one electron occupies the *p*- π AO on each carbon. A π- bond can only form if the *p*- π electrons on adjacent atoms have opposite spins. This method, known as the star/non-star method was developed by Longuett-Higgins and is useful only in odd-alternant π systems.[21] A star (*) represents an α or "up" spin and a non-star represents a β or "down" spin. Stars are arranged on a

molecule so that none are adjacent to another starred atom, and so that there are more starred than non-starred atoms.

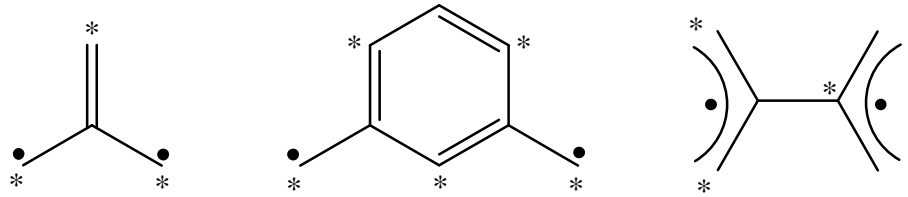

TMM (triplet) | *m*- Phenylene (triplet) | TME (singlet)

Fig 1.7. Pictorial representation of the star/ non-star method

Once the star/non-star designation is implemented, eq 1.33 can then be used to determine the ground state of the biradical;

$$S = \frac{N^* - N}{2} \qquad \textbf{eq 1.33}$$

Where S is the ground-state spin of the system, N* is the number of starred atoms, and N is the number of non-starred atoms. The predictions, using VB theory, are shown below in table 1.2 for the three molecules shown above.

Table 1.2. VB theory calculations VB theory using equation 1.16 predicts the ground states for TMM (S=1: triplet), *m*-phenylene (S=1: triplet), and TME (S=0: singlet).

	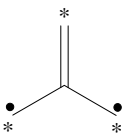	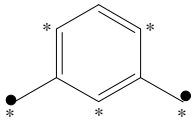	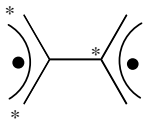
$\frac{N^* - N}{2}$	$\frac{3-1}{2}$	$\frac{5-3}{2}$	$\frac{3-3}{2}$
S =	1	1	0

Hückel Molecular Orbital theory can be used to predict the ground state of a biradical. The basis for the prediction lies in the concentration of spin density on each SOMO. Recall that the coefficients of each atom within a π-system can be calculated using Hückel theory. The square of the coefficients on these atoms is the spin density. Qualitatively, we can represent the spin density on each atom as spheres of different sizes, as shown in Figure 1.6.

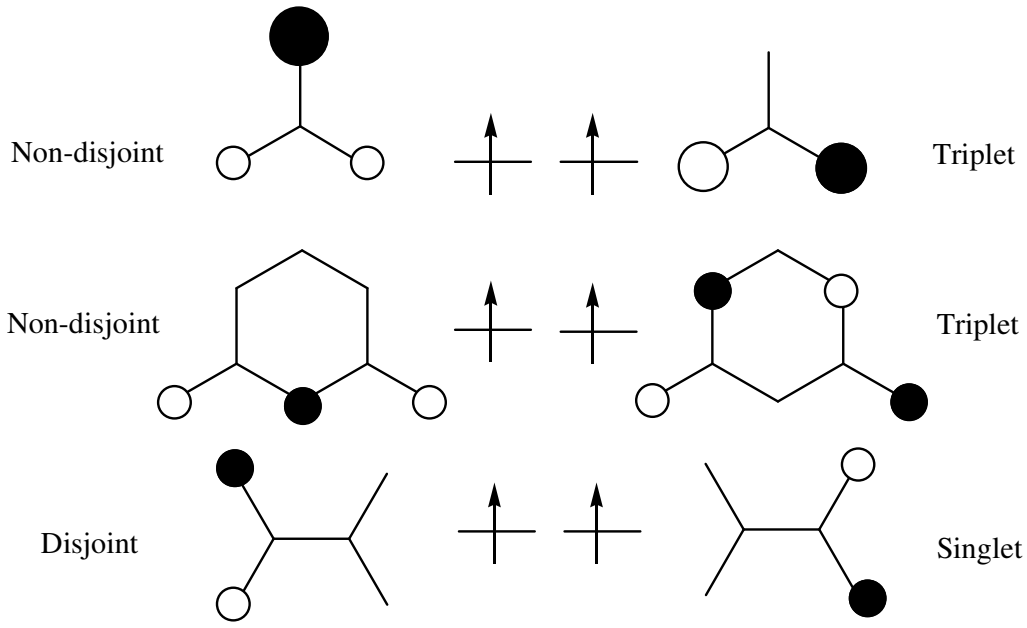

Fig. 1.8. Fragment Orbitals of Non-disjoint (TMM, *m*-phenylene) and Disjoint (TME)

If the two SOMOs do not share spin density on common atoms, they are said to be disjoint.[22] If they share spin density on common atoms, they are considered non-disjoint. The "sharing of spin density" can only occur when SOMOs overlap. This overlapping of the SOMOs is analogous to the overlap region in atomic carbon mentioned previously. Since the Pauli Exclusion Principle, (PEP), dictates the locality of the electron, in accordance with the PEP, the triplet state would be lower in energy than the singlet state

in non-disjoint molecules, e.g. *m*-phenylene. In a disjoint molecule, such as TME, there is no "overlap" region, hence no region of space for the Pauli exclusion principle to operate and so the molecule would not *save* any energy via triplet alignment and therefore a singlet ground state would persist.

Although MO theory can be used to estimate the *size* of the singlet-triplet energy gap, ΔE_{ST}, Hückel coefficients do not account for geometric configurations and symmetry. Because of this, one often chooses the Hückel MOs that "work" out of many possible NMBOs, ignoring other equally plausible MOs.

One can predict whether a system will be non-disjoint or disjoint based on the connectivity of simpler components and the coefficients of these fragments rather than the MO picture.[22] Consider the allyl radical, which contains two types of atoms, active, (A - having spin density) and inactive, (I – having no spin density) as shown in Figure 1.7.

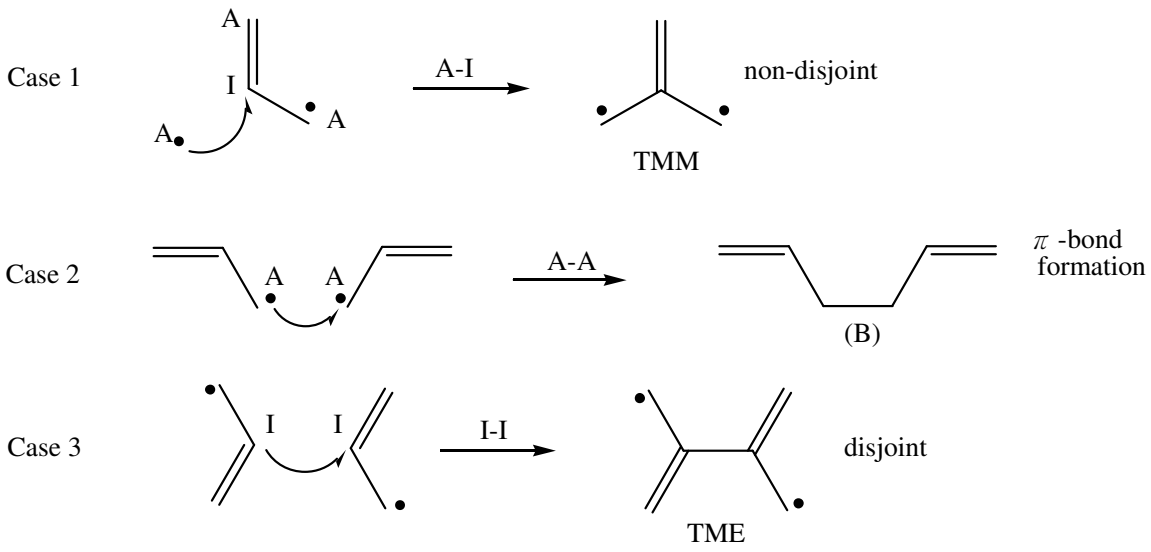

Fig. 1.9. A=active; I=inactive. Case 1: active to inactive leads to non-disjoint; Case 2: active to active leads to bond formation; Case 3: inactive to inactive leads to disjoint.

The active atoms are the two carbon atoms on either end. The inactive atom is the middle carbon. If one attaches an active radical (·CH2) to the inactive site (A -I) (Case 1), TMM is formed and a non-disjoint system is made. If one attaches an active radical (·CH2) to one of the active sites (A-A) (Case 2), a bond is formed to give (B) in Figure 1.7. Finally, if you attach two allyl radicals at both of the inactive sites (I-I) (Case 3), TME is formed, and a disjoint system is made.

From the above mentioned facts, we conclude that TMM and *m*-phenylene are coupling units that promote ferromagnetic interactions and subsequently, triplet ground states. They are classified as non-Kekulé hydrocarbons. Non-Kekulé refers to a molecule with a resonance structure that has as many π-bonds as possible, but has at least two atoms not included in a π-bond.[20] TMM and *m*-phenylene are therefore said to be cross-conjugated.[22] The ferromagnetic coupling unit, *m*-phenylene is ubiquitous throughout the research done in the Shultz group and is featured in the biradical moities under study.

When two spins are exchange coupled, thermally accessible states are created with different multiplicities. The Heisenberg Hamiltonian is used to predict the resulting spin states. To describe exchange coupled spins, one uses the Heisenberg-Dirac-van Vleck Hamiltonian, equation (1.39).[11]

$$H_{ab} = -2\boldsymbol{J}_{ab}\hat{S}_a \cdot \hat{S}_b \qquad \textbf{eq. 1.34}$$

This empirical Hamiltonian describes the spin angular momentum operators ($\hat{S}_a$ and $\hat{S}_b$) and the magnitude of the interaction depends on $\boldsymbol{J}_{ab}$, the isotropic exchange parameter. The product of the spin operators can be expressed in terms of the component spin operators and the $_{Tot}$al spin operator: $\hat{S}_{Tot} = \hat{S}_a + \hat{S}_b$.

$$\hat{S}^2_{Tot} = (\hat{S}_a + \hat{S}_b)^2 = \hat{S}_a{}^2 + \hat{S}_b{}^2 + 2\hat{S}_a\hat{S}_b \qquad \textbf{eq. 1.35}$$

$$\text{Therefore, } \hat{S}_a\hat{S}_b = \tfrac{1}{2}\,(\hat{S}^2_{Tot} - \hat{S}_a{}^2 - \hat{S}_b{}^2) \qquad \textbf{eq. 1.36}$$

Since the eigenvalue of S^2 is S(S+1), one can determine the energy of the state by substituting in the appropriate terms. The general equation is given by:

$$E_{Tot} = -\boldsymbol{J}_{ab}\,[S_{Tot}(S_{Tot}+1)-S_a(S_a+1)-S_b(S_b+1)] \qquad \textbf{eq. 1.37}$$

Since the final two terms are constants, (eq. 1.50) reduces to:

$$E_{Tot} = -\boldsymbol{J}_{ab}[S_{Tot}(S_{Tot}+1)] \qquad \textbf{eq. 1.38}$$

Thus, the energy of the triplet state (S=1), the singlet state (S=0), and the energy gap between the two can be determined.

$$E_T = -\boldsymbol{J}[1(1+1)] = -2\boldsymbol{J} \qquad \textbf{eq. 1.39}$$

$$E_S = -\boldsymbol{J}[0(0+1)] = 0\boldsymbol{J} = 0 \qquad \textbf{eq. 1.40}$$

The singlet-triplet gap energy is then:

$$\Delta E_{ST} = E_S - E_T = 0 - (-2\boldsymbol{J}) = 2\boldsymbol{J} \qquad \textbf{eq. 1.41}$$

Now, the magnetic susceptibility (χ) for an S=1 system is given by the HDVV equation (eq. 1.42):

$$\chi = \frac{Ng^2\beta^2}{3k_BT} \bullet \frac{\{\sum S(S+1)(2S+1)\,e^{Es/kT}\}}{\sum\{(2S+1)\,e^{Es/kT}\}} \qquad \textbf{eq 1.42}$$

Substituting:

$$\chi = \frac{Ng^2\beta^2}{3k_BT} \bullet \frac{\{(0)(1)e^{0/kT} + (2)(3)\,e^{-2J/k_BT}\}}{1\,e^{0/kT} + 3e^{-2J/k_BT}}$$

Multiplying through by T and accounting for intermolecular interactions (θ) gives:

$$\chi_T = \frac{2Ng^2\beta^2 T}{k_B(T-\theta)} \bullet \frac{e^{-2J/k_BT}}{1+3e^{-2J/k_BT}} \qquad \textbf{eq 1.43}$$

Lastly, the value of $\boldsymbol{J}$ can be determined experimentally by either Electron Paramagnetic Resonance (EPR) or magnetometry. Because of the sign of the Hamiltonian being used, (eq 1.34), by definition, $\boldsymbol{J} > 0$ describes ferromagnetic coupling and $\boldsymbol{J} < 0$ describes antiferromagnetic coupling.

References

1. Dougherty, D.A. *Acc.Chem.Res.* **1991**, *24*, 88.

2. Itoh, K; Kinoshita, M. *Molecular Magnetism*; Gordon & Breach Science Publishers: Australia, **2000**.

3. University of Winnipeg website. http://theory.uwinnipeg.ca/mod_tech/node83.htm., **1999**.

4. Wolf, S.A. *Science.* **2001**, *294*, 1488.

5. Gupta, J.A.; Knobel, R.; Samarth, N.; Awschalom, D.D. *Science* **2001**, *292*, 2458.

6. Shultz, D.A.; Boal, A.K.; Driscoll, D.J.; Farmer, G.T.; Kitchin, J.R.; Miller, D.B.; Tew, G.N. *Mol.Cryst.Liq.Cryst.***1997**, *305***,** 303.

7. Shultz, D.A.; Boal, A.K.; Lee, H.; Farmer, G.T. *J.Org.Chem.* **1999**, *64*, 4386.

8. Shultz, D.A.; Bodnar, S.H. *Inorg.Chem.* **1999**, *38*, 591.

9. Shultz, D.A.; Bodnar, S.H.; Kampf, J.W.; Kumar, R.K. *J.Am.Chem.Soc.* **1999**, *121*, 10664.

10. Shultz, D.A.; Bodnar, S.H; Kampf, J.W. *Chem.Commun.* **2001**, *93*.

11. Kahn, O. *Molecular Magnetism*; VCH Publishers, Inc: New York, **1993**.

12. Hurd, C. M. *Contemp.Phys* **1982**, *23*, 469.

13. Jakubovics, J.P. *Magnetism and Magnetic Materials* 2nd Ed.; Harvard University Press: Cambridge, **1994**.

14. Moore, W. *Physical Chemistry* 4th Ed.; Prentice Hall: New Jersey, **1972**.

15. Livingstone, J.D. *Driving Force: The Natural Magic of Magnets;* Harvard University Press: Cambridge, **1997**.

16. Wenthold, P. G.; Hu, J.; Squires, R. R.; Lineberger, W. C. *J.Am.Chem.Soc* **1996**, *118*, 475.

17. Levine, I.N. *Quantum Chemistry* 4th Ed.; Prentice Hall: New Jersey, **1991**.

18. Rajca, A. *Chem. Rev.* **1994**, *94*, 871.

19. Atkins, P. *Physical Chemistry* 5th Ed.; W.H. Freeman and Co.: New York, **1994**.

20. Borden, W.T. *Magnetic Properties of Organic Materials*; Marcel Dekkar, Inc., **1999**, 66-102,

21. Borden, W. T.; Davidson, E. R. *J. Am. Chem. Soc.* **1977**, *99*, 4587.

22. Phelan, N.F.; Orchin, M.J. *J.Chem.Ed.* **1968**, *45*, 633.

Chapter 2. The Biradical as a Probe for Testing Exchange Coupling Limits

2.1. Biradicals: Molecular Analogs of Bulk Magnetic Materials

Biradicals are a class of molecules that are especially relevant to a multidisciplinary frontier of science concerned with weak intermolecular interactions in large systems.[1] Many interesting characteristics of bulk materials are associated with weak interactions between electrons leading to a characteristic spin state. Most recently, research efforts have been geared towards studying spin-based electronic devices. The result of these efforts has given birth to a new technology known as "spintronics".[2,3] Spintronic molecular materials exploit the inherent spin of an electron, in addition to its charge, to yield devices that bear data storage capacities far beyond that of their traditional analogs. The attractiveness of spin-based devices lies in the additional degrees of freedom provided by the electron spin.[4-6]

Spintronics emerged in the 80's after French and German physicists discovered a very powerful effect called giant magnetoresistance (GMR).[7] It manifests itself as a decrease in electrical resistance resulting from electron-spin coupling effects within ultra-thin 'multilayers' of magnetic materials, upon application of an external magnetic field. GMR is 200 times stronger than ordinary magnetoresistance. A typical GMR device consists of a three-layer sandwich of a magnetic metal such as cobalt with a nonmagnetic metal filling like silver, as shown in the schematic drawing, Figure 2.1.

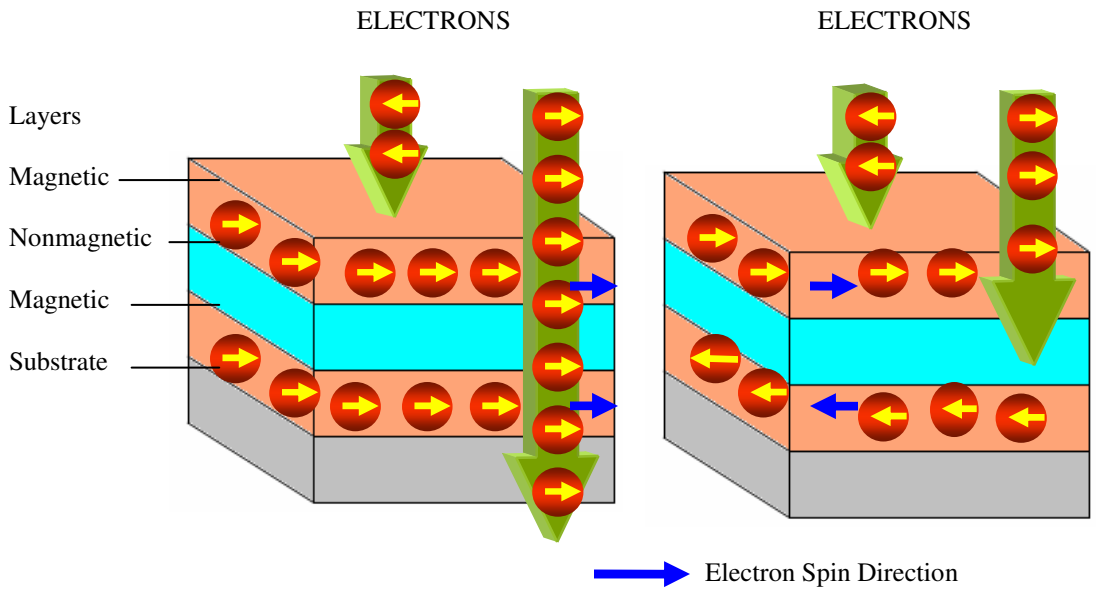

Fig 2.1. Schematic Representation of a Giant Magnetoresistive (GMR) Device

A current is passed through layers consisting of spin-up and spin-down electrons. Those oriented in the same direction as the electron spins in a magnetic layer pass through quite easily, while those oriented in the opposite direction are scattered. If the orientation of one of the magnetic layers can easily be changed by the presence of a magnetic field then the device will act as a filter, or 'spin valve',[6] letting through more electrons when the spin orientations in the two layers are the same and fewer when electrons are oppositely aligned. The electrical resistance of the device can therefore be altered dramatically. Spin valves are therefore ideal for use as high-sensitivity magnetic sensors[8] and can also be used as switches[9] if the magnetization of one of the layers is flipped.

If new magnetic materials are to be made, the intricacies of design and synthesis will have to be incorporated in the molecular "blue print". Research in the Shultz group is centered on studying fundamental concepts of magnetism. By probing fundamental

concepts such as exchange coupling between unpaired electrons, new information can be uncovered so that viable building blocks of magnetic materials can be made. Although understanding how to facilitate intramolecular ferromagnetic exchange coupling of electrons is a key component of a molecular magnet, it is by far not all that is required when designing a high spin organic species. In fact, parallel alignment of spins is not even required if a *ferrimagnetic* interaction can be achieved. The requirement at the molecular level is a species with a net magnetic moment. In addition, long range order between high-spin molecules in a 2D or 3D arrangement must also be achieved for a viable molecular magnet to be made.

The intermolecular interactions within these bulk solids are critical in the realization of a bulk material that exhibits magnetic ordering. However, long range intermolecular interactions are very difficult to control. Although one may design and synthesize a molecule with a high degree of specificity, it is hard to control the spatial distribution of the molecules within the crystal lattice. This is the major drawback to designing inorganic based molecular magnet candidates. Like their inorganic counterparts, predicting the crystal packing of organic species is equally difficult.

Supramolecular chemistry is often pursued to develop new functions that cannot appear from a single molecule.[10] One such function is the magnetic properties of a system. The field of supramolecular chemistry utilizes weak, non-covalent interactions, such as hydrogen bonding, metal coordination, hydrophobic forces, van der Waals forces, π-π interactions, and/or electrostatic effects to assemble molecules into 3D molecular complexes. Steady progress is being made to make the intermolecular interactions aforementioned significant enough to cause molecules to pack in predictable ways.[11,12]

2.2. Approaches for Studying Electronic Structure of Organic Open-Shell Systems.

There are a number of practical approaches to studying electronic phenomena of molecule-based magnetic materials. One way is to make macromolecular assemblies containing a large number of interacting spins. Rajca was successful at synthesizing a macromolecule bearing a spin value ~ 5000 that orders below 10K.[1] These species are very challenging to synthesize and are made from various triarylmethane radicals (Figure 2.2) that are only stable at very low temperatures and under inert atmospheres. So, although extremely high spin values have been achieved, practical applications of these species at ambient conditions are not tenable.

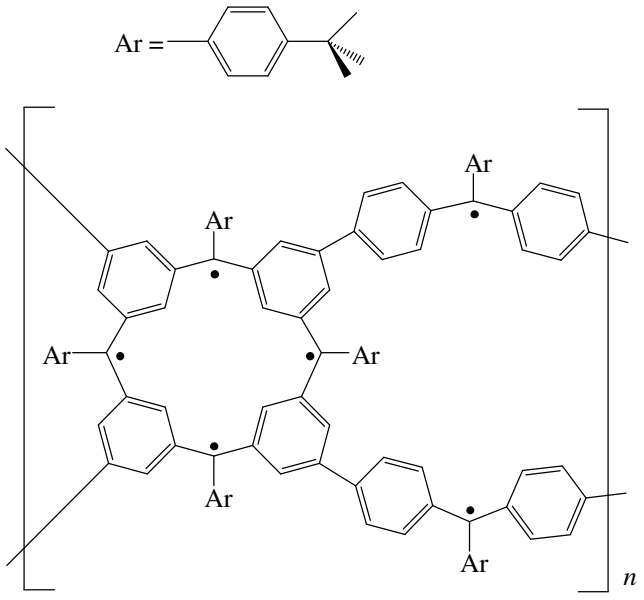

Fig. 2.2. Repeating unit in Rajca's macrocycle. Total S~5000

Iwamura and Gatteschi were among the first to use coordination polymers to produce a species that ordered as a magnet.[12-14] These polymers can take on many forms, including 1-D chains, 2-D sheets, and 3-D structures, and are usually composed of a

high-spin organic coupler that incorporates paramagnetic transition metals. Gatteschi used nitronylnitroxides (NIT) to coordinate $Cu(hfac)_2$ through oxygen atoms in order to form a linear chain - Figure 2.3.

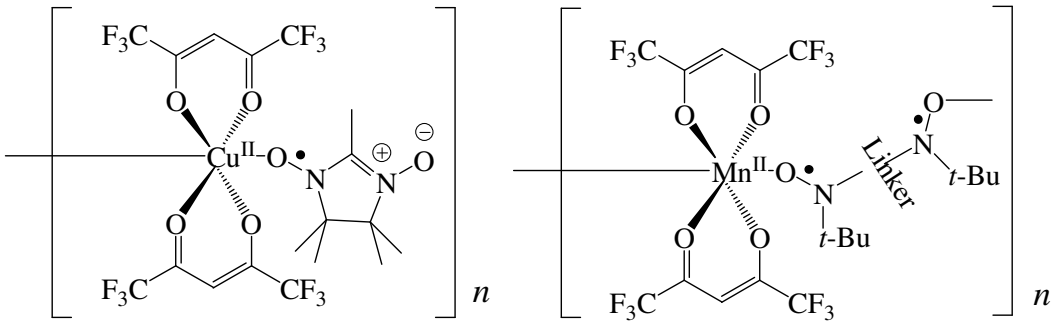

Fig. 2.3. Left. $Cu(hfac)_2(NIT)Me$ - repeating unit in Gatteschi's coordination polymer.
Right. $Mn(hfac)_2$bis(nitroxide) - repeating unit in Iwamura's coordination polymer.

Iwamura used $Mn(hfac)_2$ and a high-spin bis(nitroxide) as the coupler in his studies. The possibilities for these polymers are virtually limitless due to the variety of organic synthetic approaches and numerous metals that can be used.

The hexafluoroacetoacetonate is used to make the metal sufficiently Lewis acidic because nitroxides of this sort are known to be quite weak Lewis bases. This actually becomes a strength of the system. The crystals of these structures are typically grown through a process of slow evaporation. While an excess amount of solvent is present, the nitroxides are in equilibrium of being coordinated or uncoordinated to the metal center. As the solvent slowly evaporates, the nitroxides become "locked" in place within the structure as it crystallizes.

2.3. Shultz Group Research and Impetus

The Shultz group approach to studying electronic phenomena on a mesoscopic scale is embodied in biradical systems. Our research efforts have been centered on achieving conformational modulation of exchange coupling. Large amplitude bond torsions between the spin containing group and the coupling unit can dramatically affect delocalization of spin into the coupling unit and subsequently affect the exchange coupling in organic biradicals.[15-25] A series of TMM linked bis(semiquinone)s and bis(nitroxide)s (Figure 2.4) were used to demonstrate the relationship between conformation and exchange coupling.[17,26-28]

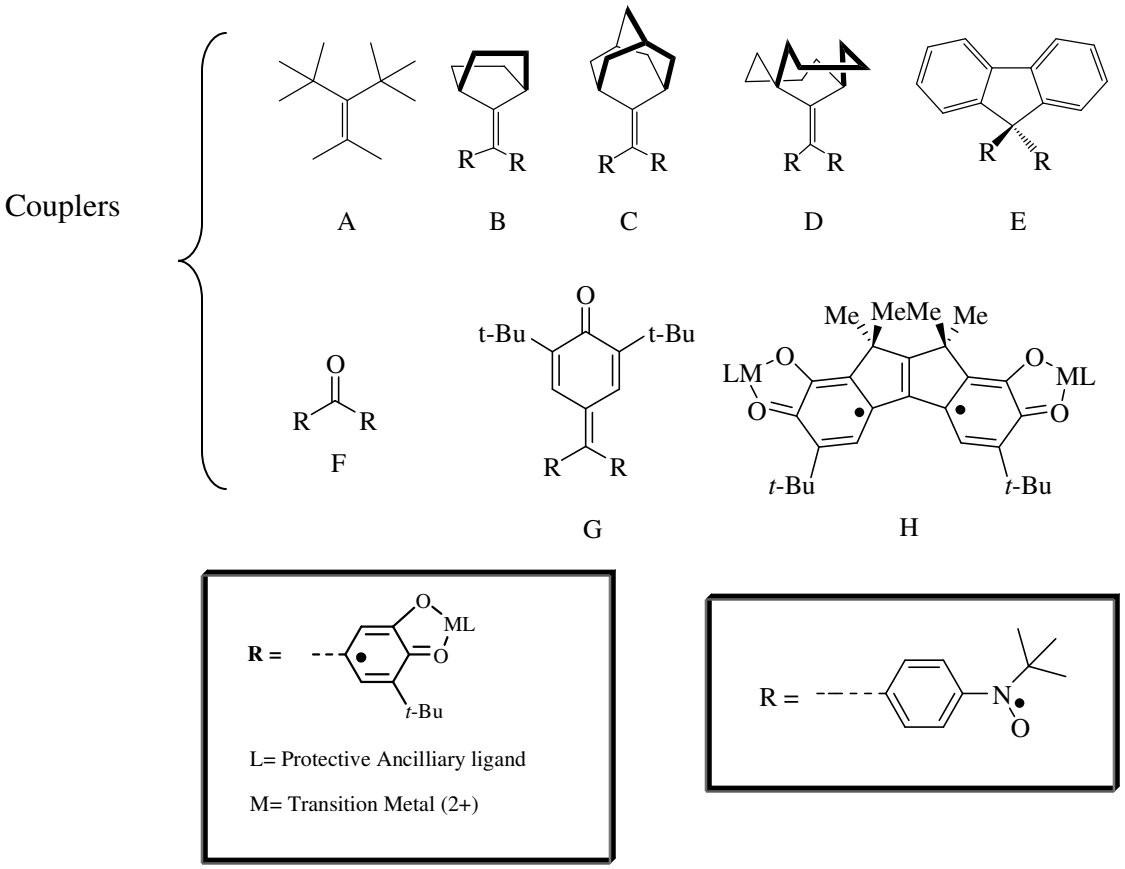

Fig 2.4. Series of TMM-linked bis (semiquinone)s and bis(nitroxide)s.

The couplers were dubbed as “bicyclic caps” that served to vary the angle, θ (Figure 2.5), to show that exchange coupling would be attenuated as the rings were twisted out of planarity in relation to the TMM coupling unit.

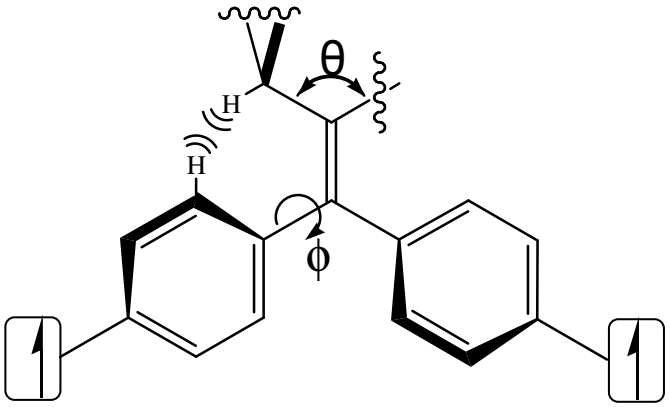

Fig. 2.5. Structure shows how the size of the bicyclic “cap” can vary the angle θ and thus the steric interaction between the two hydrogen atoms shown. That steric interaction will then affect the amount of twisting angle, ϕ and thus affect the strength of exchange coupling within the biradical.

The data in Tables 2.1 and 2.2 show that as the size of the bicyclic ring is increased, so does the angle, θ and consequently, the twisting angle, ϕ. This results in significant attenuation of the exchange coupling parameter, *J*.[27]

Table 2.1. Phenyl and Nitroxide torsion angles and ***J*** value for TMM bis(nitroxides).
* $2J = \Delta E_{ST}$ $J>0$ FM coupling; $J<0$ AFM coupling

	Phenyl Torsion	Nitroxide Torsion	J (cm^{-1}) *
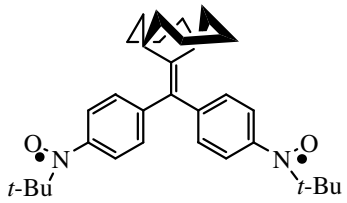	65.92 ± 0.05 82.37 ± 0.05	40.68 ± 0.1 23.14 ± 0.1	-14.03 ± 0.12 -11.8 ± 1.2
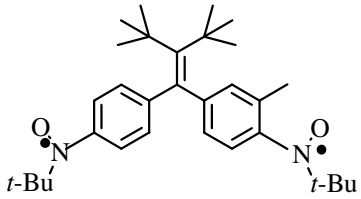	54.3 ± 0.1 55.5 ± 0.1	9.8 ± 0.2 11.1 ± 0.2	-5.75 ± 0.31
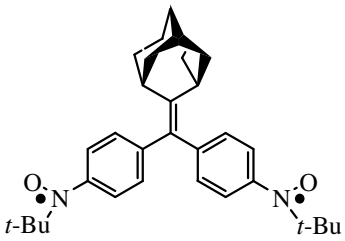	54.73 ± 0.08 53.47 ± 0.08	11.23 ± 0.07 9.9 ± 0.1	hysteresis -5.11 ± 0.24
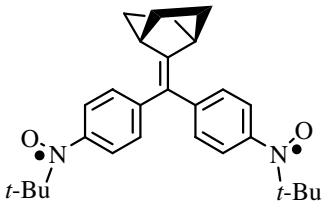	43.19 ± 0.11 50.84 ± 0.11	31.4 ± 0.2 31.3 ± 0.2	+6.79 ± 0.18 +6.07 ± 0.15
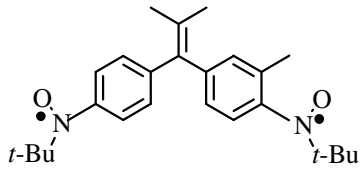			+5.24
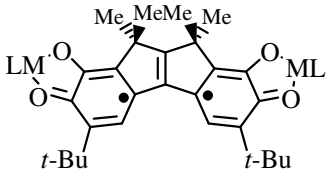	1.9 ± 0.3 1.8 ± 0.3	30.1 ± 0.2 28.4 ± 0.2	+25.5 ± 1.6 +26.35 ± 1.73
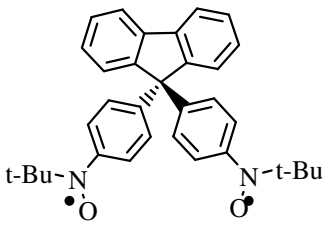	39.2 ± 0.5 41.0 ± 0.5	13.5 ± 0.4 24.3 ± 0.5	-2.61 ± 0.01 -2.85 ± 0.13

Table 2.2. Semiquinone ring torsion angles and ***J*** values for TMM bis(semiquinone).
* $2J = \Delta E_{ST}$ $J>0$ FM coupling; $J<0$ AFM coupling

	Semiquinone Ring Torsion	J (cm^{-1})*
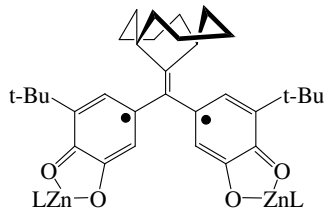	64.10 ± 0.13 78.04 ± 0.13	-30.3 ±0.8
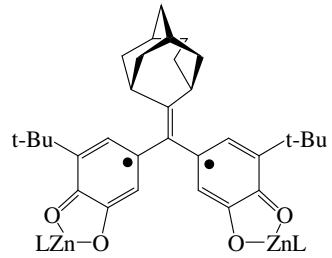	47.51 ± 0.18 48.94 ± 0.27	+24.4 ±0.6
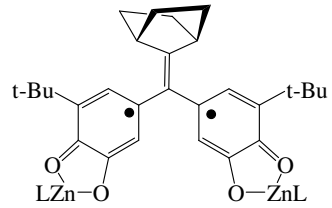	48.37±0.29	+87.0 ±3.0
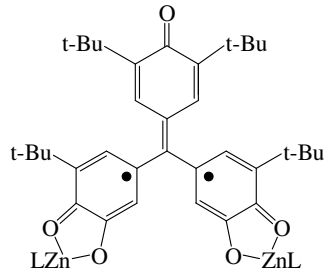	50.3 ± 0.3 42.6 ± 0.8	+209.4 ±1.4
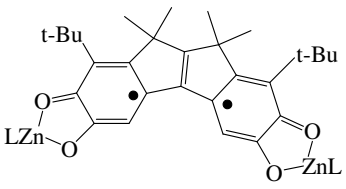	4.9 ± 0.8, 9.7 ± 0.8	+163.6 ±1.6
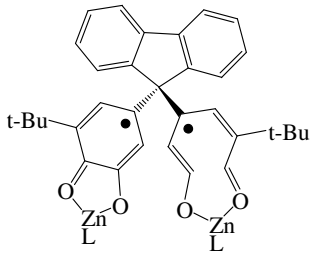	42.3 ± 0.9 52.4 ± 0.1	+0.99 ±0.06

Biradicals like the types shown in Tables 2.1 and 2.2 are termed homospin. As the name suggests, both paramagnetic functionalities attached to the coupler bear equal spin values. Conversely, heterospin biradicals have paramagnetic functionalities that bear unequal spin values. A heterospin biradical bearing nitronylnitroxide and phenyl paramagnetic functionalities is shown below as 2.3.

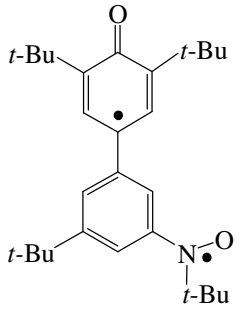

2.3

In addition to the biradicals mentioned above, there is a third type of biradical that we have dubbed Heterospin *Donor-Acceptor* biradicals. Heterospin donor-acceptor biradicals differ from homo- and heterospin biradicals in that:

1. Paramagnetic functional groups carry different spin values ($S_1 \neq S_2$),

2. A coupler is not used to facilitate exchange coupling,

3. Atoms of positive spin density are attached to atoms of negative spin density.

In heterospin *donor-acceptor* biradicals, the interaction of the SOMO of one spin carrier - the donor, with the LUMO of the other spin carrier - the acceptor, is responsible for ferromagnetic interaction of spins. A donor radical is a paramagnetic functional group having positive spin density at the point of attachment; whereas the acceptor radical is a paramagnetic functional group having negative spin density at the point of attachment, as shown for the semiquinone and galvinoxyl functionalities in Figure 2.8.

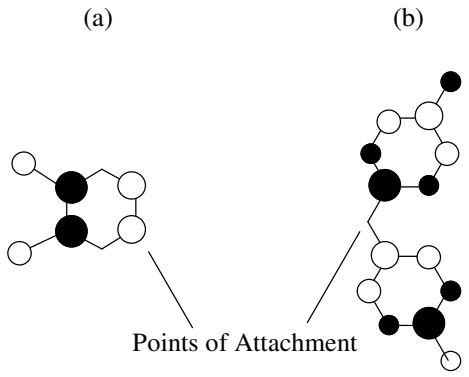

Fig. 2.6. Hückel SOMOs of (a) SQ (donor) and (b) galvinoxyl (acceptor).

In the case of a semiquinone-galvinoxyl biradical system, the SOMO of the donor (SQ) mixes with the LUMO of the acceptor (galvinoxyl) as depicted in MO diagram in Fig. 2.9. The result of this mixing is a new SOMO that is non-disjoint with the SOMO of the donor – a primary requirement for ferromagnetic coupling of spins. Shultz group member, Candice Brannen prepared a series of semiquinone- nitronyl nitroxide biradicals to evaluate the effect of donor-acceptor (D-A) interactions on the ferromagnetic coupling of D-A heterospin biradicals. A molecular orbital description was used to evaluate the *contributions* that D-A interactions have on the ferromagnetic coupling of D-A heterospin biradicals and a valence bond description was used to explain the electronic origin of strong ferromagnetic exchange coupling in this new type of biradical.

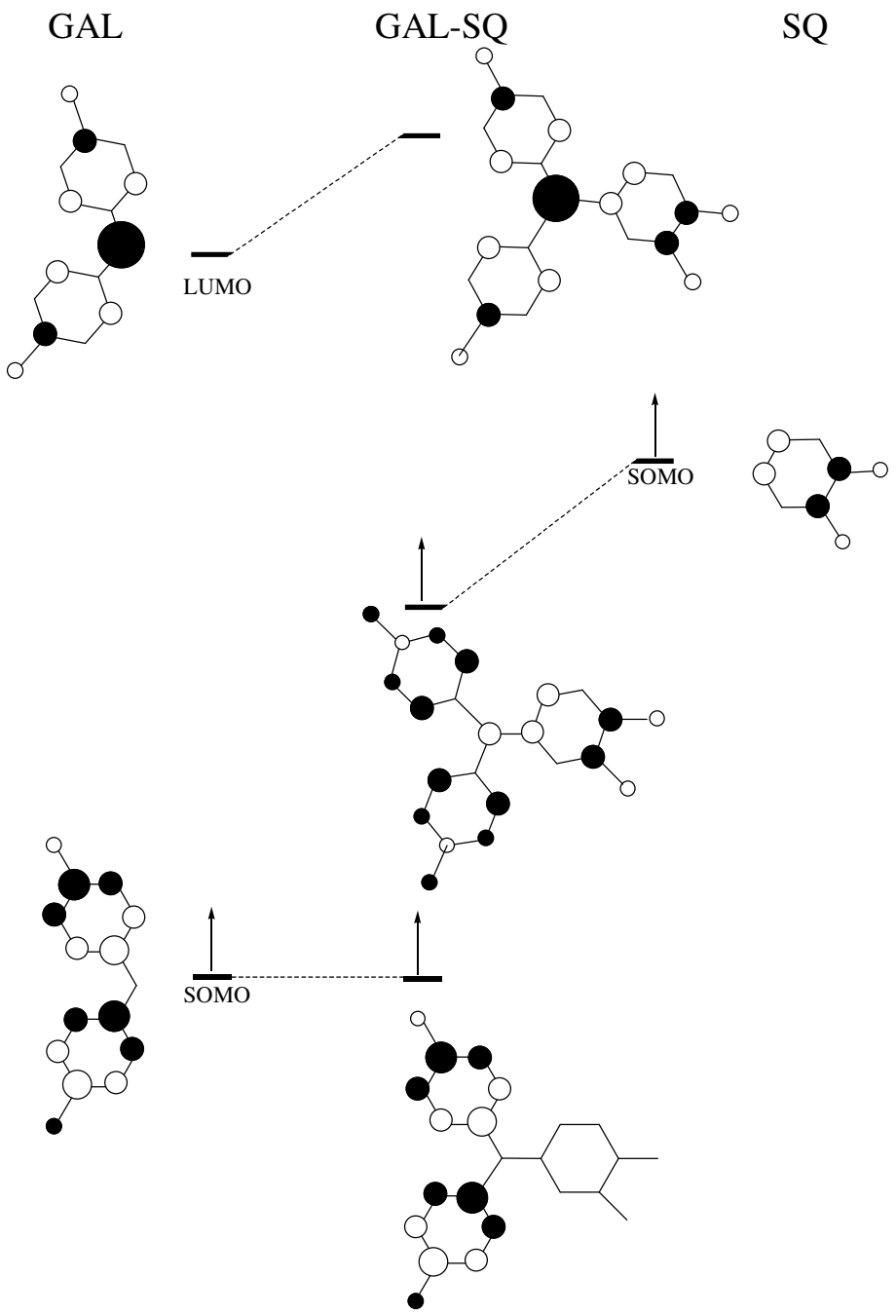

Fig. 2.7. (SQ)$SOMO_{donor-}$ (Gal)$LUMO_{acceptor}$ interaction that creates non-disjoint heterospin biradical SOMOs.

Mixed-valent species are a highly studied class of compounds with many interesting characteristics.[29]Inorganic compounds exhibiting mixed valency have been well

studied.[30] In an effort to formulate new design principles based on mixed-valency of organic compounds, the Shultz group synthesized and used triradical **2.1** in Figure 2.7 as a probe. Complex **2.1** is ideally suited for correlating exchange coupling in the biradical oxidation states with spin/charge delocalization in the mixed-valent oxidation states because it features an inherently weak antiferromagnetic coupler.[31] The weak coupler was chosen based on the fact that the effects of mixed valency might be modest and difficult to observe in a strongly coupled system. The first example of enhanced ferromagnetic coupling in a mixed-valent molecule that lacks an effective π-type ferromagnetic coupler, labeled as **2.2**, formed from one-electron reduction of an antiferromagnetically coupled triradical, **2.1** has been realized. It has been shown that delocalization enhances ferromagnetic coupling in a molecule that lacks an intrinsic ferromagnetic coupler.

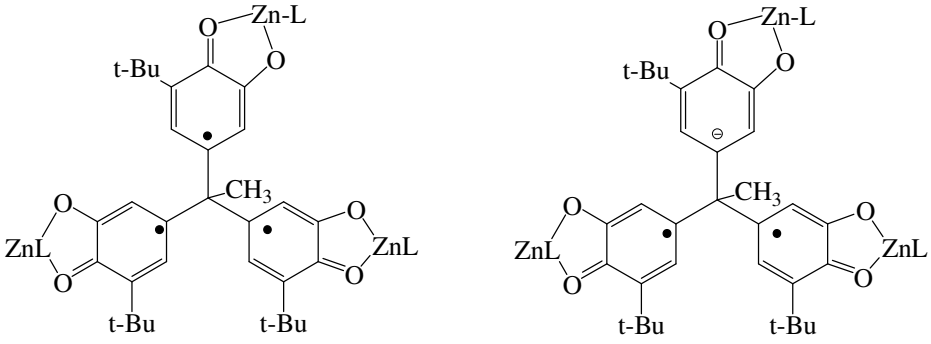

Fig. 2.8. Tri-radical $(LZn)_3(SQ_3)$, where $J<0$, and mixed valent biradical $Na+[(LZn)_3(SQ_3Cat)]-$; $J \geq 0$.

Another facet of Shultz group research and the focus of this dissertation is the effect of substituents on the exchange coupling of biradical species. Until recently there had been no experimental demonstration of controlling ΔE_{ST} of a triplet ground state biradical,

other than by bond torsions. Berson reported that electron-withdrawing substituents modulate the singlet-triplet gaps of singlet ground-state tetramethyleneethane-type biradicals.[32,33] In addition, Borden,[34] Dougherty,[35] Hadad,[36] and Yamaguchi[37]reported substituent effects on exchange coupling in computational studies. However the Shultz group pioneered *pure* electronic modulation of coupling within an *iso*-structural series of triplet ground-state, conjugated *m*-phenylene (MPH) coupled bis(semiquinone) biradicals.[38] The *m*-phenylene substituted bis(semiquinone) biradicals **1-NMe$_2$, 1-*t*-Bu,** and **1-NO$_2$** shown below were chosen to demonstrate the effect.

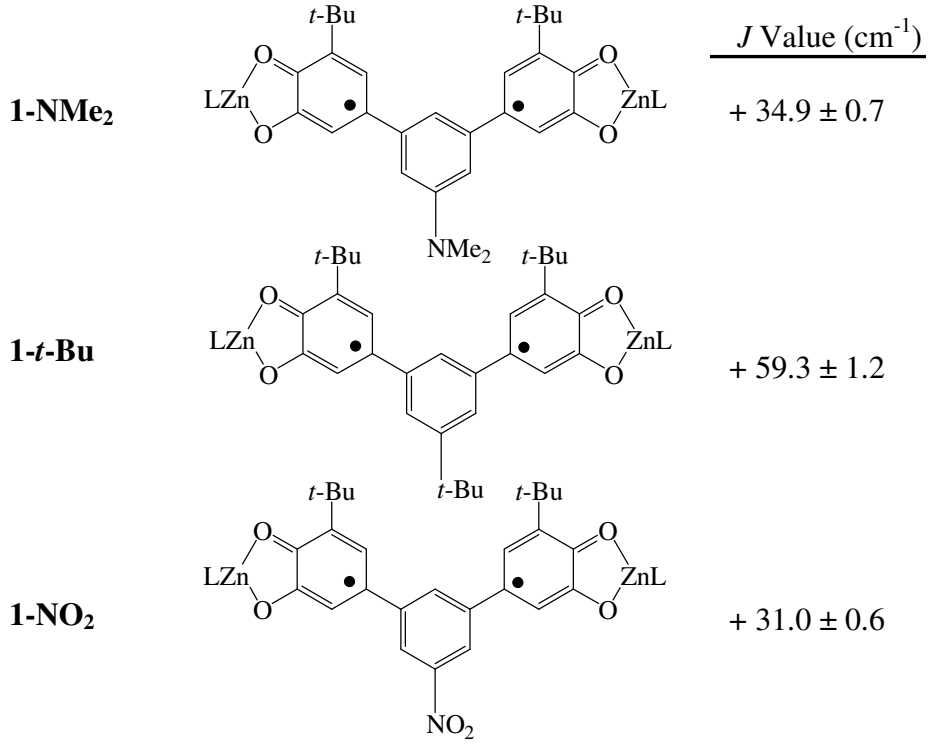

Fig. 2.9. *m*-Phenylene-type coupled bis(semiquinone)s.

We were then prompted to demonstrate that substituents modulate *J* whether in antiferromagnetically or ferromagnetically coupled species. A metal and a radical site

may couple either ferromagnetically or antiferromagnetically depending on the properties of the metal and ligand. Manganese (II) species are known to couple antiferromagnetically to radical ligands[13] with typical exchange coupling values ~ -300cm^{-1}, while copper (II) ferromagnetically couples to radical ligands, often producing exchange coupling ~ +70cm^{-1}.[36] These cases are of interest in this study, in that it is expected that coupling $Mn^{II}Tp^{Cum,Me}$ and $Cu^{II}Tp^{Cum,Me}$ with our substituted semiquinones will produce S=2 and S=1 systems, respectively. Figure 2.7 depicts the net antiferromagnetic interaction between Mn^{II} (through d_{xy}, and d_{yz} orbitals) and delocalized semiquinone ligand *p* orbitals. Manganese (II) has five half-filled *d* orbitals, and thus, five possible exchange pathways when complexed to ligands containing an unpaired electron. It is important to note that although the ferromagnetic interactions arising from the remaining three *d* orbitals are present, the antiferromagnetic interactions provide for extensive overlap and are much larger.

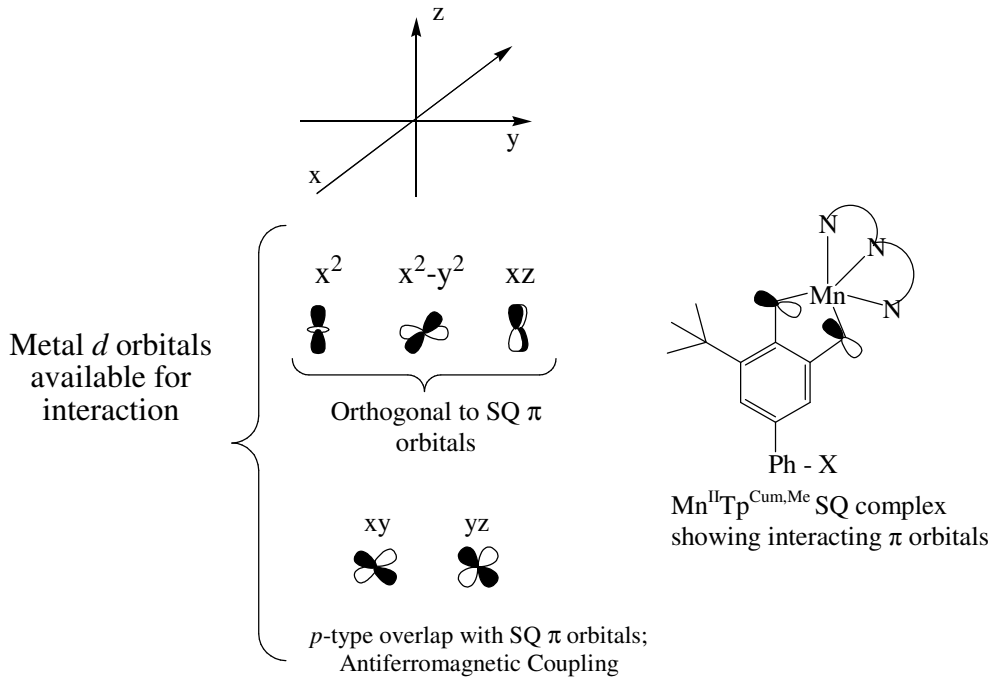

Fig. 2.10. Antiferromagnetic coupling of a metal and delocalized ligand π orbitals.

Copper (II) contains only one *d* electron, and therefore, only one exchange pathway is possible when complexed to a monoradical species. In the case of $Cu^{II}Tp^{Cum,Me}$ complexes, interactions of the delocalized ligand *p* orbitals of the semiquinone occur not with the "normal" *d* metal orbitals, but with an orbital which results from mixing the *d* orbitals. This reduces the symmetry of the complex, giving rise to net ferromagnetic coupling. The *J*-values of the series of monoradical semiquinones bearing Mn^{II} and Cu^{II} ions are shown below.

$Tp^{Cum,Me}Mn^{II}$(SQ-Ar)	*J* (cm^{-1})	$Tp^{Cum,Me}Cu^{II}$(SQ-Ar)	*J* (cm^{-1})
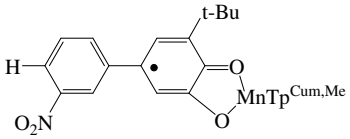	*-68.7*	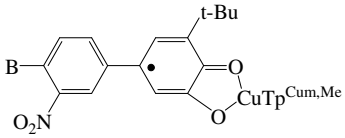	+146.2
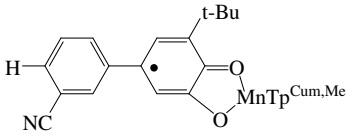	-75.4	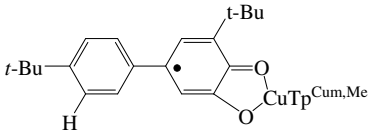	+97.9
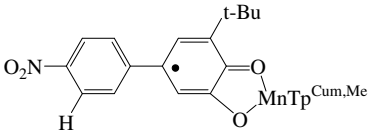	-110.4	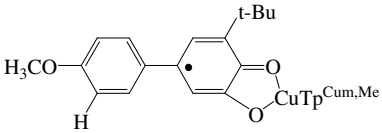	+48.7
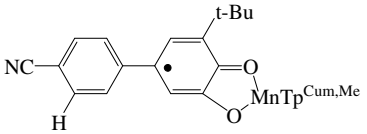	-82.2	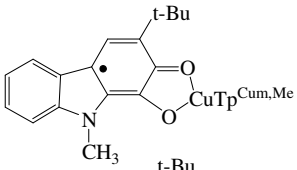	+81.5
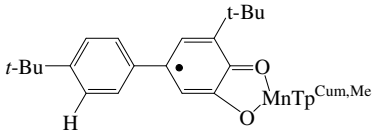	-120.0	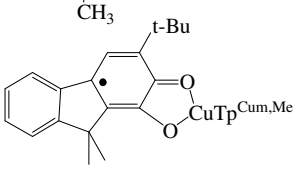	+77.6

Fig 2.11. Mn^{II} – and Cu^{II}(SQ)$Tp^{Cum,Me}$ complex exchange coupling *para*meters.[37]
2J= ΔE_{ST} J>0 FM coupling; J<0 AFM coupling.

Although there was no clear trend in the *J*-values as a function of semiquinone substituent, for the Mn^{II} complexes, for the Cu^{II} complexes, it was evident that electron-withdrawing substituents on the phenyl ring had greater ferromagnetic *J*- values than the Cu^{II} complexes of semiquinone ligands with electron-donating substituents.[40] The absence of a correlation between exchange coupling and substituents in the Mn^{II} complexes may be accounted for by considering that Mn^{II}, with its five *d* electrons, will undergo direct exchange with then semiquinone radical through five possible exchange pathways. The complexity of this exchange mechanism in $Mn^{II}(SQ)Tp^{Cum,Me}$ complexes is further complicated by the fact that each substituent will raise or lower the semiquinone SOMO energy differently, causing interactions between the metal *d* orbitals to attenuate or strengthen.

As with any substituent effect study, it is important to have several variants on which to base viable conclusions. Because of this, we thought it was important to enlarge the library of compounds that were being studied. The result of our efforts on the substituent effect in homospin biradicals is detailed in this work.

References

1. Rajca, A. *Chem. Rev.* **1994**, 94, 871.

2. Wolf, S.A. *Science.* **2001**, 294, 1488.

3. Gupta, J.A.; Knobel, R.; Samarth, N.; Awschalom, D.D. *Science* **2001**, 292, 2458.

4. Allen, G.J.; Kirschman, V.N.; Sirisathitkul, C.; Schille, J.; Gester, M.; Thompson, S.; Sparks, P.; Ounadjela, V.; Skvarla, K. J. *Magn.Magn.Mater.* **1997**, 175, 1.

5. Coey, J.M.D. *Magn.Magn.Mater*. **1999**, 197, 1.

6. Lodder, J.C.; Monsma, D.J.; Vlutters, R.; Shimatsu, T.J. *Magn.Magn.Mater*. **1999**, 199, 119.

7. Hirota, E.; Sakakima, H.; Inomata, K. Giant Magneto-Resistance Devices; Springer: New York, **2002**.

8. Clifford, K.; Robinson, A.; Miller, D.; Davis, M. *Sensors* **2005**, 5, 4.

9. Liu, R; Ke, S; Baranger, H.U.; Yang, W. *Nano. Lett* **2005**, 5, 1959.

10. Reinhoudt, D.; Crego-Calama, M. *Science* **2002**, *295*.

11. Lehn, J.M. *Science*. **1993**, 260, 5115.

12. Iwamura, H.; Inoue, K.; Hayamizu, T. *Pure and Appl. Chem.* **1996**, *68*, 243.

13. Caneschi, A.; Gatteschi, D.; Sessoli, R.; Rey, P. *Acc. Chem. Res.* **1989**, *22*, 392.

14. Gatteschi, D.; Caneschi, A.; Laugier, J.; Rey, P. *J. Am. Chem. Soc.* **1987**, *109*, 2191.

15. Silverman, S. K.; Dougherty, D. A. *J. Phys. Chem.* **1993**, *97*, 13273.

16. Shultz, D. A. *Conformational Exchange Modulation in Trimethylenemethane (TMM)-Type Biradicals*; In *Magnetic Properties of Organic Materials*; in ref Lahti, P., Ed.; Marcel Dekker, Inc.: New York, 1999.

17. Shultz, D. A.; Boal, A. K.; Lee, H.; Farmer, G. T. *J. Org. Chem.* **1999**, *64*, 4386.

18. Shultz, D. A.; Boal, A. K.; Farmer, G. T. *J. Am. Chem. Soc.* **1997**, *119*, 3846.

19. Dei, A.; Gatteschi, D.; Sangregorio, C.; Sorace, L.; Vaz, M. G. F. *Inorg. Chem.* **2003**, *42*, 1701.

20. Fujita, J.; Tanaka, M.; Suemune, H.; Koga, N.; Matsuda, K.; Iwamura, H. *J. Am. Chem. Soc.* **1996**, *118*, 9347.

21. Okada, K.; Imakura, T.; Oda, M.; Murai, H.; Baumgarten, M. *J. Am. Chem. Soc.* **1996**, *118*, 3047.

22. Adam, W.; van Barneveld, C.; Bottle, S. E.; Engert, H.; Hanson, G. R.; Harrer, H. M.; Heim, C.; Nau, W. M.; Wang, D. *J. Am. Chem. Soc.* **1996**, *118*, 3974.

23. Fang, S.; Lee, M.-S.; Hrovat, D. A.; Borden, W. T. *J. Am. Chem Soc.* **1995**, *117*, 6727.

24. Kanno, F.; Inoue, K.; Koga, N.; Iwamura, H. *J. Am. Chem. Soc.* **1993**, *115*, 847.

25. Dvolaitzky, M.; Chiarelli, R.; Rassat, A. *Angew. Chem., Int. Ed. Engl.* **1992**, *31*, 180.

26. Shultz, D. A.; Fico, R. M., Jr.; Bodnar, S. H.; Kumar, R. K.; Vostrikova, K. E.; Kampf, J. W.; Boyle, P. D. *J. Am. Chem. Soc.* **2003**, *125*, 11761-11771.

27. Shultz, D. A.; Fico, R.M.; Lee, H.; Kampf, J.W.; Pinkerton, A.A.; Boyle, P.D. *J. Am. Chem. Soc.* **2003**, *125*, 15426.

28. Shultz, D. A.; Lee, H.; Fico, R. M., Jr. *Tetrahedron* **1999**, *55*, 12079.

29. Hendrickson, D. N. *Mixed Valence Systems: Applications in Chemistry, Physics, and Biology*; Kluwer Publishing Co.: Dordrecht, The Netherlands., 1991.

30. Ward, M. D. *Chem. Soc. Rev.* **1995**, 121-134.

31. Shultz, D. A.; Kumar, R. K. *J. Am. Chem. Soc.* **2001**, *123*, 6431.

32. Bush, L. C.; Heath, R. B.; Feng, X. W.; Wang, P. A.; Maksimovic, L.; Song, A. I.; Chung, W.-S.; Berinstain, A. B.; Scaiano, J. C.; Berson, J. A. *J. Am. Chem. Soc.* **1997**, *119*, 1406.

33. Berson, J. A. *Acc. Chem. Res.* **1997**, *30*, 238.

34 Adam, W.; Borden, W. T.; Burda, C.; Foster, H.; Heidenfelder, T.; Heubes, M.; Hrovat, D. A.; Kita, F.; Lewis, S. B.; Scheutzow, D.; Wirz, J. *J. Am. Chem. Soc.* **1998**, *120*, 593.

35 West, A. P., Jr.; Silverman, S. K.; Dougherty, D. A.; *J. Am. Chem. Soc.* **1996**, *118*, 1452.

36 Geise, C. M.; Hadad, C. M. *J.Org.Chem* **2000**, *65*, 8348.

37 Mitani, M.; Yamaki, D.; Takano, Y.; Kitagawa, Y.; Yoshioka, Y.; Yamaguchi, K. *J.Chem.Phys* **2000**, *113*.

38. Shultz, D. A.; Bodnar, S. H.; Lee, H.; Kampf, J. W.; Incarvito, C. D.; Rheingold, A. L. **2002**, *124*, 10054.

39. Shultz, D. A.; Bodnar, S. H.; Vostrikova, K. E.; Kampf, J. W. *Inorg. Chem*. **2000**, *39*, 6091.

40. Shultz, D.A.; Sloop, J.; Coote, T.; Beikmohammadi, M.; Kampf, J.; Boyle, P.; *Inorg. Chem*. **2007,** *46*, 273-277.

Chapter 3. Characterization and Spectroscopy of Exchange Coupled Systems

3.1. Electron Paramagnetic Resonance (EPR) Spectroscopy

Electron Paramagnetic Resonance (EPR) is a spectroscopic technique that is used to detect unpaired electrons in a molecule. The basic role of EPR spectroscopy is identification of the chemical species being studied. Often, identification of paramagnetic species is realized solely from analysis of the EPR spectrum. In addition, EPR spectroscopy is capable of providing molecular structural details inaccessible by any other analytical tool. Hence, its use in the studies described within is invaluable.

When an atom or molecule with an unpaired electron is placed in a magnetic field, the spin of the unpaired electron can align either in the same direction or in the opposite direction as the applied field. In the absence of an external magnetic field, the energies of both α ($+\frac{1}{2}$) and β ($-\frac{1}{2}$) spin states are degenerate as shown in Figure 3.1.

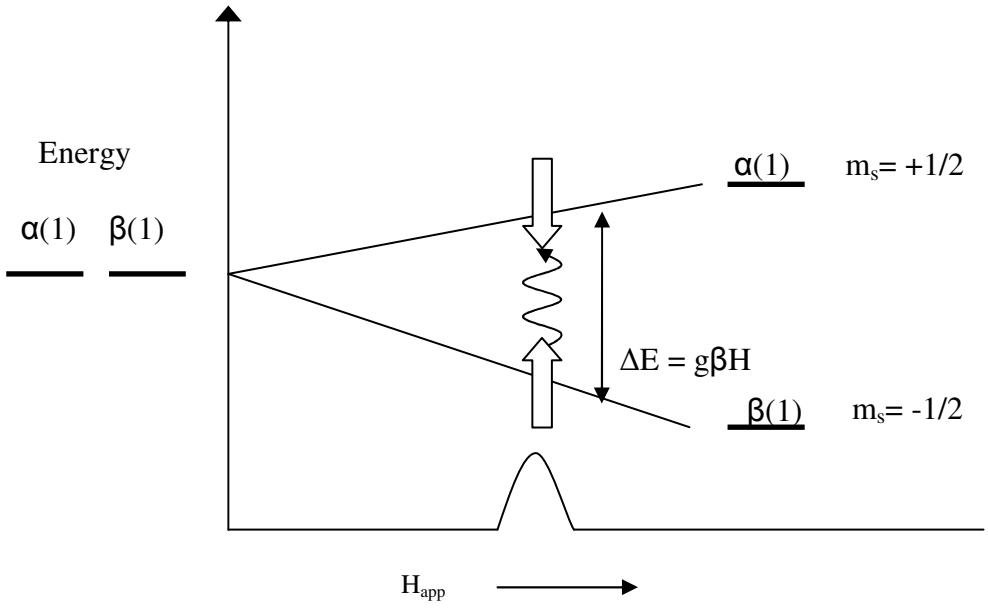

Fig. 3.1. The removal of the degeneracy of the α and β electron spin states by a magnetic field in a one-electron system.

Upon application of a magnetic field, these two electron alignments have different energies. This splitting of energies is referred to as the Zeeman Effect. The energy of each state is given by equation 3.1,

$$E = g_e \beta m_s H \qquad \textbf{eq. 3.1}$$

where g_e is the electronic g-factor of an electron (Lande's constant), β is the Bohr magneton, m_S is the spin quantum number, and H is the applied magnetic field. As is seen in the figure, the energies of the spin states diverge linearly as the magnetic field increases. The energy differences between the two spin states can be altered by varying the magnetic field strength. This sets a basis for collecting EPR spectra. The electromagnetic radiation frequency is held constant as the magnetic field is varied. A peak in the absorption occurs when the magnetic field tunes the two spin states so that their energy difference, ΔE, matches the energy of the radiation. The field at which this occurs corresponds to the resonance frequency of the electrons.

The total spin of a molecule can have 2S+1 different orientations when in a magnetic field. S is the total spin quantum number of the molecule. The 2S+1 orientations correspond to 2S+1 values of the magnetic energy. In the absence of a field there is said to be 2S+1-fold degeneracy in the energy. Magnetic degeneracy can either be lifted or abolished by external magnetic fields. A situation where the total spin due to the electrons is zero is called a singlet state because 2S+1 = 2(0)+1 = 1. A monoradical molecule has a doublet state corresponding to two magnetic energy levels, because $S = \frac{1}{2}$ and 2S+1 = 2. A biradical molecule has a triplet state and a spin multiplicity of 3, corresponding to three magnetic energy levels because S = 1. This is shown in Figure 3.2.[1]

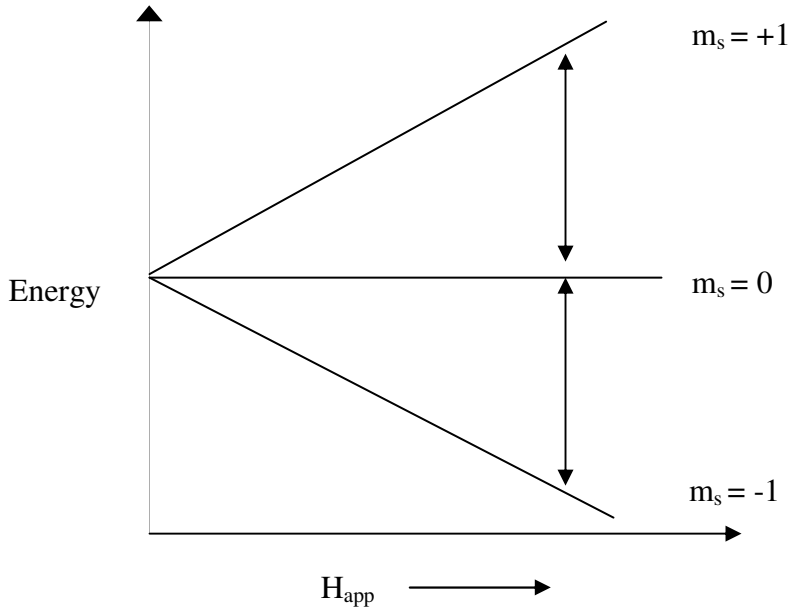

Fig. 3.2. The effect of increasing external magnetic field on the energy of a system of two *para*llel spins when the mutual interaction of the spins is neglected.

In the EPR of biradical molecules, in addition to the interaction of the magnetic moment of the molecule as a whole with the external magnetic field, the dipolar interaction of the two electron spins must also be considered.[2] From Figure 3.2, we can see that the energy of the molecules for which m_s is zero is not dependent upon the external magnetic field. The energy of the other two states increases or decreases with increased field as shown above. In this uncomplicated system, there would only be one line visible in the EPR spectrum since the difference of energy between the m_s= -1 state and the m_s 0 state is the same as the difference in energy between the m_s = 0 state and the m_s = 1 state. Also, in this case, the transition from the lowest energy level to the highest energy level is forbidden since it would be a $\Delta m_s = 2$ transition. The spins are now independent of each other so we would be flipping two independent spins with one quantum. Only if two spins are dependent can the system as a whole be "flipped" from the m_s= -1 to the m_s=1 state.

In real situations, the dipolar interaction energy is usually of the same order of magnitude as the interaction of the magnetic moment of the molecule with the laboratory field. So in a real situation, the energy levels are modified by this dipolar interaction and the distance between the lower and middle energy level is no longer the same as the difference between the middle energy level and the highest energy level. Consequently, there are two se*para*te and different lines representing the transitions between these adjacent energy levels and a three line pattern that is a result of the transition between the m_s=0 to m_s= -1, m_s= 1 to m_s= 0 and m_s= 1 to m_s = -1 states would be seen. In addition, the formerly forbidden $\Delta m_s = 2$ transition is also seen.

3.2. Zero field splitting and frozen EPR spectra of triplet molecules.

Each electron in a two electron system has its own magnetic field. These fields interact in a dipole-dipole fashion. This interaction occurs, even in the absence of an applied magnetic field, causing the triplet microstates to split, thus the term Zero Field Splitting (ZFS).[3] Dipole-dipole interactions are repulsive in nature, and to avoid the higher energy associated with the interaction of the two electrons, they prefer to be further apart. The state where the electrons are furthest apart will be lowest in energy and conversely, the state in which the electrons are closest will be highest in energy. The splitting of the triplet microstates arises, in large part, from the geometry of the molecule of interest. Figure 3.3 depicts how the geometry of the molecule affects the triplet energy states of three simplistic molecules. The *T* state is the state in which the spin axes of the two electrons have been quantized and are confined to the ***XY*** plane, resulting in a zero

spin angular momentum in the Z direction. The T_X and T_Y states are similar to the T_Z state with the appropriate axes and planes substituted.

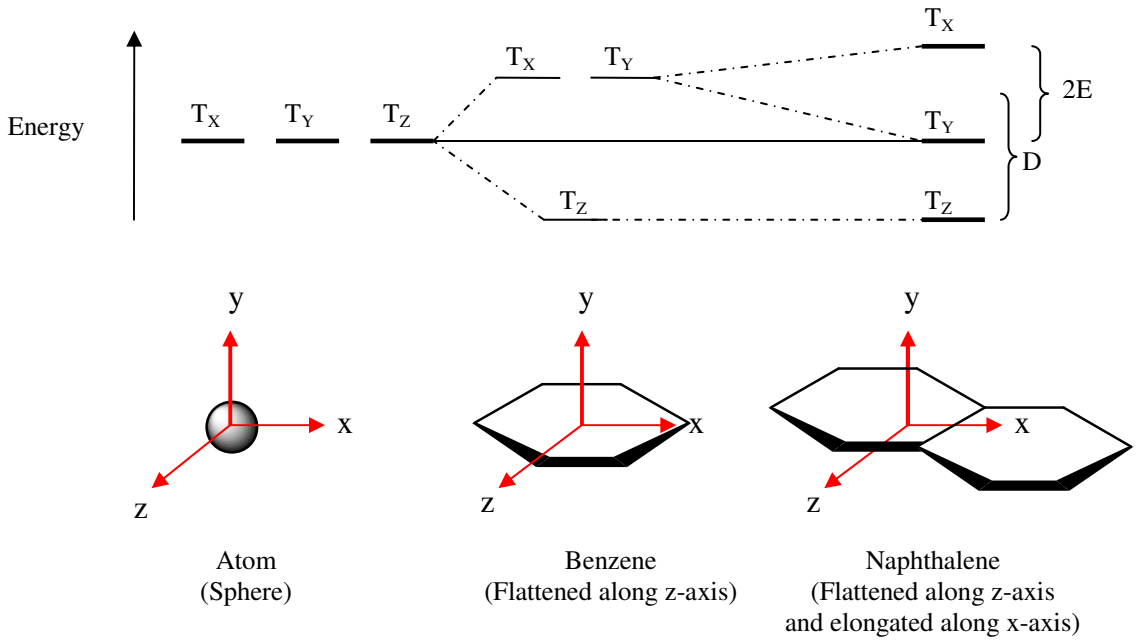

Fig 3.3. Energy se*para*tion of microstates in relation with the molecular geometry of an atom, triplet excited benzene, and triplet excited naphthalene.

Figure 3.3 depicts compression and elongation along certain axes in which the two electrons are confined to a certain plane, **XY**, **XZ**, or **YZ**. In an atom, the repulsive dipole-dipole interaction between the unpaired electrons cannot be minimized because there is no direction along which the electrons can move further apart. In benzene compression along the **Z**-axis maximizes the dipole-dipole interactions in the **XY** plane resulting in a lower energy Z state. In naphthalene, compression along the **Z**-axis and elongation along the **X**-axis maximizes dipole-dipole interaction along the **YZ** plane resulting in a splitting of the two highest energy states. The sign of the ZFS parameter **D** is dictated by the compression along the **Z**-axis, or elongation along the **Z**-axis, to yield a

positive value. Therefore, the geometrical shape of the spin distribution can be estimated from both the sign and magnitude of **D** and **E**.[1]

The three triplet species in Figure 3.3 can be characterized to have three different types of symmetry; cubic, axial, and rhombic. An atom possesses cubic symmetry (x = y = z) but ZFS is nullified by virtue of the high symmetry. For a triplet species to have axial (x = y ≠ z) symmetry the species must possess three-fold or higher rotational symmetry, and a magnetically isotropic plane perpendicular to the symmetry axis, as with benzene (D_{6h}).[1]

When a triplet species with axial symmetry is placed in an external applied field this field is aligned, for example, with the **Z**-axis of the species, and only the electrons in the **XZ**- or **YZ** planes will be split by the field. The electrons in the **XY** plane will not be affected since they are perpendicular with the applied field. With axial symmetry there are two allowed transitions but only one will be seen since they are at the same field strength. The ZFS would be dictated by the **D** parameter only (**E** = 0).

For a triplet species to have rhombic symmetry (x ≠ y ≠ z) the species must possess lower symmetry elements than a species of axial symmetry, for example naphthalene (D2h). The ZFS would be dictated by both parameters **D** and **E**. Each symmetry type will result in three distinctly different EPR spectra, where the number of signals increases as the symmetry is lowered, as shown in Figure 3.4. Each signal represents where the magnetic field is oriented along one of the axes of the system.

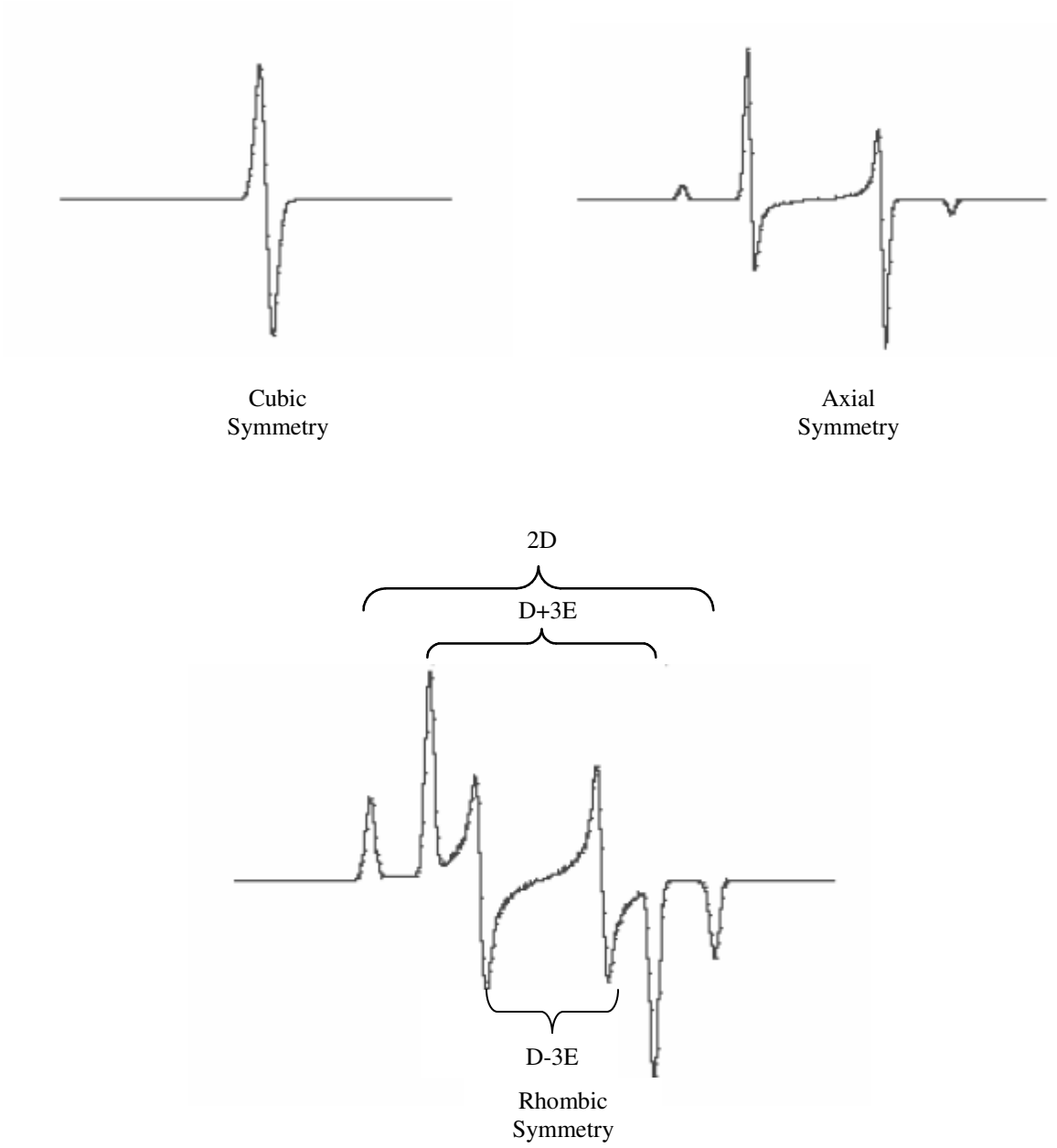

Fig 3.4. Simulated spectra for a triplet excited species with cubic symmetry (D = 0), axial symmetry (D ≠ 0; E = 0), and rhombic symmetry (D ≠ 0; E ≠ 0)

A species with axial symmetry has six allowed transitions, but as shown in Figure 3.4, there are only four. This is due to the degeneracy of two of the axes. A species with rhombic symmetry has six allowed transition and as shown in Figure 3.4, there are six displayed due to all the axes being different.[1]

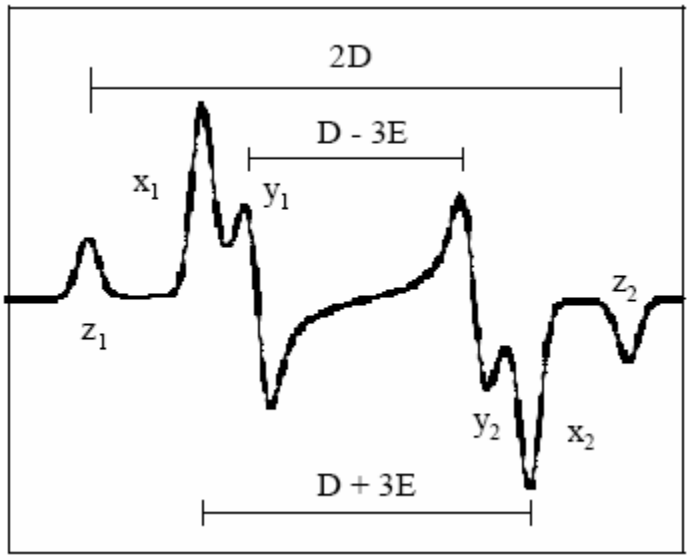

Fig 3.5. Simulated EPR spectrum for rhombic triplet from Figure 2.9. ZFS *para*meters shown.

Figure 3.5 represents a typical EPR of a bis(semiquinone) in the Shultz group. The x1 and y1 and x2 and y2 absorptions may collapse on each other, reducing the spectral complexity. It should be reiterated that the orientation of the applied magnetic field matters. In the axial example, two absorptions occur for each of the three different applied field directions, but since two of the axes are degenerate, only four absorptions are seen. In the rhombic system, again, two absorptions occur for each of the three different applied field directions. In this case, all axes are different, giving a total of six absorptions. The value of obtaining ZFS parameters for a triplet species is two-fold. First, ZFS is an indicator of the molecular geometry. Also, the dipole-dipole interaction between electrons, and thus **D**, is related to the average distance, *r*, between the electrons.[2] As this distance becomes smaller, **D** becomes larger.

$$\frac{1}{r^3} \propto D \qquad \textbf{eq. 3.1.}$$

3.3. Super Conducting Quantum Interference Device (SQUID).

In Chapter 1 it was presented that the magnetization of a material is directly proportional to the magnetic susceptibility of that material and the applied magnetic field,[4]

$$M = \chi_{exp} H \qquad \textbf{eq. 3.2}$$

The magnetic susceptibility is a constant; it is the sum of the diamagnetic and paramagnetic susceptibilities,

$$\chi_{exp} = \chi_{dia} + \chi_{para} \qquad \textbf{eq. 3.3}$$

The diamagnetic susceptibility of a material can be tabulated from Pascal's constants.[5] The paramagnetic susceptibility of a material is temperature dependent and follows the Curie Law.[6]

$$\chi_{para} = \frac{C}{T} \qquad \textbf{eq. 3.4}$$

The SQUID is the magnetometry device that is used to generate χ_{para}. SQUID magnetometry is one of the most sensitive forms of magnetometry. It uses a combination of superconducting materials and Josephson junctions to measure magnetic fields with resolutions up to ~10^{-14} kG or greater. Experimentally it requires that one place the biradical sample in a sample holder within the experimentation cavity of the instrument. The center field of the sample is then found and a saturation plot is generated. A saturation plot is the applied field vs. magnetic moment. The saturation plot is used to identify the Curie region of the biradical – the region where there is a linear relationship between applied field and magnetic moment. A sample saturation plot is shown in Figure 3.6.

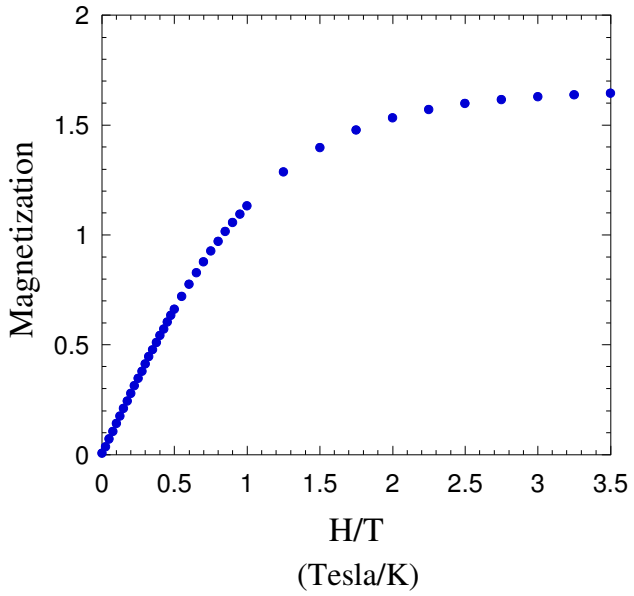

Fig 3.6. Magnetization plot showing linear Curie region.. Magnetization (μ_B) versus Applied Field/Temperature.

The Curie region indicates the field at which the experiment should be run. From the above graph, it is clear that an ideal field to run the SQUID experiment would be 10,000 Gauss. The field is held constant at 10,000G and a reversible temperature sweep is run from 2 – 300K. Parameters such as the time, field, temperature and long moment are generated.

We are primarily concerned with exchange-coupled spins. As described in Chapter 1, using the Heisenberg-Dirac-Van Vleck (HDVV) Hamiltonian the energy levels of the system can be predicted:

$$H_{12} = -2J_{12}\hat{S}_1 \cdot \hat{S}_2 \qquad \textbf{eq. 3.5}$$

By this definition, $J > 0$ denotes ferromagnetic coupling and $J < 0$ denotes antiferromagnetic coupling of spins. It is important to know the sign of the Hamiltonian, as this dictates the definition of J. If $H_{12} = -2J_{12}\hat{S}_1 \cdot \hat{S}_2$, it follows that ΔE_{ST} is equal to $2J$.

Van Vleck derived a field-independent expression relating magnetic susceptibility

and the exchange coupling parameter, J,[3,11]

$$\chi = \frac{Ng^2\mu_B^2}{3k_BT} \bullet \frac{\{\sum S(S+1)(2S+1)\, e^{Es/kT}\}}{\sum\{(2S+1)\, e^{Es/kT}\}} \qquad \textbf{eq 3.6}$$

where g is the electron g-value, μ_β is the Bohr magneton, E_S is the energy of the exchange coupled spins determined using the HDVV Hamiltonian and the other constants have their usual meaning. Substituting the energy of the singlet (S=0) and triplet (T=2J) states.

$$\chi = \frac{Ng^2\mu_B^2}{3k_BT} \bullet \frac{\{6e^{-2J/k_BT}\}}{1+3e^{-2J/k_BT}} \qquad \textbf{eq. 3.7}$$

From here, a plot of χ versus T can be generated.

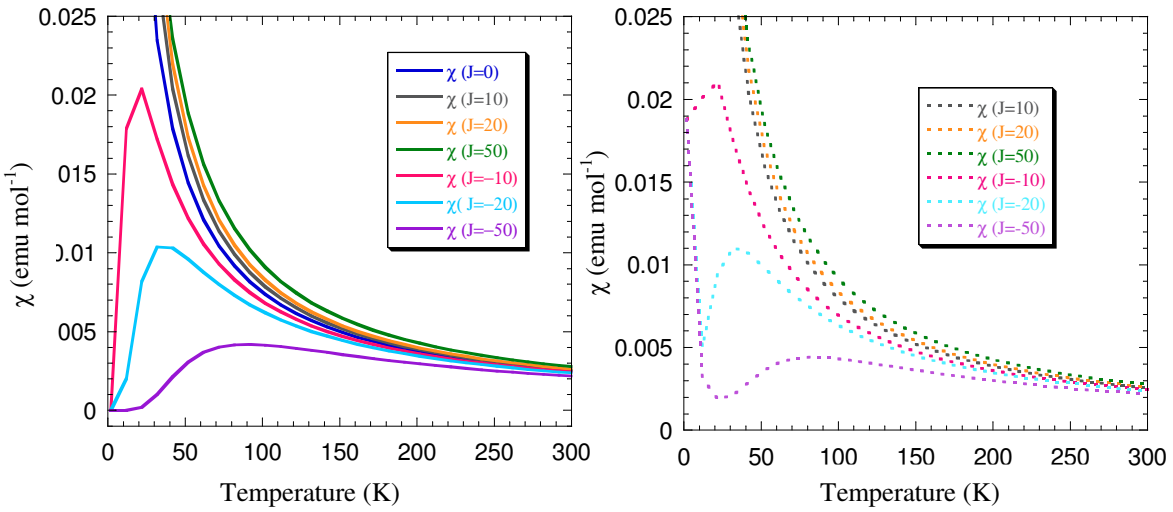

Fig. 3.7. Left Plot of χ vs. T for various ***J***-values using Eq. 3.8.
Right Plot of χ vs. T for various ***J***-values using Eq. 3.9. (with 5% monoradical impurity)

From Figure 3.6, one is able to see that there is a vast difference in the plots of ferromagnetically coupled spins versus antiferromagnetically coupled spins. More information can be *resolved* in the plots corresponding to negative *J* values. Because of this, antiferromagnetically coupled spins are typically plotted as χ vs. T, which exhibits a maximum at $T_{max} = 1.285\ J/k$.[3] Thus, a maximum in the plot of χ vs. T is characteristic of antiferromagnetic coupling. Figure 3.6 (right) is a plot of χ vs. T for a biradical with a 5% monoradical impurity. Similar to Figure 3.6 (left), there is very little difference in the plots of the ferromagnetically coupled spins. A χ vs. T for a biradical with a 5% monoradical impurity shows a sharp upturn at low temperatures. A derivative of equation 3.7 is equation 3.8 shown below.

$$\chi_T = \frac{2Ng^2\mu_B^2 T}{k_B(T-\theta)} \bullet \frac{e^{-2J/k_BT}}{1+3e^{-2J/k_BT}} \qquad \textbf{eq 3.8}$$

Equation 3.8 can be used to generate a χT vs. T plot. A sample χT plot is shown in Figure 3.8

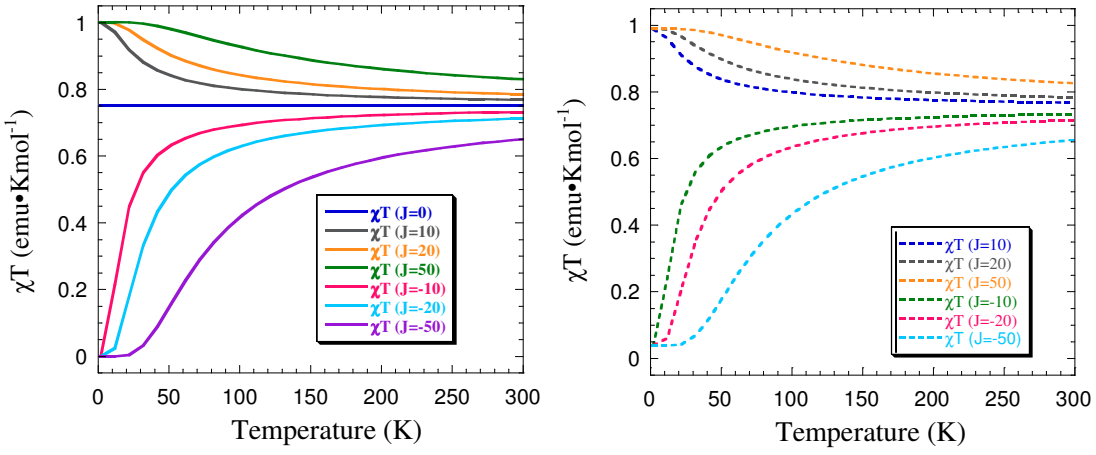

Fig. 3.8. Left. Plot of χT vs. T for various ***J***-values using eq. 3.8.
Right. Plot of χT vs. T for various ***J***-values Using Eq. 3.9. (with 5% monoradical impurity)

A χT plot is the plot of choice when ferromagnetically coupled spins are being examined. Figure 3.8 (left) shows theoretical *J*-values. Notice that in the χT plot, ferromagnetically coupled spins, (positive *J*-values) can be differentiated quite easily. Hence, the reason it is generated when ferromagnetically coupled spins are examined is simply because it provides a better visual representation. For a ferromagnetically coupled biradical, χT approaches unity at low temperatures and for spins that are antiferromagnetically coupled, χT approaches zero. Both tend towards χT = 0.75 emu•Kmol^{-1} at high temperatures, which is the expected value for two uncorrelated spins, based on the calculation:

$$\mu_{eff} = \sqrt{8\chi T} = \sqrt{n(n+2)} \qquad \textbf{eq 3.9}$$

$$\chi T = \frac{n(n+2)}{8} \qquad \textbf{eq 3.10}$$

Monoradical impurities can be observed within SQUID magnetometry data. These impurities can be modeled by adding the susceptibility of a monoradical to the field-independent Van Vleck expression, equation. 3.9, assuming that the monoradical also displays Curie like behavior.[5]

$$\chi = (1-\rho)\frac{2Ng^2\mu_B{}^2}{kT\left[3+e^{-2J/kT}\right]} + \rho\frac{Ng^2\ \mu_B{}^2}{2kT} \qquad \textbf{eq 3.11}$$

The plot of χT vs. T for a monoradical is a straight line. Figure 3.8 (right) is a plot of χT vs. T for a biradical with a 5% monoradical impurity. The effect on the χT plot is simple-ferromagnetically coupled spins approach a value below one, and antiferromagnetically coupled spins approach a value greater than zero at low temperatures.

Our primary concern is intr*a*molecular exchange coupling, but in crystalline form there can also be intermolecular exchange coupling. Intermolecular exchange coupling can be accounted for with a Weiss mean-field correction, using the expression

$$\chi_{eff} = \frac{\chi}{1-\theta\chi} \qquad \textbf{eq 3.11}$$

where $\theta = \frac{zJ'S(S+1)}{3k_B}$.[7] The origin of zJ' may be zero-field splitting, intermolecular interactions, saturation effects, or some combination of all three.[8]

References

1. Wertz, J. E.; Bolton, J. R. *Electron Spin Resonance*; Chapman and Hall:New York, **1986**.

2. Berson, M.; Baird, J.C. *An Introduction to Electron* Paramagnetic *Resonance*; W.A. Benjamin, Inc.: New York,**1966**.

3. El-Sayed, M. A. *Pure and Appl. Chem.* **1970**, *24*, 475-493.

4. Hurd, C. M. *Contemp.Phys* **1982**, *23*, 469.

5. Kahn, O. *Molecular Magnetism*; VCH: New York, **1993**.

6. Carlin, R. L. *Magnetochemistry*; Springer-Verlag: New York, **1986**.

7. Lahti, P. M. *Magnetic Properties of Organic Materials*; Marcel Dekker, Inc.: New York, **1999**.

8 Van Vleck, J. H. *The Theory of Electric and Magnetic Susceptibilities*; Oxford University Press: Oxford, **1932**.

Chapter 4. Orbital Control of Exchange Coupling by way of Substituents.

4.1. Background and Previous Work Associated with Modulation of the Singlet-Triplet Gap in Biradicals.

Much of the research done in the Shultz group has been centered on structure-property relationships of biradical molecules. In order to understand the fundamental concepts underlying the observed physical properties of biradicals, we have developed a systematic 'mode of study' within our group. It involves taking an *iso*-structural series of molecules that have one modification. In the study being reported here, that modification is that of the substituent on the ferromagnetic coupler in a series of bis(semiquinones).

Numerous studies have shown that bond torsions can modulate the energy gap between the singlet and triplet states (ΔE_{ST}) of biradicals by controlling the delocalization between spin-containing units and spin-coupling units.[1-12]. Usually, these studies discuss the angular limitations of intramolecular exchange coupling – that is the range of angles within which delocalization of spin into a ferromagnetic coupler is facilitated. On the other hand, there are only a limited number of examples where substituents have been used in alternate fashions, besides steric bulk, to alter singlet-triplet gaps.[13-19] Many of the previous studies were limited to computational work.[16-19] Dougherty carried out computational studies on the effects of substituting a pyridine ring and various pyridinium analogs for the ubiquitous *m*-phenylene coupler.[17]

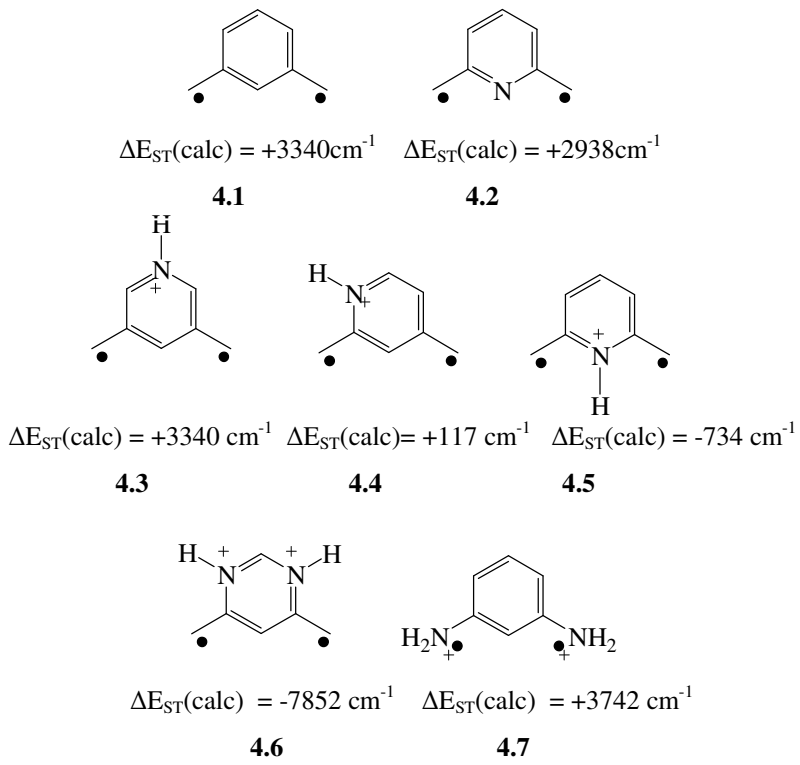

Figure 4.1. *m*-Xylylene (**4.1**) and the pyridine-based derivatives (**4.2**-**4.6**) that Dougherty studied computationally to see how the heteroatom and charges affected singlet-triplet gaps relative to **4.1** (values are in wavenumbers). $\Delta E_{ST} > 0$ = ferromagnetic ; $\Delta E_{ST} < 0$ = antiferromagnetic.

Using the pyridine coupler had a minimal effect on the singlet-triplet gap (ΔE_{ST}). However transforming a pyridine into a pyridinium ring showed significant changes in ΔE_{ST} as a function of the resonance structure, as shown in Figure 4.1. In **4.3,** the triplet is still strongly favored as the ground-state. This is not too surprising as the heteroatom is introduced at a "non-star" position where, to first order, there is no spin density in the NBMO. Compounds **4.4** and **4.5** both have the substituents at "starred" positions and should lead to significant perturbation. Compound **4.4** has singlet and triplet states that are nearly degenerate. In compound **4.5** the singlet state is the ground state.

The important feature of **4.5** is that even though it is planar, the substituent has transformed it into a weak antiferromagnetic coupling unit. It has been shown that two radicals coupled through a planar, cross-conjugate π-system result in a ferromagnetic interaction, unless the planarity is disrupted by bulky substituents.[4-9] The main reason that both **4.4** and **4.5** stabilize the singlet state preferentially is that the singlet state benefits from zwitterionic resonance structures as well as the biradical resonance structures. Since **4.5** has an additional resonance structure compared to **4.4**, its singlet state is even lower in energy relative to the triplet.

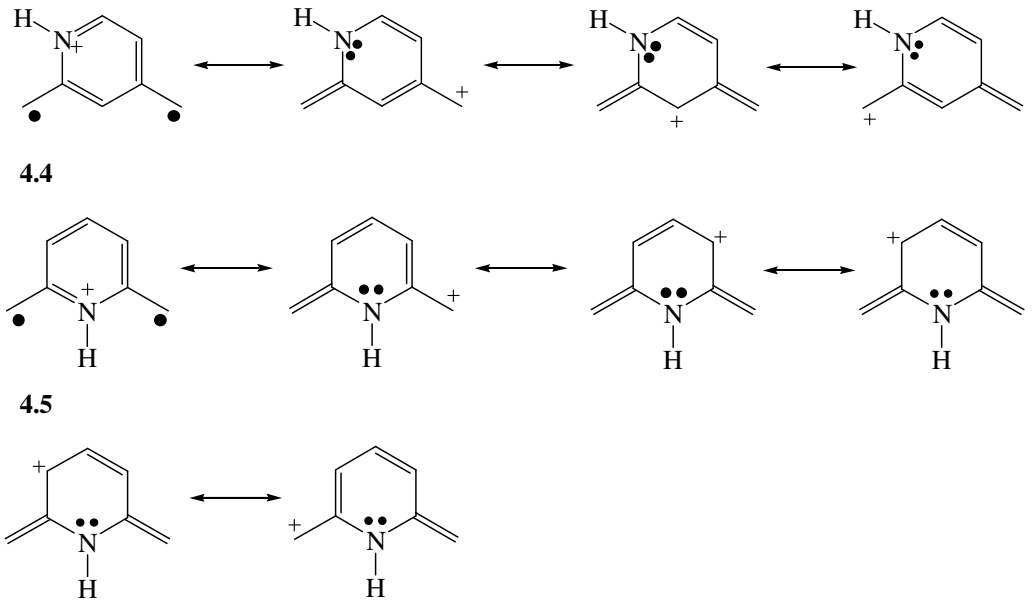

Fig. 4.2. Zwitterionic resonance structures of **4.4** and **4.5** that show why the singlet is preferentially stabilized.

Finally, **4.6** has two substituents that perturb the same NBMO and virtually leaves the other NBMO unaffected. This gives rise to a significant HOMO-LUMO gap which naturally leads to a strong preference for the singlet as the ground-state. Compound **4.7**

has substituents that interact with both NBMOs and therefore results in no significant perturbation. This results in a triplet ground-state. Experimental work was also performed that generally supported the computational work.[17]

Berson conducted a significant amount of computational studies on TME-based derivatives.[13] As can be seen in Figure 4.3, he attached various heteroatoms to see if he could effectively tune the singlet-triplet gap. TME starts with nearly degenerate NBMOs, so any perturbation is typically going to lead to an increase in stabilization of the singlet as the ground-state.

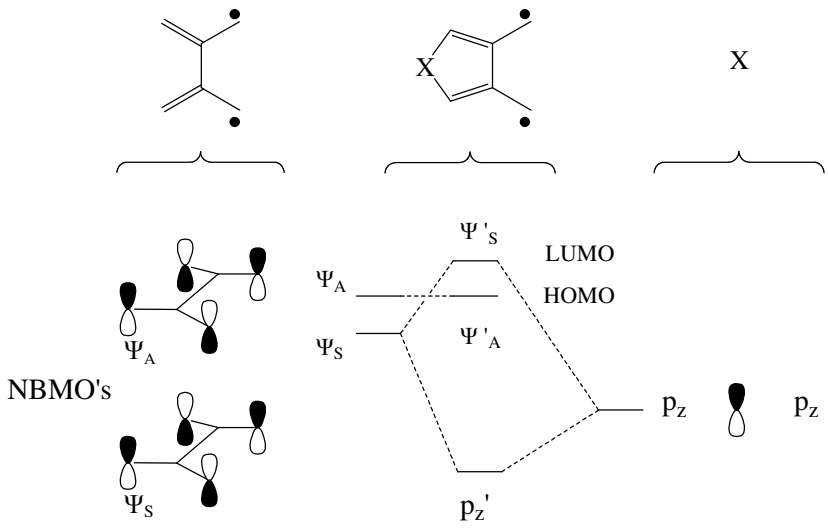

Fig. 4.3. Perturbation interaction of the filled heteroatomic p-π-orbital with the NBMOs of TME. Copyright 1997 ACS. X = O, S, NH, and many NR where R is a series of electron withdrawing groups.

The lone-pair on the X substituent can only perturb Ψ_S according to symmetry compatibility. The conclusion is that, the stronger the interaction of the p_z orbital with the Ψ_S NBMO, the stronger the stabilization of the singlet state as the ground state. This was extended further using the substituted nitrogen. The singlet-triplet gap became tunable

based on the strength of the electron-withdrawing group attached to the nitrogen. When there was only one hydrogen atom, the perturbation of orbitals was relatively significant, leading to a strong stabilization of the singlet-state. As electron withdrawing groups became stronger, effectively lowering the p_z orbital, resulted in the perturbation becoming significantly attenuated and matched the characteristics of the parent TME compound.

Finally, Hadad performed computational studies on substituted phenylcarbenes.[18] Phenylcarbenes with various substitution patterns such as *ortho*, *meta*, and *para*, were studied.

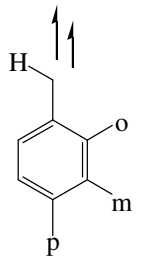

Fig. 4.4. Phenylcarbenes substituted at the *ortho*, *meta*, and *para* positions with donating and withdrawing groups ranging from NH_2, OH, OCH_3, CH_3, F, H, Cl, CF_3, CO_2CH_3, CN, CHO, NO_2.

As would be expected, substitution at the *para*-position affects the singlet-triplet gap the most. It is allowed to interact mesomerically through a direct conjugation pathway. The *ortho*-substituted carbene might be expected to have similar characteristics as the *para*; however, due to its proximity to the carbene center, complications arose. Therefore, the *ortho*-substitution pattern results will not be given in detail here. Based on examination of the EPR generated D-parameter, the carbene was determined to remain fairly localized, regardless of the substituents. This is important because it simplifies the role of the substituent as the main perturbation, rather than delocalization of the carbene into the phenyl ring. It was concluded that strong donors stabilize the singlet state and strong

withdrawers destabilize the singlet-state leading to the triplet state preferentially becoming the ground-state. In the *meta*-substituted series, strong mesomeric donors had very little effect on ΔE_{ST}. However, strong inductive withdrawing groups destabilized the singlet-state. The trends are very similar between the *para* and *ortho* substituted carbenes, however in the *ortho* series, the perturbation is not as significant. The authors conclude that both mesomeric (*para*) and inductive (*meta*) substitution lead to significant perturbations of the (ΔE_{ST}). Most of the studies conducted on tuning the singlet-triplet gap have involved species with singlet ground states. Many of these studies have been computational in nature as well. Presented in this chapter is the electronic modulation of exchange coupling within an *iso*-structural series of *m*-phenylene coupled bis(semiquinone)s with triplet ground states.

Substituents could affect ΔE_{ST} in a triplet ground-state biradical in several ways. They could alter the singlet selectively, alter the triplet selectively, or alter both states simultaneously. The substituents also could easily affect higher lying closed-shell excited states, which in turn could have influences on the lower lying open-shell states. Using a *m*-phenylene coupling unit, there are several different substitution patterns that could be employed to result in significant substituent effects.

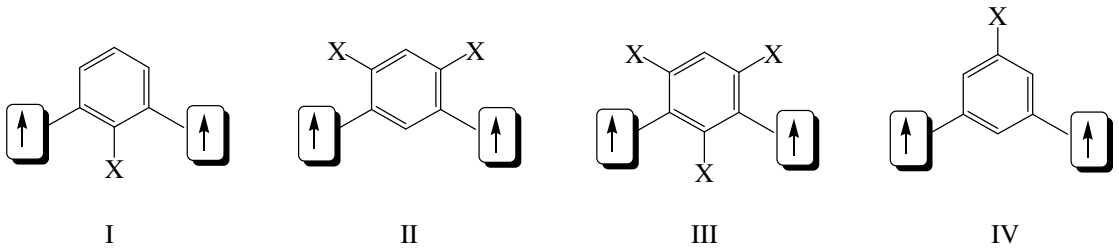

Fig. 4.5. Various substitution patterns for C*2*-symmetric *m*-phenylene type biradicals.

The substitution pattern that involves the substituent being placed at a position that would allow for mesomeric interactions with the spin-containing groups would result in the largest effect. This type of placement is seen in Figure 4.5, Cases I-III.

Case I has a substituent *ortho* to both spin-containing groups, and Case II has two substituents *ortho/para* to both spin-containing groups. Case III has three substituents mesomerically positioned, two at the *para* positions, and one in the *ortho* position. Case III would be expected to give the largest substituent effect. However, one has to consider that planarity affects delocalization of the spin-containing groups into the coupling unit and therefore exchange coupling.[1,4,7-11] Therefore, although Cases I-III, would be the choice to demonstrate significant substituent effects, their mesomeric positioning and close proximity to spin containing groups render them poor candidates for this study. Close proximity between spin-containing groups and substituents will cause significant twisting between the semiquinone and *m*-phenylene rings, and subsequently cause large attenuation of exchange coupling. In addition, it would be nearly impossible to differentiate between the effect of the substituent and the effect of the twisting.

The final case, Case IV, places the substituent in the *meta*-position relative to the spin-containing groups. Although the effect of the substituent would be limited to an inductive effect, this has been shown before to affect exchange coupling significantly.[18] Synthetic ease and feasibility also need to be considered, and Case IV provides the most facile synthetic route. Prior work on this structure-property relationship project was done by Dr. Scott Bodnar.[19] Since then, we have enlarged our library of substituents to include phenyl, proton and methoxy substituents - three functional groups whose synthesis was facile and whose chemistry would significantly lend to our previously established

molecular orbital description of the effect of substituents on exchange coupling.[19] Our current library of compounds is shown below.

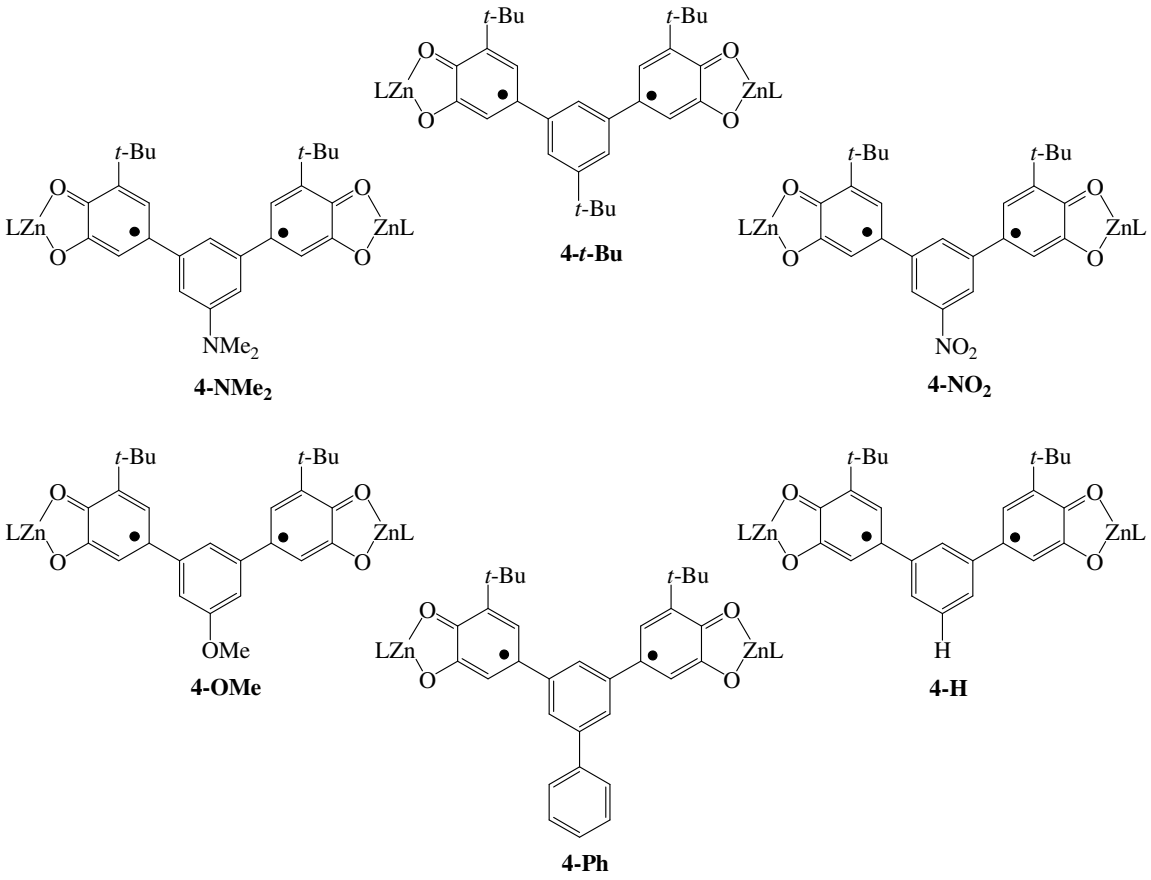

Figure 4.6. *meta*-Phenylene-type coupled bis(semiquinone)s. Note the *meta* substitution pattern relative to the spin-containing groups (semiquinones). Typical electron donors (NMe_2, OMe), electron withdrawer (NO_2), and mild donor (*t*-Bu, Ph).

4.2. Synthesis of the Bis(Semiquinone)s.

Synthesis of biradicals, **4-NMe_2**, **4-NO_2** and **4-*t*-Bu** were previously reported.[19] Once the respective aryldibromides are synthesized, the synthetic scheme becomes identical for all three species.

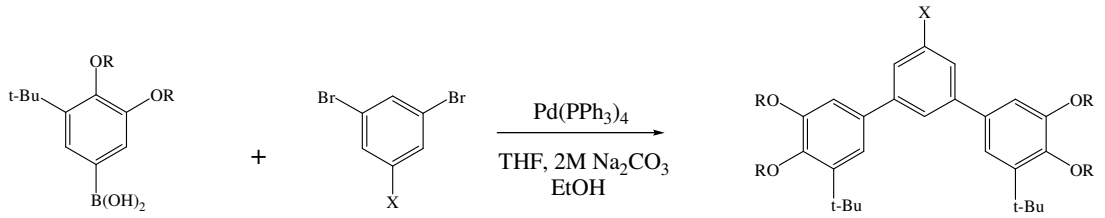

4.8

4.9 (X= Ph)
4.10 (X= H)
4.11 (X= OMe)

4.12 (X = Ph); 80%
4.13 (X = H); 88%
4.14 (X = OMe); 75%

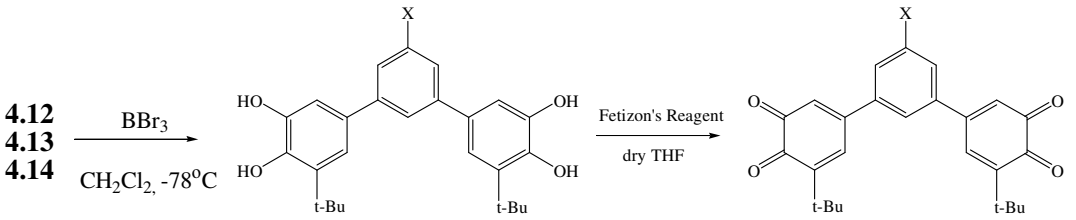

4.15 (X = Ph); 100%
4.16 (X = H); 100%
4.17 (X = OMe); 96%[a]

4.18 (X = Ph); 89%
4.19 (X = H); 90%
4.20 (X = OMe); 95%

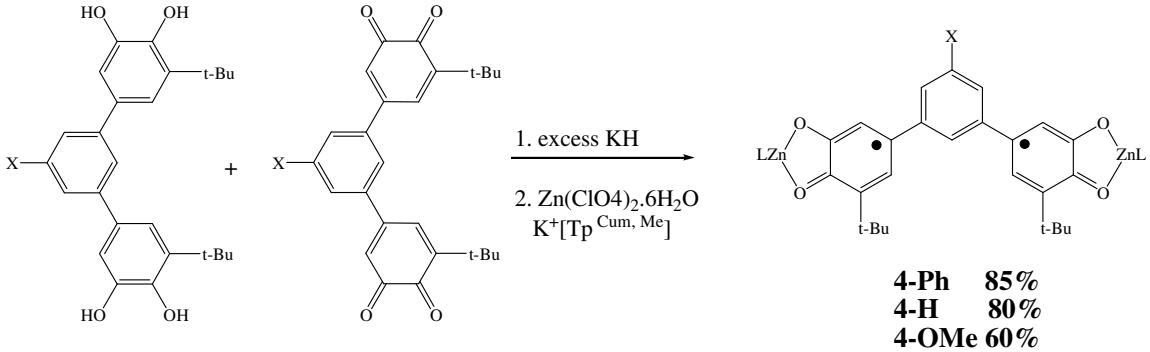

4-Ph 85%
4-H 80%
4-OMe 60%

Compound	R	X
4.12	OMe	Phenyl
4.13	OMe	H
4.14	OMOM	OMe

Scheme 4.1. Synthesis of bis(semiquinone)s **4-OMe, 4-H** and **4-Ph**, from boronic acid starting material (**4.8**) and appropriate diarylbromides (**4.9**, **4.10**, **4.11**). [a] deprotection of MOM groups require the use of MeOH and a catalytic amount of HCl.

Compound **4.8** is the precursor to the semiquinone fragment used in Shultz research.[21] Two equivalents of the boronic acid **4.8** were coupled to the three differently substituted aryldibromides via a Suzuki coupling to yield the protected bis(catechol)s **4.12-4.14**. A ten equivalent excess of boron tribromide using methylene chloride as a solvent was used to deprotect compounds **4.12** and **4.13**, while compound **4.14** was deprotected using MeOH as a solvent and a catalytic amount of concentrated HCl to give the bis(catechol)s, **4.15-4.17** in very good yields. The bis(catechol)s were then oxidized using Fetizon's reagent (Ag_2CO_3 on celite) to afford the bis(quinone)s. Subsequent comproportionation between the bis(catechol) and bis(quinone) using potassium hydride as a base gave the *in situ* bis(semiquinone) product. Complexation of the bis(semiquinone) in the presence of zinc perchlorate hexahydrate and hydrotris(3-p-isopropylphenyl-5-methylpyrazolyl)borate[22] resulted in the formation of the olive green biradical in each case.

4.3. Results and Discussion of Substituent Effect Modulation of Singlet-Triplet Gap in Triplet-State Bis(Semiquinone)s.

We now have six molecules in our bis(semiquinone) series with which to compare the effect of substituents on exchange coupling. The results of our findings are in stark contrast to our initial hypothesis. Semiquinones are radical anions. Strong electron withdrawers should pull both the electron and spin density into the middle coupling *m*-phenylene ring. The result of this would be an increase in the communication between the radical centers and subsequently, stronger exchange coupling. However, upon characterization of our library of semiquinones, this hypothesis was not able to be

confirmed. We have developed and reported an explanation of our findings based on Hückel MO theory that persists for all of the molecules under study.[23]

The frozen solution (77K) EPR spectra are seen in Figure 4.7. The miniaturized spectra show the presence of a $\Delta m_s = 2$ transition – a fingerprint that indicates the presence of triplet states - for all of the complexes. We initially had hoped to see differences in the zero-field splitting parameters for all three bis(semiquinone)s. This would be an indication that the substituents were affecting the spin-density distribution. If they were indeed different, we would expect the exchange coupling to be different as well. As can be seen in Figure 4.7, all the EPR spectra are very similar and there are no significant differences in zero-field splitting.

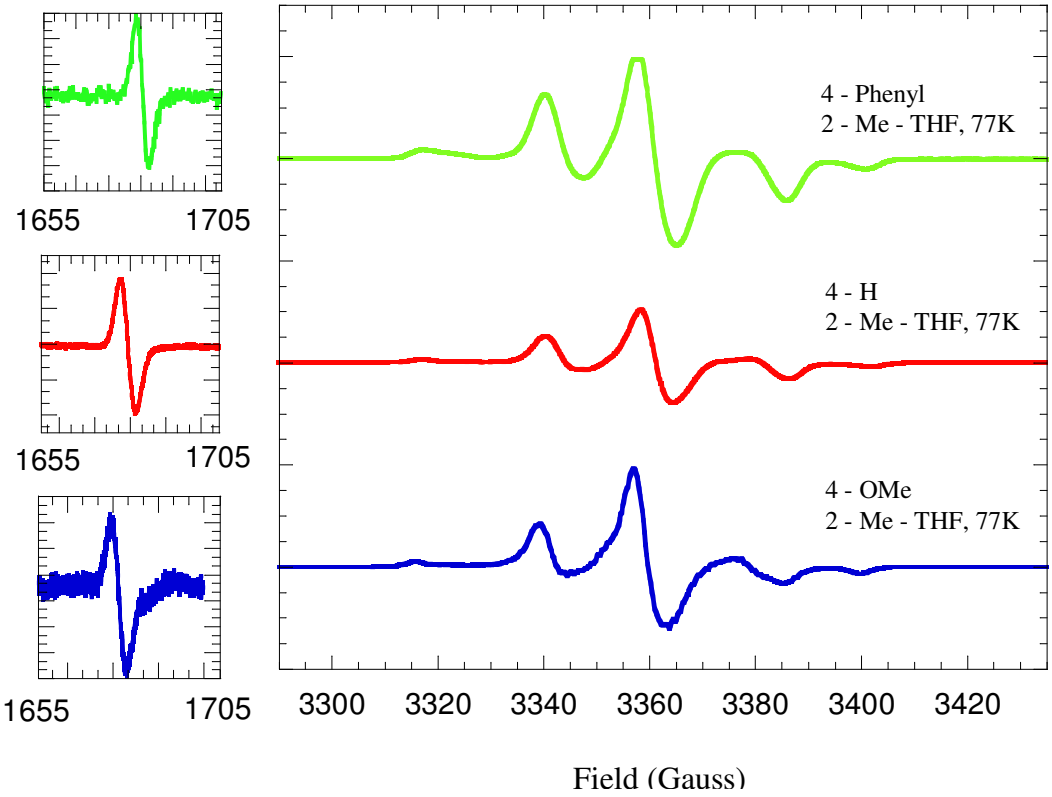

Figure 4.7. EPR spectra of **4-Phenyl**, **4-H**, **4-OMe** taken at 77K in 2-Me-THF. The zero-field splitting *para*meters were estimated by simulations: **4-Phenyl**, $|D/hc| = 0.00364$ cm^{-1}, $|E/hc| = 0.000183$ cm^{-1}; **4-H**, $|D/hc| = 0.00392$cm^{-1}, $|E/hc| = 0.000224$ cm^{-1}; **4-OMe**, $|D/hc| = 0.00378$ cm^{-1}, $|E/hc| = 0.000122$ cm^{-1}. The miniaturized spectra are the $\Delta m_s = 2$ transitions indicating the presence of a triplet state in all of the bis(semiquinone)s.

The zero-field parameters estimated by simulation were as follows: **4-Phenyl**, $|D/hc|$ = 0.00364 cm^{-1}, $|E/hc|$ = 0.000183 cm^{-1}; **4-H**, $|D/hc|$ = 0.00392cm^{-1}, $|E/hc|$ = 0.000224 cm^{-1}; **4-OMe**, $|D/hc|$ = 0.00378 cm^{-1} $|E/hc|$ = 0.000122 cm^{-1}. The similarity in zero-field splitting parameters leads us to conclude that the spin densities for all three complexes are nearly identical.

The crystal structures of two of the three complexes were resolved. The ORTEP representation of each complex is seen below in Figure 4.8. Attempts to crystallize complex **4-OMe** were futile. Because the magnetic data collected for complex **4-OMe** is within range of our previous and current findings, we do not believe that omitting the crystal structure will compromise our conclusions.

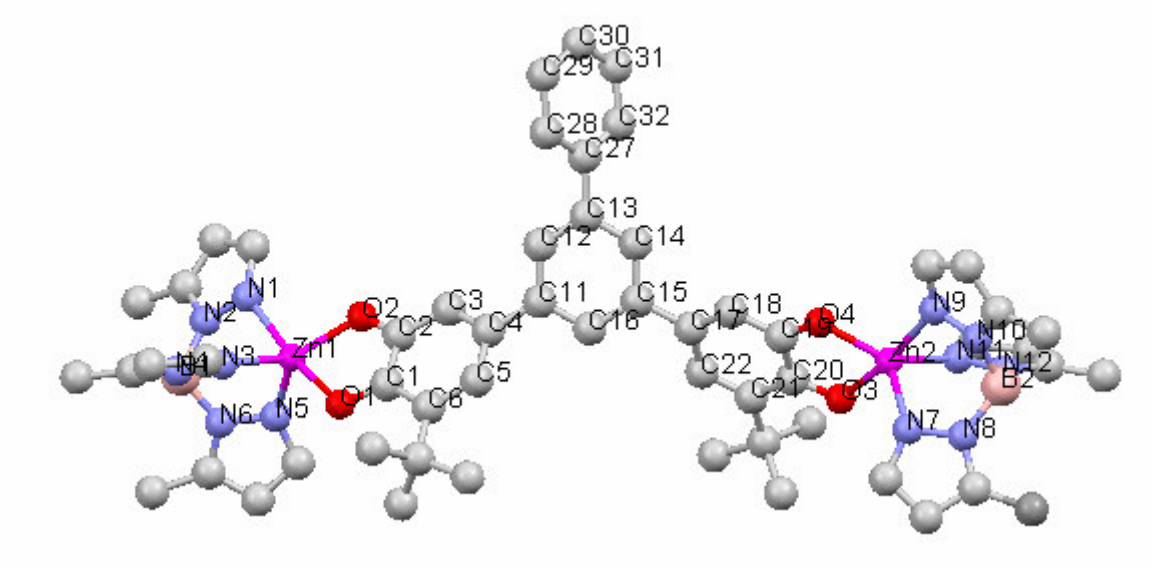

4-Phenyl

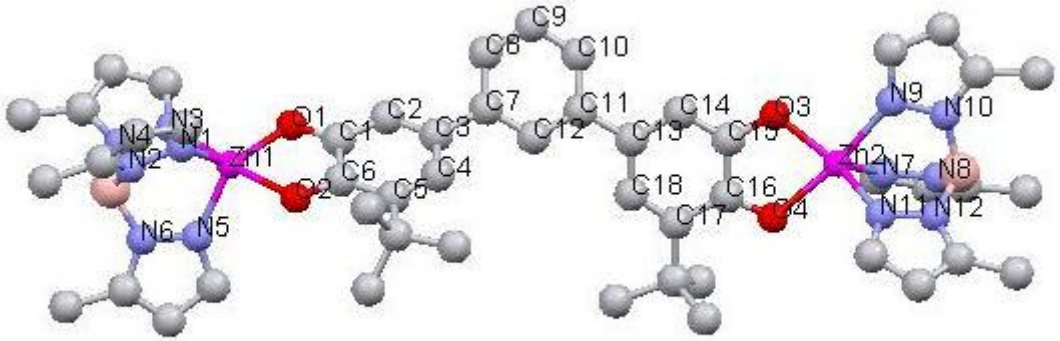

4-H

Figure 4.8 ORTEP representations of the crystal structures of **4-Phenyl and 4-H.** Thermal ellipsoids are drawn at the 50% probability level. Cumenyl groups and hydrogens are excluded for clarity.

Important bond lengths of the **4-Phenyl** and **4-H** complexes are given in Table 4.1.

Table 4.1 Bond lengths for **4-Phenyl and 4-H**.

Biradical	**Bond**	**Length (Å)**	**Bond**	**Length (Å)**
4-Phenyl	C1-O1	1.263(7)	C19-O4	1.284(6)
SQ-rings	C2-O2	1.290(6)	C20-O3	1.281(6)
	C1-C2	1.479(7)	C20-C19	1.462(7)
	C2-C3	1.391(7)	C19-C18	1.401(7)
	C3-C4	1.370(7)	C18-C17	1.372(7)
	C4-C5	1.442(8)	C17-C22	1.433(8)
	C5-C6	1.378(8)	C22-C21	1.372(8)
	C6-C1	1.436(7)	C21-C20	1.434(7)
SQ-phenylene	C4-C11	1.480(8)	C17-C15	1.489(8)
m-phenylene-ring	C11-C12	1.401(8)	C14-C15	1.416(7)
	C12-C13	1.365(9)	C15-C16	1.367(8)
	C13-C14	1.402(9)	C16-C11	1.402(8))
Metal bonds	Zn1-O1	2.177(3)	Zn2-O3	2.123(3)
	Zn1-O2	1.990(3)	Zn2-O4	1.985(3)
	Zn1-N1	2.148(4)	Zn2-N7	2.046(4)
	Zn1-N3	2.066(4)	Zn2-N9	2.155(4)
	Zn1-N5	2.040(4)	Zn2-N11	2.059(4)
Biradical	**Bond**	**Length (Å)**	**Bond**	**Length (Å)**
4-H	C1-O1	1.294(6)	C15-O3	1.302(6)
SQ-rings	C6-O2	1.272(6)	C16-O4	1.279(6)
	C6-C1	1.449(7)	C16-C15	1.459(7)
	C1-C2	1.411(7)	C15-C14	1.404(7)
	C2-C3	1.377(7)	C14-C13	1.379(7)
	C3-C4	1.415(7)	C13-C18	1.425(7)
	C4-C5	1.369(7)	C18-C17	1.354(7)
	C5-C6	1.4547)	C17-C16	1.434(7)
SQ-phenylene	C3-C7	1.481(7)	C11-C13	1.486(7)
m-phenylene-ring	C7-C8	1.386(7)	C11-C12	1.403(7)
	C8-C9	1.389(7)	C12-C7	1.395(7)
	C9-C10	1.399(8)		
	C10-C11	1.397(8)		
Metal bonds	Zn1-O1	1.958(4)	Zn2-O3	1.9759(3)
	Zn1-O2	2.140(3)	Zn2-O4	2.125(4)
	Zn1-N1	2.0554)	Zn2-N7	2.037(4)
	Zn1-N3	2.169(4)	Zn2-N9	2.149(5)
	Zn1-N5	2.027(4)	Zn2-N11	2.041(5)

A significant and useful measure to compare the deviation in bond length between a reference and an unknown compound is the structural deviation factor: $\Sigma|\Delta_i|$. The bond lengths of interest are the semiquinone ring bonds that we have chosen to compare to Pierpont's (3,5-DBSQ) semiquinone seen in Figure 4.9.

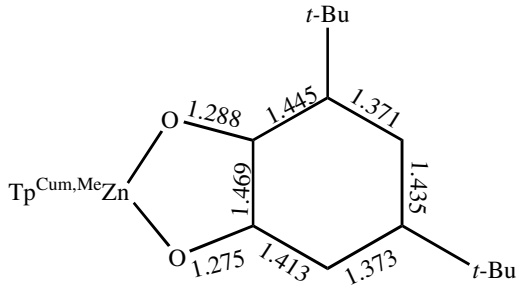

Fig 4.9. (3,5-DBSQ)Semiquinone synthesized by Pierpont being used as a reference.[24]

If the bond lengths are similar to the reference, then the dioxolene ring has "normal" semiquinone character. However, large deviations could indicate that the dioxolene is of a different oxidation state or that the dioxolene ring is a semiquinone that is delocalized into other parts of the compound, effectively lessening its "normal" semiquinone character. If the amount of delocalization of the semiquinone is large, the structural deviation will be large. Conversely, if the amount of delocalization of the semiquinone is small, the structural deviation will be small.

Eight bonds are used in the comparison between our synthesized complexes and the "reference" complex. These bonds are: all six dioxolene ring bonds, as well as the two bonds from the dioxolene ring to the two oxygens. The structural deviation parameters are shown in Table 4.2. Pierpont's complex (Fig 4.11) was chosen because of several similarities between its molecular construct and our bis(semiquinones): (1) the semiquinone ring has the same substitution pattern as all of our complexes, (2) it contains

Zn^{II} as the metal ion, as do all the complexes to which we intend to apply the structural deviation factor, (3) it contains the same ancillary ligand ($Tp^{Cum,Me}$) as our complexes, (4) it represents a "pure" semiquinone, in that, there is no delocalization of the semiquinone into the substituents (two *t*-Bu groups).

The structural deviation parameter is a *qualitative* measure between similar complexes, and as such, whole scientific merit can not be given to its meaning. The reason for this is that there are numerous factors that affect the bond lengths of a crystalline lattice. Variations can occur in the quality of the crystal data collection and the related standard deviations of bond lengths. Other factors that preclude obtaining a completely symmetric molecule are ring torsions and crystal packing forces. The structural deviation parameter is therefore best used as a trend identifier between related complexes rather than an absolute comparison technique.

Table 4.2 Structure Deviation Parameters ($\Sigma|\Delta_i|$) (Å) for **4-Phenyl**, **4-H**, **4-NMe_2**, **4-NO_2** and **4-*t*-Bu**

Biradical	Ring with O1 (Å)	Ring with O2 (Å)	Avg. Deviation (Å)
4-Phenyl	0.114	0.086	0.1000
4-H	0.134	0.127	0.1305
4- NMe_2	0.266	0.103	0.1845
4-*t*-Bu	0.175	0.154	0.1645
4- NO_2	0.102	0.151	0.1265

The semiquinone rings of all of the complexes are similar to Pierpont's reference molecule. The complex with the largest structural deviation is **4-NMe_2**. The data suggests that the strongly electron donating NMe_2 substituent is more delocalized into the semiquinone ring than its NO_2 counterpart. Based on our original hypothesis, we thought we would see the most delocalization in the **4-NO_2** complex, and thus the largest structural deviation. This trend should be taken lightly however, as all of the values are

fairly close, the errors involved are relatively large, and the difference may not be as significant as they appear.

The bonds that deviated the most significantly from the "typical" semiquinone were the bonds of the carbons attached to the oxygens to the contiguous carbons within the ring. These two bonds in each of the semiquinone rings contributed a large component of the deviation from the "typical" semiquinone. Most of the other bonds matched very well to the compared semiquinone. This large deviation may be caused by the *m*-phenylene coupling unit. It is an aromatic ring and may affect the delocalization of the semiquinone rings significantly.

The other very critical structural data is the torsion angles of the semiquinone rings in relation to the *m*-phenylene ring. It is important that these torsion angles be identical, or nearly so, so that the effect of degree of planarity can be ruled out as a variable that affects the exchange coupling. This allows us to attribute any differences in exchange coupling to the effect of the substituent and not the combination of the substituent and bond torsions. Table 4.3 shows the torsion angles of the semiquinone rings in relation to the *m*-phenylene rings of the complexes: **4-Phenyl , 4-H, 4-NMe2, 4-*t*-Bu**, and **4-NO2**.

Table 4.3. Semiquinone Torsion Angles[a] for **4-Phenyl, 4-H, 4-NMe_2, 4-*t*-Bu**, and **4-NO_2**.

Biradical	Semiquinone Ring Torsion angles (deg)	Average Semiquinone Ring Torsion Angles (deg)
4-Phenyl	40.5 ± 0.4, 42.3 ± 0.5	41.4 ± 0.5
4-H	42.7 ± 0.3, 27.2 ± 0.4	35.0 ± 0.4
4-NMe_2	36.0 ± 0.5, 31.0 ± 0.5	33.5 ± 0.5
4-NO_2	33.3 ± 0.3, 33.5 ± 0.4	30.5 ± 0.4
4-t-Bu	30.2 ± 0.3, 30.8 ± 0.4	33.4 ± 0.4

[a] The torsion angle is defined as the angle between the plane of a semiquinone ring and the plane of the central phenylene ring.

Table 4.3 shows that the torsion angles of all the semiquinone rings are nearly identical. The average semiquinone ring torsion is 34.8° ± 2.0° relative to the central *m*-phenylene ring. We feel that the range of torsion angles (only 12º) is not significant enough to have a measurable effect on the exchange coupling. This hypothesis is supported by the magnetic data, which will be discussed next.

The magnetic saturation plots of **4-Phenyl, 4-OMe**, and **4-H** were measured at 2K and the field strength was swept from 0 Tesla to 5 Tesla using a SQUID magnetometer. The saturation plots for the other complexes had been measured and reported previously.[19]

Because there is no significant difference in the plots, they are not being shown here. The results of saturation plots for the three most recently synthesized biradicals are seen in Figure 4.12. The theoretical maximum of magnetization for S = 1 at H/T = 2.5 Tesla/K is 1.55 μ_B. The higher experimental value could be due to saturation effects. Although, this value is slightly high, the data for all three complexes approaches a saturation value of $2_{\mu B}$ that is consistent with species that have an S = 1 ground-state at 2K. As the field increases, a deviation from linearity can be seen in Figure 4.10 at approximately 0.5 μ_B (1 Tesla). This is therefore the chosen field strength to perform the susceptibility studies.

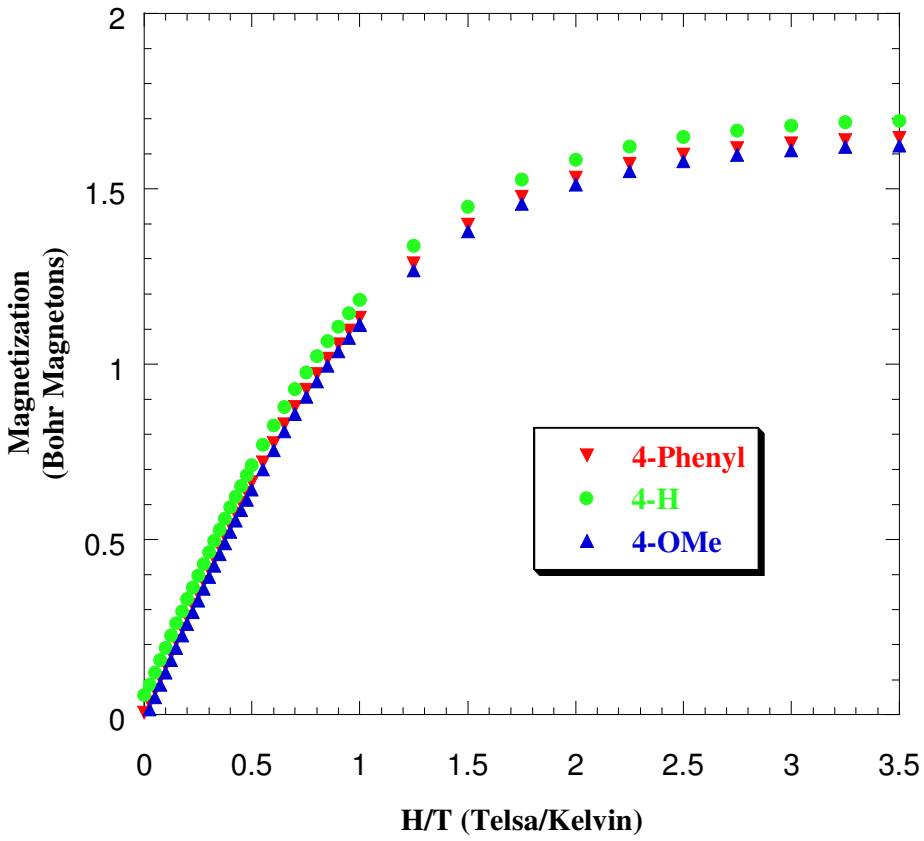

Fig. 4.10. Magnetization plots at 2K for **4-Phenyl, 4-H**, and **4-OMe**. Theoretical magnetization for S=1 @ H/T = 3.5 is 1.55 μ_B.

The magnetic susceptibilities of **4-Phenyl, 4-H** and **4-OMe** were measured from 2 to 300K using an applied field strength of 1 Tesla. As a means of comparison, the susceptibilities for all six complexes are plotted as χT products and are seen in Figure 4.11.

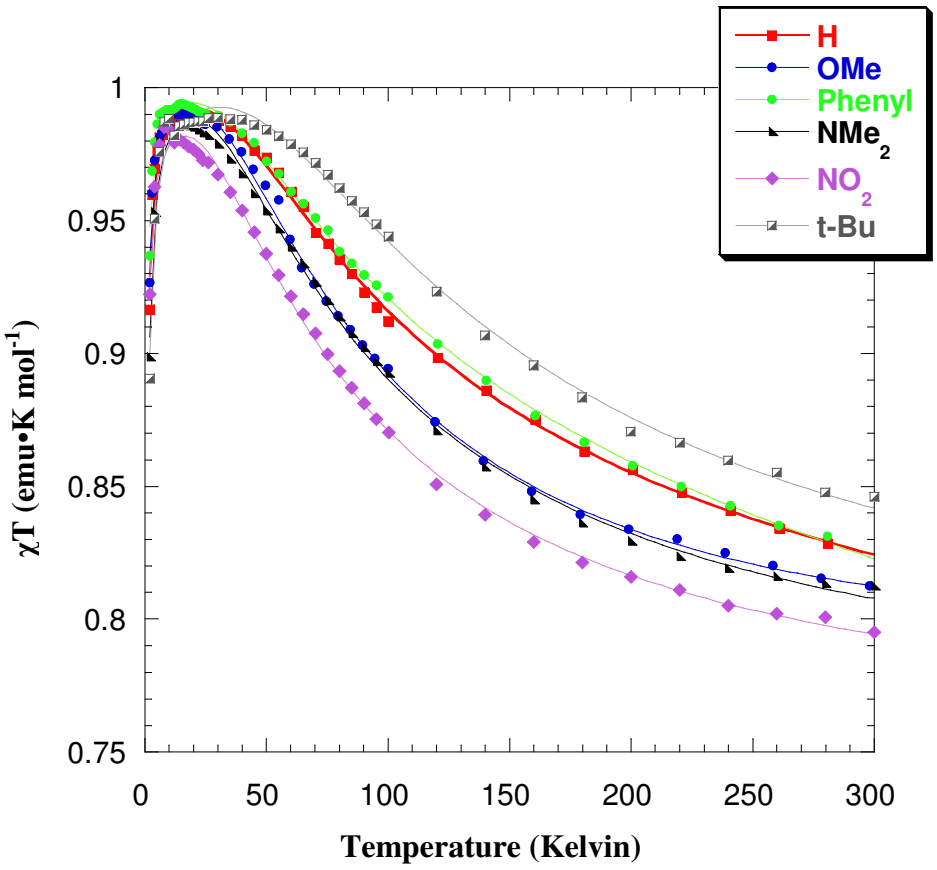

Fig. 4.11. Temperature dependence of χT for bis(semiquinone) complexes **4-NMe$_2$, 4-t-Bu 4-NO$_2$, 4-OMe, 4-Phenyl and 4-H.**

The χT values for all six complexes at room temperature are greater than the value for two uncorrelated spins (χT = 0.75 emu•K•mol^{-1}), which is consistent with intramolecular ferromagnetic exchange interactions. As the temperature decreases from 300K, the values of χT for all six complexes increases, also indicating that the triplet is the ground-state and that a ferromagnetic interaction is present. The strength of exchange coupling can be determined by fitting the magnetic data to a field-independent van Vleck expression (using $H = -2J\hat{S}_1 \cdot \hat{S}_2$), Equation 4.1,[25,26]

$$\chi T = \frac{2Ng^2\beta^2}{k\left[3 + e^{-2J/kT}\right]} \qquad \textbf{eq. 4.1}$$

where g is the isotropic Landé constant (g = 2.0023), μ_B is the Bohr magneton, T is the temperature in Kelvin, k is Boltzmann's constant, J is the intramolecular exchange coupling parameter ($2J = \Delta E_{ST}$), and $\hat{S}_1$ and $\hat{S}_2$ are the spin operators for the semiquinones. The decrease of the χT value at very low temperatures (below 5K) is typical and was accounted for with a Weiss correction, using the expression $\chi_{eff} = \chi/(1 - \vartheta\chi)$, where $\vartheta = 2z J'/(Ng^2\beta^2)$.[29] The origin of J' can be zero-field splitting, intermolecular interactions, saturation effects, or some combination of these.[30] The curve fit results are seen in Table 4.4.

Table 4.4 χT Variable Temperature Susceptibility Fit Parameters for **4-Phenyl, 4-H , 4-OMe 4-NMe_2, 4-*t*-Bu**, and **4-NO_2**.[a]

Biradical	J (cm^{-1})[b]	zJ' (cm^{-1})[c]
4-Phenyl	+ 41.5 ± 0.7	- 0.17 ± 0.01
4-H	+ 42.1 ± 0.6	- 0.19 ± 0.01
4-OMe	+ 36.8 ± 0.5	- 0.13 ± 0.01
4-NMe_2	+ 34.9 ± 0.7	- 0.11 ± 0.01
4-t-Bu	+ 59.3 ± 0.2	- 0.11 ± 0.01
4-NO_2	+ 31.0 ± 0.6	- 0.07 ± 0.01

[a] The fits used g = 2.002. [b] $J > 0$ for the triplet ground-state. [c] Intermolecular interaction term.

Based on all of the characterization data of the six complexes, **4-Phenyl, 4-H, 4-OMe**, **4-NMe_2, 4-*t*-Bu,** and **4-NO_2**, there is an effect on the exchange coupling due to the different substituents. The small zJ' values are consistent with weak intermolecular interactions which become apparent only at very low temperatures. This conclusion is strongly grounded in the very similar structural data from the crystal structures showing only a small variation in torsion angles of the semiquinone rings relative to the *m*-phenylene ring. Although we have enlarged our library of compounds, we do not see a clear trend from either donor to withdrawer or *vice versa.* However, we can infer from

the magnetic data that strong electron π-donors *and* π-withdrawers (**4-OMe**, **4-NMe$_2$** and **4-NO$_2$**) attenuate exchange coupling relative to the unsubstituted complex, **4-H**, while, weak inductively donating groups (**4-Phenyl**) attenuate exchange coupling less.

Prior to synthesizing the three additional bis(semiquinones), **4-Phenyl, 4-H** and **4-OMe,** we had used **4-*t*-Bu** as a reference molecule to compare our substituted complexes. However, now that we have enlarged our library of compounds to include the unsubstituted bis(semiquinone), **4-H**, barring any contribution to exchange coupling other than the electronic effect of these substituents, **4-H** seems like a better "reference" molecule. As a result of this change, it now seems as if the weak inductive donor, **4-*t*-Bu** exhibits anomalous behavior.

We cannot be certain of the effect of the small differences in torsion angles, but it seems reasonable that ***J*** should vary as $\cos^2(\phi)$, where ϕ is the torsion angle between the spin-containing unit (semiquinones in this case) and the spin coupling unit (*m*-phenylene ring in this case). The range of *average* torsion angles is from 30° to 43°, giving $\cos^2(\phi)$ values of 0.75 and 0.56 respectively. This small difference in $\cos^2(\phi)$ values may have an effect on the exchange coupling, but we feel that it is not significant to result in the differences seen in Table 4.4. Therefore, we feel confident that the differences seen in exchange coupling amongst all the complexes are due to the substituent.

4.4. Proposed Mechanism of Substituent Modulation of Exchange Coupling.

An accurate calculation of the exchange coupling parameter using MO theory must include configuration interactions.[25] This consists of the antiferromagnetic component of the exchange coupling that arises from interaction with low lying excited states. However, MO theory alone can give a reasonable qualitative description of the magnitude of the ferromagnetic contribution to the overall exchange parameter.[11,16, 23]

Using Hückel MO theory coupled with simple perturbation theory can give a reasonable explanation for the substituent effect on the exchange coupling seen in this work. If we look at the attachment of the a_2 and b_2 symmetry-adapted linear combinations (SALCs) for the CH_2 radical fragments (Figure 4.12; right) and how they interact with the $1a_2/2a_2$ and $2b_2/3b_2$ frontier MOs of benzene (Figure 4.12; left) (formally e_{1g} and e_{2u} for D_{6h} symmetry), we see how the *m*-xylylene SOMOs (Figure 4.12; middle) can be constructed. The *m*-xylylene SOMOs have been discussed previously in Chapter 1 under disjoint and non-disjoint SOMOs.

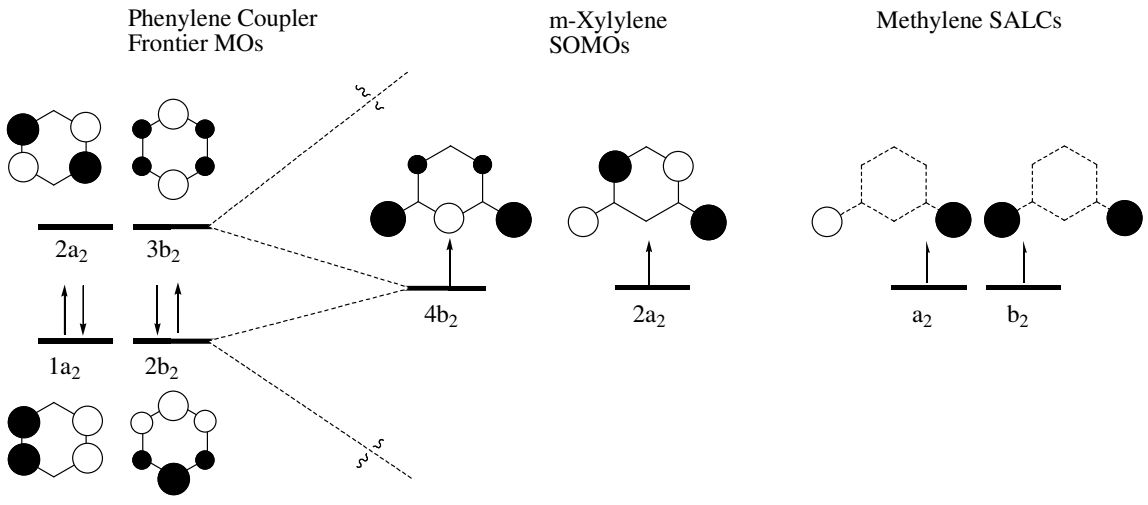

Fig. 4.12 Construction of *m*-Xylylene SOMOs using group theory as a guide.

Because of the pairing theorem,[27] each set of interactions between the methylene SALCs and the frontier MOs of benzene are equal in magnitude, resulting in two accidentally degenerate SOMOs, $4b_2$ and $2a_2$.

If a mesomeric substituent is attached to the benzene ring, the $2b_2/3b_2$ MOs will mix with the substituent AO, but the $1a_2/2a_2$ will not interact with the substituent AO because the attachment is at nodal positions in these MOs (Figure 4.13; left). If the newly formed benzyl coupler frontier MOs (Figure 4.13; left) are interacted with the a_2 and b_2 SALCs of the CH_2 radical fragments, the interaction of the a_2 CH_2-SALC will be identical to that in *m*-Xylylene, but the interaction of the b_2 CH_2-SALC will be attenuated because of the larger energy gap between the b_2 CH_2-SALC and the benzyl $2b_2$ and $4b_2$ MOs.

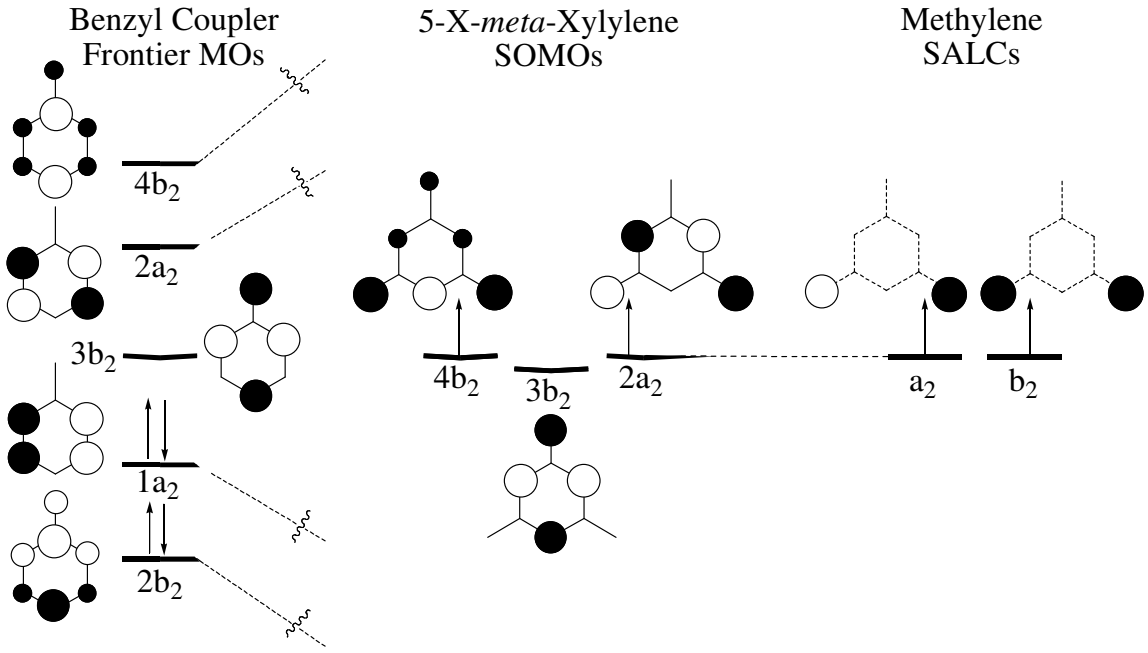

Fig. 4.13. Construction of 5-X-*m*-Xylylene SOMOs using group theory as a guide. For X=EDG, $3b_2$ of 5-X-*m*-xylylene is filled, while for X = EWG, $3b_2$ is empty.

This weaker interaction leads to smaller coefficients in the $4b_2$ SOMO and therefore less overlap density of coefficients between the two 5-X-*m*-xylylene SOMOs compared to

that of the original *m*-phenylene.[17,23,28] The attenuated overlap density of coefficients of the 5-X-*m*-xylylene SOMOs can also be thought of as more disjoint in nature relative to the unsubstituted *m*-phenylene SOMOs.

Another, more simplistic, explanation of the attenuation of exchange coupling is the spin dilution resulting from the attachment of the substituent. The OMe, NMe_2 and NO_2 substituents have atoms (Oxygen and Nitrogen atoms) that are part of the π-system. In each case, the additional atom to the π- system results in the spin density being delocalized over a larger number of atoms and effectively attenuates the coefficients at other atoms. This can be seen in Figure 4.13 in the SOMO $4b_2$, where the coefficient on the substituent atom is non-zero. In the phenyl substituted complex, the attenuated effect is similar, yet not as great – as is expected, because of the moderate change in the electronic structure going from the unsubstituted complex to the phenyl substituted complex, as compared to introducing a π–donor/withdrawer to the system.

With the *t*-Bu substituent, the quaternary carbon is sp^3-hybridized and is not part of the π-system. The spin-density dilution into this substituent is significantly smaller than the others, and the data shows that the exchange coupling is stronger in the **4-*t*-Bu** bis(semiquinone) complex than in the reference **4-H.** Unfortunately, there is no way to explain this anomaly with our above arguments unless further research is done using other alkyl groups as substituents.

It makes no difference whether the $3b_2$ 5-X-*m*-xylylene orbital is filled or unfilled; both strong and weak electron pair withdrawers and donors are predicted to attenuate the exchange integral. This prediction is supported by the magnetic data discussed here and by Borden and Squires' previous work with 1,3,5- trimethylene benzene monoanion. The

singlet-triplet gap in this species was calculated to be approximately 50% of the prototype *m*-xylylene.[23] Their explanation included less overlap of spin-density between SOMOs (more disjoint) as a significant factor in the attenuation of the exchange coupling.

A relationship between the substituent effect and traditional Hammett parameters was examined. Equation 4.1 shows the relationship between the exchange coupling parameters of the substituted and unsubstituted semiquinones to the substituent constant, σ and the reaction constant, ρ.

$$\log (J_x / J_o) = \sigma_m \rho \qquad \textbf{eq. 4.1}$$

Table 4.5 shows various reported σ values for the functional groups under study.[33,34]

Table 4.5. Hammett σ values

Substituent	σ_{meta}	σ_{para}	σ^+	σ^-	$\sigma^\bullet$
OMe	0.12	-0.27	-0.78	-0.20	0.23
NMe_2	-0.16	-0.83	-1.70	-0.12	1.00
NO_2	0.71	0.78	0.79	1.24	0.36
H	0.0	0.0	0.0	0.0	0.0
Phenyl	0.06	-0.01	-0.17	0.02	0.47
t-Bu	-0.10	-0.20	-0.26	-0.13	0.26

A plot of log (J_x/J_o) vs. σ_m was generated. The results of that plot are shown in Figure 4.14.

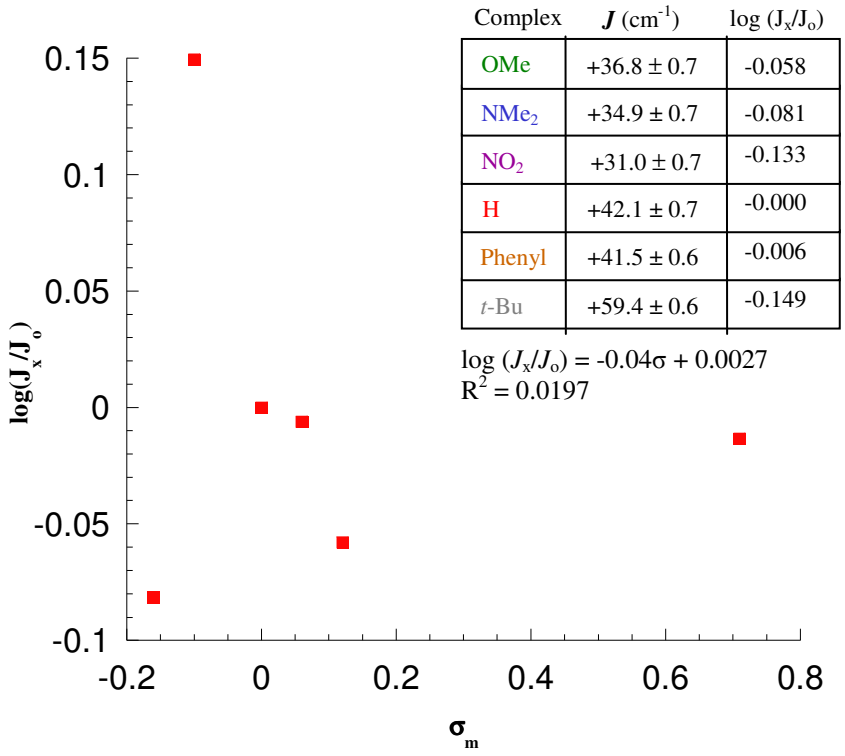

Complex	J (cm^{-1})	log (J_x/J_o)
OMe	+36.8 ± 0.7	-0.058
NMe_2	+34.9 ± 0.7	-0.081
NO_2	+31.0 ± 0.7	-0.133
H	+42.1 ± 0.7	-0.000
Phenyl	+41.5 ± 0.6	-0.006
t-Bu	+59.4 ± 0.6	-0.149

$\log (J_x/J_o) = -0.04\sigma + 0.0027$
$R^2 = 0.0197$

Fig. 4.14 Plot of log (J_x/J_o) vs. σ_m for **4-OMe, 4-NMe_2, 4-NO_2, 4-H, 4-Phenyl, 4-*t*-Bu.**

A linear relationship between J and σ_m was not evident. The results were not surprising, as the semiquinone species is a radical anion and it is difficult to correlate a magnetic parameter, J that is concerned with the mixing of electronic states with a Hammett σ parameter that was generated for a series based solely on the stability of a carboxylate anion species. The energies of the four electronic states of the semiquinone involved in mixing are represented qualitatively in Figure 4.15.

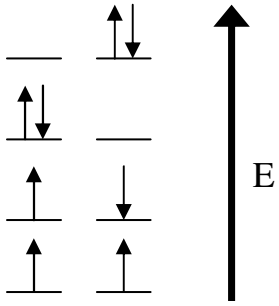

Fig. 4.15. Representation of the triplet ground state and three excited singlet states involved in energy mixing and subsequent determination of ΔE_{ST}.

The mixing of the energies of the four electronic states conspires to give the ΔE_{ST} of the two lowest lying states. How these states interact is extremely difficult to predict, hence the lack of correlation with σ_m. We could have proposed a new σ scale based on the equation $\log (J_x/J_o) = \sigma\rho$; where $\rho = 1$. However, this scale would probably be of minimal utility to the small portion of the scientific community – at best!

J-modulation has been achieved by varying the substituent in a series of ground state triplet bis(semiquinone) complexes. Both strong electron pair donors (NMe_2, OMe) and strong electron pair withdrawers (NO_2) have been shown to attenuate exchange coupling relative to a neutral substituent. While, weak electron pair donors attenuate exchange coupling lesser. Simple Hückel arguments and previous computational work support the results of this work. The attenuation is contributed to spin-density dilution and orbital interactions that lead to a more disjoint nature of the SOMOs associated with the substituted species.

4.5. Experimental Section.

Compound **4.8** was prepared according to literature methods.[21] **4.10** (1,3-dibromobenzene) was purchased from Aldrich Chemicals and was used without further purification. Compounds **4.9** (3,5-dibromobiphenyl)[31] and **4.11** (3,5-dibromoanisole)[32] were prepared according to literature methods. All reactions, solvent distillations and EPR sample preparation were conducted under nitrogen atmosphere. Solvents were purchased from Fisher Scientific or Aldrich, and unless otherwise noted, were freshly distilled immediately prior to use. THF was distilled from sodium benzophenone-ketyl, while CH_2Cl_2 and CH_3OH were distilled from CaH_2.

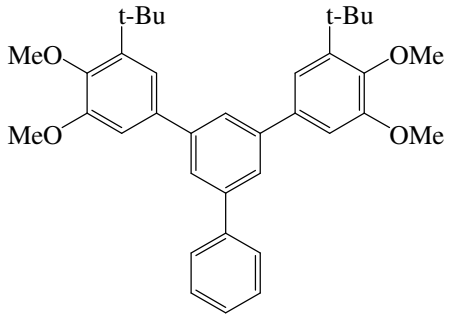

4.12

3,5-Bis-(5-*t* –butyl-3,4-dimethoxyphenyl)-biphenyl

A 100 mL Schlenk flask containing dibromide **4.9** (1g, 3.21 mmol), boronic acid **4.8** (2.12 g, 6.42 mmol), $Pd(PPh_3)_4$ (5 mol%), EtOH (5 mL), and 40 mL of distilled THF was pumped and purged three times under nitrogen atmosphere. 2M Na_2CO_3 (5 mL) was then added and the reaction mixture was pumped and purged three more times. This reaction mixture was refluxed for 7h. Once cool, the solvent was removed under reduced pressure,

ether was added and the reaction mixture was filtered on celite to remove inorganic salts. The remaining crude mixture was purified by column chromatography with 20:80 (ether: petroleum ether) to give **4.12** (1.69 g, 80%). m.p. 232-235°C. ^{1}H NMR (300MHz, $CDCl_3$): δ = 7.70 (m, 5H), 7.51 (t, *J*=7.20Hz, 2H), 7.43 (d, *J*=7.20Hz, 1H), 7.23 (d, *J*=1.89Hz, 2H), 7.11 (d, *J*=1.77Hz, 2H), 3.95 (s, 6H), 3.94 (s, 6H), 1.45 (s, 18H).

^{13}C NMR (300MHz, $CDCl_3$): δ =153.5, 150.1, 148.7, 148.5, 143.7, 142.9, 142.3, 140.3, 136.1, 133.1, 129.6, 128.2, 126.8, 124.5, 119.3, 118.7, 111.7, 110.4, 57.6, 56.2, 35.3, 30.5. HRMS (FAB+): *Calcd for* $C_{36}H_{42}O_4$: 538.3083. *Found*: 538.4409.

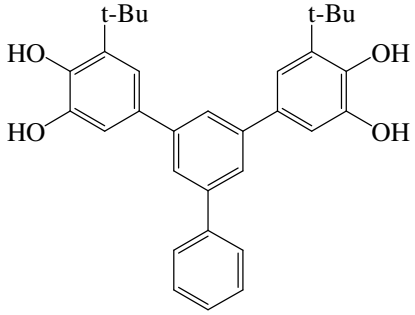

4.15

3,5-Bis-(5-*t* –butyl-3,4-dihydroxyphenyl)-biphenyl

To a 50 mL flask containing **4.12** (0.16 g, 0.297 mmol), 15 mL of CH_2Cl_2 was added. The reaction mixture was then cooled to -78°C. After 15mins of stirring, boron tribromide (0.28 mL, 2.97 mmol) was added via syringe. The reaction was allowed to stir for 6h. The reaction was quenched with cold aq. NaCl. The solvent was removed under reduced pressure to yield **4.15** (143 mg, 100%). m.p. 100-103°C. ^{1}H NMR (300 MHz, $CDCl_3$): δ =7.68 (d, *J*=7.2 Hz, 2H), 7.63 (s, 2H), 7.62 (d, *J*=9.0 Hz,2H), 7.49 (t, *J*=7.35 Hz, 3H), 7.42 (d, *J*=6.9 Hz, 1H), 7.37 (d, 2H), 7.19 (d, *J*=2.1 Hz, 2H), 7.06 (d, *J*=1.8 Hz, 2H),

1.47(s,18H). ^{13}C NMR (300MHz, $CDCl_3$): δ = 143.6, 142.7, 136.5, 132.7, 129.0, 127.6, 124.5, 123.2, 121.5, 118.5, 112.3, 35.1, 29.8. IR (film from CH_2Cl_2) ν (cm^{-1}): 3391. High Res MS (FAB+): *Calcd for* $C_{32}H_{34}O_4$: 482.2457. *Found*: 482.2453.

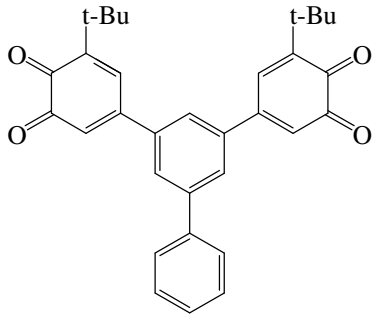

4.18

3,5-Bis-(5-*t* –butyl-3,4-ortho-quinone)-biphenyl

To a 50 mL flask containing **4.15** (100 mg, .207 mmol) was added 20mL of anhydrous THF and Fetizon's reagent (1 g). The reaction flask was wrapped in aluminum foil and the solution was stirred at room temperature for 12 h. The reaction mixture was then run through a celite plug to remove inorganic impurities and further purified via column chromatography with 20:80 (hexanes: ethyl acetate) to give **4.18** (86 mg, 89%) ^{1}H NMR (300 MHz, $CDCl_3$): δ =7.68 (d, *J*=7.2 Hz, 2H), 7.63 (s, 2H), 7.62 (d, *J*=9.0 Hz,2H),, 7.48 (t, *J*=6.6 Hz, 3H), 7.43 (d, *J*=7.8 Hz, 1H), 7.20 (d, *J*=3.6 Hz, 2H), 7.21 (s, 2H), 6.63 (s, 2H), 1.36 (s,18H). ^{13}C NMR (300 MHz, $CDCl_3$): δ = 143.6, 142.7, 136.5, 132.7, 129.0, 127.6, 124.5, 123.2, 121.5, 118.5, 112.3, 35.1, 29.8. IR (film from CH_2Cl_2) ν (cm^{-1}): 1652.

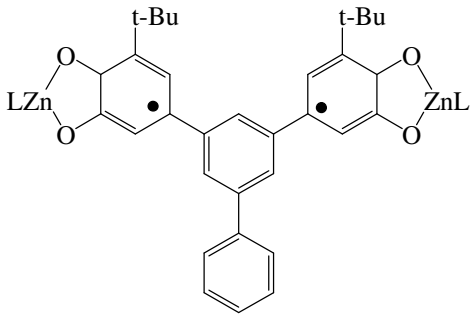

4-Phenyl

Complex Biphenyl Bis(Semiquinone).

The bis(semiquinone) complexes were prepared in a glove box via a comproportionation reaction between the appropriate bis(catechol)s and bis(quinone)s. The bis(catechol) **4.15** (100 mg, 0.207 mmol) and bis(quinone) **4.18** (100 mg, 0.207 mmol) were weighed outside the glove box, then placed in a 10 mL glass vial (vial no.1). A second vial (vial no.2) containing $Zn(ClO_4)_2.6H_2O$ (0.344 g, 0.922mmol) and $KTp^{Cum,Me}$ (0.599 g, 0.922 mmol) was similarly prepared. Both vials were then purged and taken into the glove box. Excess KH was added to vial no. 1, then 4mL of anhydrous *m*-THF were added to both vials and the solutions were then stirred for 15 minutes. Vial no. 1, now containing the *in situ* generated bis(semiquinone) was filtered into vial no.2. The reaction was then stirred for an additional 15 minutes, then filtered to yield the olive green complex **4-Phenyl**. Recrystallized from hexanes to yield green, plate-like crystals. IR (film from CH_2Cl_2) ν (cm^{-1}): 2953, 2547, 1521, 1440, 1365. UV-Vis (cm^{-1}): 21500, 12619.

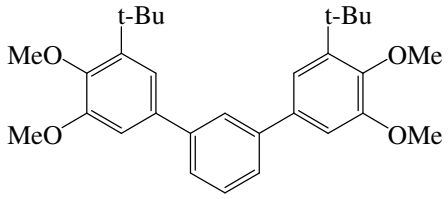

4.13

3,5-Bis-(5-*t* –butyl-3,4-dimethoxyphenyl)-phenyl

A 100 mL Schlenk flask containing dibromide **4.10** (1 g, 4.24 mmol), boronic acid **4.8** (2.79 g, 9.38 mmol), $Pd(PPh_3)_4$ (5 mol%), EtOH (5 mL), and 40 mL of distilled THF was pumped and purged three times under nitrogen atmosphere. 2M Na_2CO_3 (5 mL) was then added and the reaction mixture was pumped and purged three more times. This reaction mixture was refluxed for 5 h. Once cool, the solvent was removed under reduced pressure, ether was added and the reaction mixture was filtered on celite to remove inorganic salts. The remaining crude mixture was purified by column chromatography with 10:90 (ether: petroleum ether) to give **4.13** (1.7 g, 88%). m.p. 112-114°C. ^{1}H NMR (300 MHz, $CDCl_3$): δ =7.77 (s, 1H), 7.50 (m, 3H), 7.24 (s, 2H), 7.13 (s, 2H), 3.98 (s,12H), 1.35 (s, 18H). ^{13}C NMR (300MHz, $CDCl_3$): δ = 153.5, 148.4, 143.6, 142.3, 136.2, 129.0, 126.2, 125.9, 118.1, 110.1, 60.5, 56.0, 35.3, 30.7. *Anal. Calcd for* $C_{30}H_{38}O_4$: C: 77.88, H: 8.27. *Found:* C: 77.64, H: 8.23.

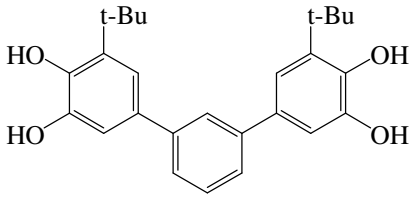

4.16

3,5-Bis-(5-*t* –butyl-3,4-dihydroxyphenyl)-phenyl

To a 50 mL flask containing **4.13** (0.50 g, 1.08 mmol), 40 mL of CH_2Cl_2 was added. The reaction mixture was then cooled to -78°C. After 15mins, boron tribromide (10 mL, 0.11 mmol) was added via syringe. The reaction was allowed to stir for 6 h. The reaction was quenched with cold aq. NaCl. The solvent was removed under reduced pressure to yield **4.16** (0.43 g, 100%). m.p. 164-167°C. ^{1}H NMR (300MHz, $CDCl_3$): δ =7.62 (s, 1H), 7.44 (s, 3H), 7.15 (s, 2H), 7.01 (s, 2H), 5.69 (s,2H), 5.31 (s, 2H), 1.47 (s,18H). ^{13}C NMR (300MHz, $CDCl_3$): δ = 143.2, 143.1, 141.9, 136.7, 132.7, 129.0, 125.5, 125.3, 118.4, 112.0, 34.8, 29.6. IR (film from CH_2Cl_2) ν (cm^{-1}): 3480. *Anal. Calcd for* $C_{26}H_{30}O_4$: C: 76.81, H: 7.76, *Found:* C: 76.49, H: 7.70.

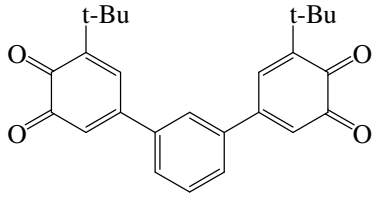

4.19

3,5-Bis-(5-*t* –butyl-3,4-ortho-quinone)-phenyl

To a 50 mL flask containing **4.16** (90 mg, 0.222 mmol) was added 20 mL of anhydrous THF and Fetizon's reagent (0.9 g). The reaction flask was wrapped in aluminum foil and the solution was stirred at room temperature for 12 h. The reaction mixture was then run

through a celite plug to remove inorganic impurities and further purified via column chromatography with 30:70 (hexanes: ethyl acetate) to give **4.19** (80 mg, 90%) ^{1}H NMR (300 MHz, $CDCl_3$): δ =7.71 (s, 2H), 7.54 (s, 1H), 7.17 (s, 2H), 6.58 (s, 2H),1.34 (s,18H). ^{13}C NMR (300 MHz, $CDCl_3$): δ = 143.2, 143.1, 141.9, 136.7, 132.7, 129.0, 125.5, 125.3, 118.4, 112.0, 34.8, 29.6. IR (film from CH_2Cl_2) ν (cm^{-1}): 1651.

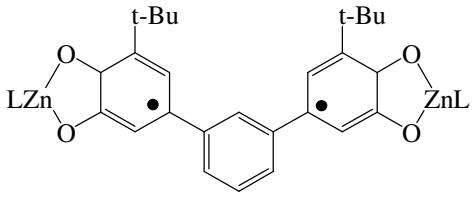

4-H

Complex Phenyl Bis(Semiquinone), 4-H

The bis(catechol) **4.16** (40 mg, 0.098 mmol) and bis(quinone) **4.19** (40 mg, 0.098 mmol) were weighed outside the glove box, then placed in a 10 mL glass vial (vial no.1). A second vial (vial no.2) containing $Zn(ClO_4)_2.6H_2O$ (141 mg, 0.216 mmol) and $KTp^{Cum,Me}$ (80 mg, 0.216 mmol) was similarly prepared. Both vials were then purged and taken into the glove box. Excess KH was added to vial no. 1, then 4 mL of anhydrous *m*-THF were added to both vials and the solutions were then stirred for 15 minutes. Vial no. 1, now containing the *in situ* generated bis(semiquinone) was filtered into vial no.2. The reaction was then stirred for an additional 15 minutes, then filtered to yield the olive green complex **4-H**. Recrystallized from hexanes to yield green, plate-like crystals. IR (film from CH_2Cl_2) ν (cm^{-1}): 2953, 2536, 1520, 1440, 1365, 1178. UV-Vis (cm^{-1}): 23000, 13623.

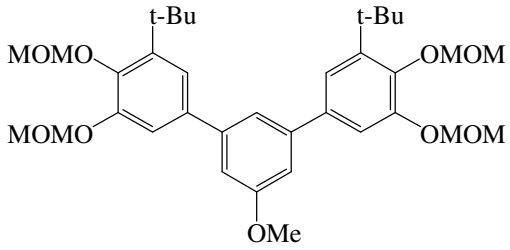

4.14

3,5-Bis-(5-*t*-butyl-3,4-methoxymethoxy)-anisole

A 100 mL Schlenk flask containing dibromide **4.11** (0.798 g, 3mmol), boronic acid **4.8** (2.15 g, 6.6 mmol), $Pd(PPh_3)_4$ (5 mol%), EtOH (5 mL), and 40 mL of distilled THF was pumped and purged three times under nitrogen atmosphere. 2M Na_2CO_3 (5 mL) was then added and the reaction mixture was pumped and purged three more times. This reaction mixture was refluxed for 5 h. Once cool, the solvent was removed under reduced pressure, ether was added and the reaction mixture was filtered on celite to remove inorganic salts. The remaining crude mixture was purified by column chromatography with 20:80 (hexanes: ethyl acetate) to give **4.14** (1.4 g, 75%) as a light yellow oil. ^{1}H NMR (300MHz,$CDCl_3$): δ =7.28 (m, 5H), 7.03 (s, 2H), 5.26 (s, 4H), 5.24 (s, 4H), 3.92 (s, 3H), 3.69 (s, 6H), 3.54 (s, 6H), 1.48 (s, 18H). ^{13}C NMR (300MHz, $CDCl_3$): δ = 160.2, 154.3, 153.8, 150.4, 145.8, 143.7, 143.2, 136.2, 124.9, 120.2, 119.5, 114.5, 111.7, 99.0, 98.3, 95.5, 94.8, 70.4, 57.2, 56.0, 35.4, 31.4. HRMS (FAB+): *Calcd for* $C_{35}H_{48}O_9$: 612.3298. *Found*: 612.3329.

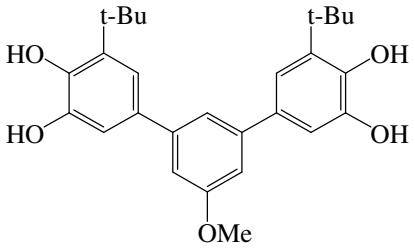

4.17

3,5-Bis-(5-*t* –butyl-3,4-dihydroxyphenyl)-anisole

To a 50 mL flask contained **4.14** (200 mg, 0.458 mmol) in 15 mL of MeOH was added three drops of concentrated hydrochloric acid (12 M). The reaction mixture was refluxed for 12 h. Once cool, the solvent was removed under reduced pressure, brought up in ether, then washed with a saturated solution of $NaHCO_3$. This was followed by an aq. wash with saturated NaCl solution. The ether was removed under reduced pressure to give bis(catechol) **4.17** (199 mg, 96%). ^{1}H NMR (300 MHz, $CDCl_3$): δ = 7.10 (s, 1H), 7.11 (s, *J*=2.9Hz, 2H), 6.97 (d, *J*=2.0Hz, 4H), 3.90 (s, 3H), 3.51 (s, 4H), 1.45 (s,18H). ^{13}C NMR (300MHz, $CDCl_3$): δ = 159.2, 146.7, 143.5, 143.3, 136.9, 132.7, 118.6, 112.2, 111.2, 55.7, 35.1, 29.8. IR (film from CH_2Cl_2) ν (cm^{-1}): 3508. HRMS (FAB+): *Calcd for* $C_{27}H_{32}O_5$: 436.2250. *Found*: 436.2241.

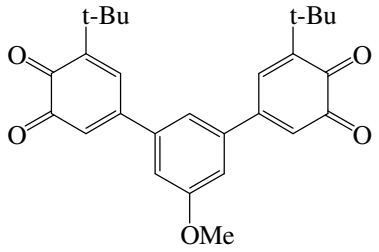

4.20

3,5-Bis-(5-*t* –butyl-3,4-ortho-quinone)-anisole

To a 50 mL flask containing **4.17** (120 mg, 0.277 mmol) was added 20 mL of anhydrous THF and Fetizon's reagent (1.2 g). The reaction flask was wrapped in aluminum foil and the solution was stirred at room temperature for 12 h. The reaction mixture was then run through a celite plug to remove inorganic impurities and further purified via column chromatography with 20:80 (hexanes: ethyl acetate) to give **4.20** (113 mg, 95%) ^{1}H NMR (300 MHz, $CDCl_3$): δ = 7.10 (s, 1H), 7.11 (s, *J*=2.9Hz, 2H), 6.97 (d, *J*=2.0Hz, 4H), 3.90 (s, 3H), 3.51 (s, 4H), 1.45 (s,18H). IR (film from CH_2Cl_2) ν (cm^{-1}): 1651.

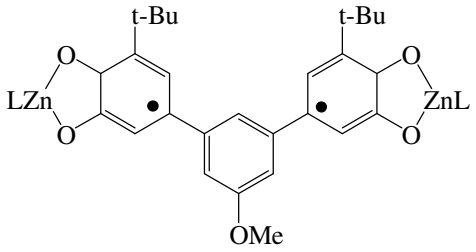

4-OMe

Complex Phenyl Bis(Semiquinone), 4-H

The bis(catechol) **4.17** (80 mg, 0.183 mmol) and bis(quinone) **4.20** (80 mg, 0.183 mmol) were weighed outside the glove box, then placed in a 10mL glass vial (vial no.1). A second vial (vial no.2) containing $Zn(ClO_4)_2.6H_2O$ (300 mg, 0.807 mmol) and $KTp^{Cum,Me}$ (524 mg, 0.807 mmol) was similarly prepared. Both vials were then purged and taken into the glove box. Excess KH was added to vial no. 1, then 4 mL of anhydrous *m*-THF were added to both vials and the solutions were then stirred for 15 minutes. Vial no. 1, now containing the *in situ* generated bis(semiquinone) was syringed into vial no.2 after Whatman filtration. The reaction was then stirred for an additional 15 minutes, then filtered to yield the yellow green complex, **4-OMe**. IR (film from CH_2Cl_2) ν (cm^{-1}): 2953, 2547, 1515, 1439, 1178. UV-Vis (cm^{-1}): 21200, 14600.

Crystal Structure Determinations.

4-Phenyl - The sample was mounted on a nylon loop with a small amount of NVH immersion oil. All X-ray measurements were made on a Bruker-Nonius X8 Apex2 CCD diffractometer at 110K. The unit cell dimensions were determined from a symmetry constrained fit of 9204 reflections with $4.36° < 2\theta < 42.31°$. The data collection strategy was a number of ω and φ scans which collected data up to 50.03° (2θ). Early in the structure analysis it was realized that the lattice contained several highly disordered mixed C_6 alkane isomers solvent molecules ("hexanes" was used as a crystallization solvent). The structure was treated with the SQUEEZE option of PLATON. After initial refinements with the "squeezed" data with SHELXTL, the trial structure and SQUEEZE modified reflection data were imported into NRCVAX and the structure was processed normally with refinement converging smoothly. The structural model was fit to the data using full matrix least-squares based on F. The calculated structure factors included corrections for anomalous dispersion from the usual tabulation.

4-H - A crystal of dimensions 0.34 x 0.24 x 0.12 mm was mounted on a standard Bruker SMART 1K CCD-based X-ray diffractometer equipped with a LT-2 low temperature device and normal focus Mo-target X-ray tube (λ = 0.71073 A) operated at 2000 W power (50 kV, 40 mA). The X-ray intensities were measured at 123(2) K; the detector was placed at a distance 4.969 cm from the crystal. A total of 3000 frames were collected with a scan width of 0.5° in ω and phi with an exposure time of 60 s/frame. The integration of the data yielded a total of 127468 reflections to a maximum 2θ value of 44.22° of which 13121 were independent and 10557 were greater than $2\sigma(I)$. The final

cell constants (Table 1) were based on the xyz centroids of 9221 reflections above 10σ(I). Analysis of the data showed negligible decay during data collection; the data were processed with SADABS and corrected for absorption. The structure was solved and refined with the Bruker SHELXTL (version 6.12) software package, using the space group P2(1)/c with Z = 4 for the formula $C_{104}H_{117}B_2N_{12}O_4Zn_2 \bullet C_6H_{14}$. All non-hydrogen atoms were refined anisotropically with the hydrogen atoms placed in idealized positions. The equivalent of 4 hexane lattice solvates per unit cell, disordered about inversion centers in the crystal lattice were modeled by use of the SQUEEZE subroutine of the PLATON program suite. Full matrix least-squares refinement based on F^2 converged at R1 = 0.0858 and wR2 = 0.1777 [based on I > 2sigma(I)], R1 = 0.1057 and wR2 = 0.1865 for all data.

Magnetic Susceptibility Measurements: Magnetic susceptibilities were measured on a Quantum Design MPMS-XL7 SQUID magnetometer using an applied field of 0.5 Tesla for Curie plots. Saturation magnetization values are consistent with the spin of the ground states mentioned in the results and discussion section of this chapter. Microcrystalline samples were loaded into the sample space of a Delrin sample holder, and mounted to the sample rod using string. Data were corrected for sample holder and molecular diamagnetism using Pascal's constants. The decrease in the χT data at low temperatures was accounted for with a Weiss correction, using the expression $\chi_{eff} = \chi/(1-\vartheta\chi)$, where $\vartheta = 2z J'/(Ng^2\beta^2)$. The origin of z$J'$ may be zero-field splitting, intermolecular interaction, saturation effects, or some combination of all three. The other terms have their usual meaning.

References

1. Shultz, D. A.; Lahti, P., Ed.. Ed.; Marcel Dekker, Inc.: New York., 1999.

2. Silverman, S. K.; Dougherty, D. A. *J. Phys. Chem.* **1993**, *97*, 13273-13283.

3 Shultz, D. A.; Boal, A. K.; Lee, H.; Farmer, G. T. *J. Org. Chem.* **1999**, *64*, 4386-4396.

4. Shultz, D. A.; Boal, A. K.; Farmer, G. T. *J. Am. Chem. Soc.* **1997**, *119*, 3846.

5. Okada, K.; Matsumoto, K.; Oda, M.; Murai, H.; Akiyama, K.; Ikegami, Y. *Tet Letts* **1995**, *36*, 6693.

6. Okada, K.; Oda, M.; Murai, H.; Imakura, T.; Baumgarten, M. *J. Am. Chem. Soc.* **1996**, *118*, 3047.

7. Iwamura, H.; Karasawa, S.; Nakazono, S. *Angew. Chem. Int. Ed. Engl.* **1998**, *37*, 1550.

8. Iwamura, H.; Matsuda, K.; Koga, N.; Suemune, H.; Tanaka, M.; Fujita, J. *J. Am. Chem. Soc.* **1996**, *118*, 9347.

9. Iwamura, H.; Inoue, K.; Koga, N.; Kanno, F. *J. Am. Chem. Soc.* **1993**, *115*, 847.

10. Dvolaitzky, M.; Chiarelli, R.; Rassat, A. *Angew. Chem. Int. Ed. Engl.* **1992**, *31*.

11. Borden, W. T.; Fang, S.; Lee, M. S.; Hrovat, D. A. *J. Am. Chem. Soc.* **1995**, *117*, 6727.

12. Adam, W.; van Barneveld, C.; Bottle, S. E.; Engert, H.; Hanson, G. R.; Harrer, H. M.; Heim, C.; Nau, W. M.; Wang, D. *J. Am. Chem. Soc.* **1996**, *118*, 3974.

13. Berson, J. A. *Acc. Chem. Res.* **1997**, *30*, 238-244.

14. Berson, J. A.; Scaiano, J.; Berinstain, A.; Chung, W.; Song, A.; Maksimovic, L.; Wang, P.; Feng, X.; Heath, R.; Bush, L. *J. Am. Chem. Soc.* **1997**, *119*, 1406.

15. Berson, J. A.; Lahti, P., Ed.. Ed.; Marcel Dekker: New York, **1999**.

16. Borden, W. T.; Adam, W.; Burda, C.; Foster, H.; Heidenfelder, T.; Heubes, M.; Hrovat, D.; Kita, F.; Lewis, S.; Scheutzow, D.; Wirz, J. *J. Am. Chem. Soc.* **1998**, *120*, 593.

17. Dougherty, D. A.; Silverman, S. K.; West, A. P., Jr. *J. Am. Chem. Soc.* **1996**, *118*, 1452.

18. Geise, C. M.; Hadad, C. M. *J. Org. Chem.* **2000**, *65*, 8348.

19. Shultz, D. A.; Bodnar, S. H.; Lee, H.; Kampf, J. W.; Incarvito, C. D.; Rheingold, A. L. *J. Am. Chem. Soc.* **2002**, *124*, 10054.

20. Vorlander, D.; Siebert, E. *Chem. Ber.* **1919**, *52*, 283.

21. Iwamura, H.; Ishida, T. *J. Am. Chem. Soc.* **1991**, *113*, 4238-4241.

22. Bhandari, G.; Rheingold, A. L.; Theopold, K. H. *Chem. Eur. J.* **1995**, *1*,199.

20. Mitani, M.; Yamaki, D.; Yakano, Y.; Kitagawa, Y.; Yoshioka, Y.; Yamaguchi, K. *J. Chem. Phys.* **2000**, *113*, 10486.

21. Shultz, D. A.; Boal, A. K.; Farmer, G. T.; Driscoll, D. J.; Kitchin, J. R.; Tew, G. N. *J. Org. Chem.* **1995**, *60*, 3578.

22. Ruf, M.; VahrenKamp, H. *Inorg. Chem.* **1996,** *35,* 6571.

23. Borden, W. T.; Squires, R. R.; Kemnitz, C. R. *J. Am. Chem. Soc.* **1997**,*119*, 6564.

24. Pierpont, C. G.; Noll, B. C.; Groner, M. D.; Yee, G. T. *Inorg. Chem.* **1997**,*36*, 4860

25. Kahn, O. *Molecular Magnetism*; VCH Publishers, Inc: New York, **1993**.

26. Bleaney, B.; Bowers, K. D. *Proc. R. Soc. London.* **1952**, *A214*, 451.

27. Salem, L. *Molecular Orbital Theory of Conjugated Systems*; W.A.Benjamin Inc.: New York, **1966**.

28. Rajca, A. *Chem. Rev.* **1994**, *94*, 871.

29. O'Connor, C. J. *Prog. Inorg. Chem.* **1982**, *29*, 203.

30. Caneschi, A.; Dei, A.; Mussari, C. P.; Shultz, D. A.; Sorace, L.;Vostrikova, K. E. *Inorg. Chem.* **2002**, *41*, 1086.

31. Kelly, T.; Bridger, G.; Zhao, C. *J. Amer. Chem. Soc.* **1990**, *112*, 8024.

32. Dorman, L. *J. Org. Chem.* **1966**, *31*, 3666.

33. Hansch, C.; Leo, A.; Taft, R. *Chem. Rev.* **1991**, *91*, 165.

34. Jiang, Xi-Kui. *Acc. Chem. Res.* **1997**, *30***,** 283.

APPENDIX

Crystal Structure and Data Refinement

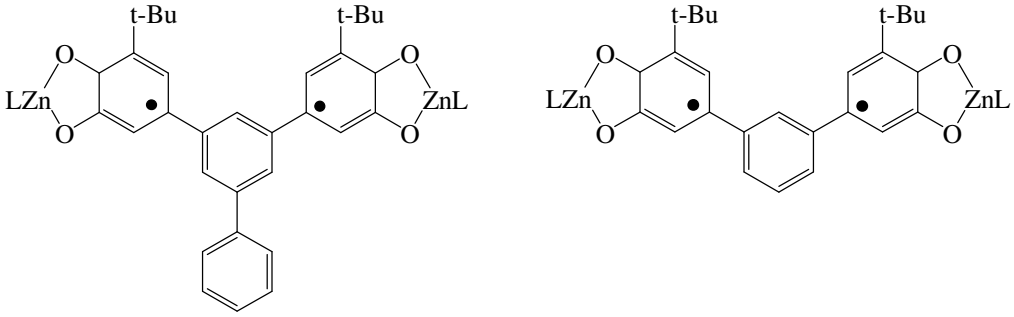

Table A.1. Crystal Data and Structure Refinement for **4-Phenyl** and **4-*t*-Bu**

Empirical Formula	$C_{110}H_{120}B_2N_{12}O_4Zn_2$	$C_{104}H_{117}B_2N_{12}O_4Zn_2$
a/Å	11.5947(9)	11.1192(12)
b/Å	18.5344(14)	21.822(2)
c/Å	29.394(2)	44.040(5)
α/deg	76.981(3)	90.00
β/deg	85.716(3)	94.885(7)
γ/deg	89.384(3)	90.00
V/ Å^3	6137.1(8)	10647(2)
Z	2	4
FW	1826.60	1837.63
Space Group	Triclinic P$\bar{1}$	Monoclinic, P 2_1/c
T/K	110K	123K
λ/ Å	0.71073	0.71073
δ_{calc}/Mg•cm^{-3}	0.988	1.146
μ/mm^{-1}	0.44	0.505
R(F)	0.118	0.1057
R_w	0.088	0.1865

Complete Crystallographic Data

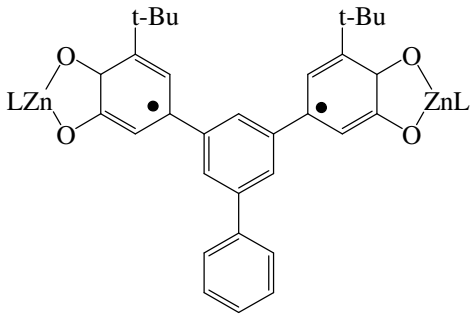

Table A.2 Atomic coordinates (x 10^4) and equivalent isotropic displacement parameters (A^2 x 10^3).
E.S.Ds. refer to the last digit printed. Biso is the Mean of the Principal Axes of the Thermal Ellipsoid

Atom	x	y	z	Biso
ZN1	0.72579(4)	0.35192(3)	0.473755(19)	2.98(3)
ZN2	0.26794(5)	-0.00414(3)	0.106131(18)	3.13(3)
O1	0.7681 (3)	0.25451(16)	0.45005 (13)	3.36(17)
O2	0.6318 (2)	0.36673(17)	0.41848 (11)	2.97(15)
O3	0.2231 (3)	-0.00870(19)	0.17809 (10)	3.48(17)
O4	0.3667 (3)	0.07690(17)	0.11612 (11)	3.11(17)
B1	0.7741 (5)	0.4010 (3)	0.5623 (2)	3.3 (3)
N1	0.6963 (3)	0.4620 (2)	0.48398 (15)	2.9 (2)
N2	0.7018 (3)	0.4618 (2)	0.53054 (15)	3.1 (2)
N3	0.8901 (3)	0.3675 (2)	0.49284 (15)	3.0 (2)
N4	0.8897 (3)	0.3915 (2)	0.53344 (15)	3.2 (2)
N5	0.6534 (3)	0.3031 (2)	0.53865 (13)	2.95(19)
N6	0.7077 (3)	0.3260 (2)	0.57357 (15)	3.3 (2)
B2	0.2121 (5)	-0.1057 (3)	0.04332 (19)	3.5 (3)
N7	0.3285 (3)	-0.1100 (2)	0.11367 (14)	3.12(20)
N8	0.2725 (3)	-0.1485 (2)	0.08673 (13)	3.4 (2)
N9	0.3047 (3)	0.0206 (2)	0.03128 (13)	3.0 (2)
N10	0.2925 (3)	-0.0426 (2)	0.01534 (13)	3.1 (2)
N11	0.1028 (3)	-0.0238 (2)	0.09036 (14)	3.4 (2)
N12	0.0999 (3)	-0.0708 (2)	0.06052 (14)	3.4 (2)
C1	0.7195 (4)	0.2530 (3)	0.41323 (19)	2.9 (2)
C2	0.6446 (4)	0.3162 (3)	0.39469 (17)	2.6 (2)
C3	0.5925 (4)	0.3206 (2)	0.35306 (18)	3.1 (2)
C4	0.6057 (5)	0.2644 (3)	0.32984 (18)	3.8 (3)
C5	0.6748 (5)	0.2012 (3)	0.34888 (19)	3.9 (3)
C6	0.7322 (4)	0.1937 (3)	0.38905 (19)	3.4 (3)
C7	0.8064 (4)	0.1270 (3)	0.40752 (20)	4.1 (3)
C8	0.7599 (5)	0.0907 (3)	0.4580 (2)	4.6 (3)
C9	0.8039 (6)	0.0689 (3)	0.3782 (2)	6.2 (4)
C10	0.9319 (5)	0.1520 (3)	0.4072 (2)	5.6 (3)
C11	0.5568 (5)	0.2709 (3)	0.28402 (18)	4.0 (3)
C12	0.5615 (6)	0.3389 (3)	0.2513 (2)	5.5 (4)
C13	0.5178 (6)	0.3483 (3)	0.20856 (20)	6.0 (4)

C14	0.4635	(6)	0.2880	(3)	0.19742	(18)	5.3	(4)
C15	0.4578	(5)	0.2181	(3)	0.22928	(18)	4.0	(3)
C16	0.5047	(5)	0.2108	(3)	0.27174	(17)	3.7	(3)
C17	0.4004	(5)	0.1555	(3)	0.21561	(17)	3.6	(3)
C18	0.4143	(4)	0.1456	(3)	0.17068	(17)	3.3	(3)
C19	0.3558	(4)	0.0885	(3)	0.15768	(17)	2.9	(3)
C20	0.2768	(4)	0.0409	(3)	0.19256	(17)	3.2	(3)
C21	0.2625	(4)	0.0504	(3)	0.23976	(16)	3.5	(3)
C22	0.3263	(5)	0.1061	(3)	0.24967	(17)	4.0	(3)
C23	0.1794	(5)	-0.0005	(3)	0.27564	(17)	4.1	(3)
C24	0.1776	(6)	0.0182	(3)	0.32420	(18)	5.8	(4)
C25	0.2168	(5)	-0.0810	(3)	0.28131	(18)	4.7	(3)
C26	0.0555	(5)	0.0087	(3)	0.25954	(18)	5.5	(3)
C27	0.5234	(10)	0.4216	(4)	0.1752	(2)	7.7	(6)
C28	0.6235	(10)	0.4622	(4)	0.1673	(2)	10.1	(7)
C29	0.6288	(12)	0.5335	(5)	0.1364	(3)	11.8	(8)
C30	0.5324	(18)	0.5618	(6)	0.1147	(4)	13.5	(12)
C31	0.4343	(15)	0.5225	(6)	0.1222	(3)	13.4	(11)
C32	0.4318	(11)	0.4510	(4)	0.1530	(3)	10.4	(7)
C33	0.6464	(4)	0.5402	(3)	0.58824	(19)	4.0	(3)
C34	0.6531	(4)	0.5246	(3)	0.54016	(20)	3.3	(3)
C35	0.6177	(4)	0.5661	(3)	0.4986	(2)	3.3	(3)
C36	0.6462	(4)	0.5267	(3)	0.46438	(18)	2.6	(3)
C37	0.6340	(4)	0.5495	(3)	0.41408	(19)	3.1	(3)
C38	0.6989	(5)	0.5179	(3)	0.3824	(2)	3.8	(3)
C39	0.6849	(5)	0.5369	(3)	0.3354	(2)	5.0	(3)
C40	0.6053	(7)	0.5908	(4)	0.3176	(2)	6.4	(4)
C41	0.5438	(5)	0.6243	(3)	0.3495	(3)	5.7	(4)
C42	0.5572	(5)	0.6047	(3)	0.3958	(2)	4.2	(3)
C43	0.5832	(10)	0.6119	(5)	0.2664	(3)	9.9	(6)
C44	0.6706	(14)	0.6206	(8)	0.2347	(3)	18.7	(11)
C45	0.4806	(9)	0.5687	(6)	0.2566	(3)	10.6	(6)
C46	1.0271	(4)	0.4332	(3)	0.5836	(2)	4.6	(3)
C47	0.9993	(4)	0.4054	(3)	0.54197	(19)	3.5	(3)
C48	1.0718	(4)	0.3899	(3)	0.50643	(20)	3.6	(3)
C49	1.0001	(4)	0.3662	(3)	0.47623	(18)	3.2	(3)
C50	1.0342	(4)	0.3484	(3)	0.4312	(2)	3.5	(3)
C51	1.1436	(5)	0.3172	(3)	0.4242	(2)	4.4	(3)
C52	1.1808	(5)	0.3068	(3)	0.3802	(3)	4.8	(3)
C53	1.1139	(6)	0.3250	(3)	0.3425	(2)	4.8	(3)
C54	1.0035	(5)	0.3548	(3)	0.3506	(2)	5.0	(3)
C55	0.9671	(5)	0.3657	(3)	0.3932	(2)	4.0	(3)
C56	1.1575	(7)	0.3155	(4)	0.2948	(3)	7.5	(4)
C57	1.1640	(12)	0.2406	(7)	0.2912	(4)	16.5	(9)
C58	1.2490	(11)	0.3738	(6)	0.2741	(3)	14.9	(8)
C59	0.7444	(4)	0.2839	(3)	0.65824	(18)	4.0	(3)
C60	0.6912	(4)	0.2759	(3)	0.61448	(18)	3.3	(3)
C61	0.6247	(4)	0.2185	(3)	0.60689	(19)	3.5	(3)
C62	0.6028	(4)	0.2379	(3)	0.55942	(18)	3.0	(3)
C63	0.5345	(4)	0.1983	(3)	0.53263	(17)	2.8	(2)
C64	0.4884	(4)	0.2344	(2)	0.49135	(17)	2.8	(2)
C65	0.4272	(4)	0.1968	(3)	0.46474	(17)	3.1	(2)
C66	0.4102	(4)	0.1202	(3)	0.47976	(18)	2.8	(3)
C67	0.4515	(4)	0.0843	(3)	0.52152	(18)	3.2	(2)
C68	0.5147	(4)	0.1222	(3)	0.54753	(17)	3.3	(2)
C69	0.3504	(4)	0.0773	(3)	0.44973	(18)	3.6	(3)
C70	0.4093	(5)	0.0900	(3)	0.40064	(20)	4.9	(3)

C71	0.2218	(5)	0.0970	(3)	0.4474	(2)	4.7	(3)
C72	0.2212	(5)	−0.2788	(3)	0.08479	(20)	5.0	(3)
C73	0.2796	(4)	−0.2220	(3)	0.10487	(19)	4.0	(3)
C74	0.3443	(5)	−0.2325	(3)	0.14347	(18)	4.0	(3)
C75	0.3730	(4)	−0.1621	(3)	0.14814	(17)	3.4	(3)
C76	0.4397	(4)	−0.1401	(3)	0.18373	(17)	3.2	(3)
C77	0.4490	(4)	−0.1894	(3)	0.22679	(18)	3.7	(3)
C78	0.5102	(5)	−0.1693	(3)	0.26131	(17)	3.8	(3)
C79	0.5611	(4)	−0.1007	(3)	0.25463	(17)	3.3	(3)
C80	0.5520	(4)	−0.0524	(3)	0.21109	(18)	3.3	(3)
C81	0.4944	(4)	−0.0711	(3)	0.17624	(16)	3.1	(2)
C82	0.6208	(5)	−0.0786	(3)	0.29335	(17)	3.9	(3)
C83	0.7465	(5)	−0.0533	(4)	0.27881	(19)	5.8	(4)
C84	0.5537	(5)	−0.0197	(3)	0.3116	(2)	5.5	(3)
C85	0.3484	(4)	−0.0921	(3)	−0.05615	(17)	4.3	(3)
C86	0.3459	(4)	−0.0335	(3)	−0.02907	(17)	3.2	(3)
C87	0.3899	(4)	0.0375	(3)	−0.04095	(17)	3.5	(3)
C88	0.3624	(4)	0.0696	(3)	−0.00304	(17)	3.0	(3)
C89	0.3819	(4)	0.1464	(3)	0.00051	(17)	3.5	(3)
C90	0.3111	(5)	0.1799	(3)	0.02952	(17)	4.1	(3)
C91	0.3348	(6)	0.2514	(3)	0.03425	(19)	5.9	(4)
C92	0.4298	(7)	0.2912	(3)	0.0079	(2)	5.7	(4)
C93	0.4922	(6)	0.2590	(4)	−0.0232	(2)	6.1	(4)
C94	0.4715	(5)	0.1893	(3)	−0.02633	(20)	4.9	(3)
C95	0.4633	(8)	0.3665	(4)	0.0134	(2)	8.1	(5)
C96	0.3662	(9)	0.4151	(5)	0.0179	(4)	11.9	(6)
C97	0.5374	(11)	0.3588	(5)	0.0566	(3)	12.7	(7)
C98	−0.0428	(4)	−0.1258	(3)	0.01852	(19)	5.0	(3)
C99	−0.0105	(5)	−0.0791	(3)	0.05055	(18)	3.8	(3)
C100	−0.0784	(4)	−0.0368	(3)	0.07401	(19)	4.1	(3)
C101	−0.0063	(4)	−0.0019	(3)	0.09853	(18)	3.7	(3)
C102	−0.0357	(4)	0.0538	(3)	0.12560	(17)	4.0	(3)
C103	−0.1467	(5)	0.0544	(4)	0.14840	(19)	4.9	(3)
C104	−0.1784	(6)	0.1102	(4)	0.1706	(2)	5.7	(4)
C105	−0.1035	(6)	0.1670	(4)	0.1721	(2)	5.7	(4)
C106	0.0067	(6)	0.1663	(3)	0.1504	(2)	5.4	(3)
C107	0.0392	(5)	0.1113	(3)	0.12758	(19)	4.5	(3)
C108	−0.1425	(8)	0.2269	(5)	0.1948	(3)	9.1	(5)
C109	−0.2005	(19)	0.2843	(7)	0.1627	(6)	28.8	(16)
C110	−0.1503	(15)	0.2028	(7)	0.2460	(4)	21.0	(12)

Table A.3. Bond Lengths (Å)and Angles (deg)

ZN1–O1	2.117(3)	C46–H46C	0.980(5)
ZN1–O2	1.990(3)	C47–C48	1.371(8)
ZN1–N1	2.148(4)	C48–C49	1.402(7)
ZN1–N3	2.066(4)	C49–C50	1.461(8)
ZN1–N5	2.040(4)	C50–C51	1.408(8)
ZN2–O3	2.123(3)	C50–C55	1.386(8)
ZN2–O4	1.985(3)	C51–C52	1.387(10)
ZN2–N7	2.046(4)	C51–H51	0.950(6)
ZN2–N9	2.155(4)	C52–C53	1.378(10)
ZN2–N11	2.059(4)	C52–H52	0.950(6)
O1–C1	1.263(7)	C53–C54	1.414(9)
O2–C2	1.290(6)	C53–C56	1.502(10)
O3–C20	1.281(6)	C54–C55	1.349(9)
O4–C19	1.284(6)	C54–H54	0.950(6)
B1–N2	1.571(7)	C55–H55	0.950(5)
B1–N4	1.561(7)	C56–C57	1.417(14)
B1–N6	1.553(7)	C56–C58	1.515(13)
B1–H1	1.120(6)	C56–H56	1.000(8)
N1–N2	1.374(6)	C57–H57A	0.980(9)
N1–C36	1.354(7)	C57–H57B	0.980(14)
N2–C34	1.365(7)	C57–H57C	0.980(14)
N3–N4	1.364(6)	C58–H58A	0.980(10)
N3–C49	1.333(6)	C58–H58B	0.980(9)
N4–C47	1.353(6)	C58–H58C	0.980(14)
N5–N6	1.388(5)	C59–C60	1.505(7)
N5–C62	1.344(6)	C59–H59A	0.980(5)
N6–C60	1.346(7)	C59–H59B	0.980(5)
B2–N8	1.554(7)	C59–H59C	0.980(5)
B2–N10	1.546(7)	C60–C61	1.387(7)
B2–N12	1.549(7)	C61–C62	1.402(7)
B2–H2	1.120(6)	C61–H61	0.950(5)
N7–N8	1.378(6)	C62–C63	1.466(7)
N7–C75	1.361(7)	C63–C64	1.389(7)
N8–C73	1.351(7)	C63–C68	1.396(7)
N9–N10	1.368(6)	C64–C65	1.392(7)
N9–C88	1.338(6)	C64–H64	0.950(4)
N10–C86	1.377(6)	C65–C66	1.399(7)
N11–N12	1.370(6)	C66–C67	1.376(7)
N11–C101	1.345(7)	C66–C69	1.521(7)
N12–C99	1.352(6)	C67–C68	1.398(7)
C1–C2	1.479(7)	C67–H67	0.950(5)
C1–C6	1.436(7)	C68–H68	0.950(5)
C2–C3	1.391(7)	C69–C70	1.519(8)
C3–C4	1.370(7)	C69–C71	1.535(7)
C3–H3	0.950(5)	C69–H69	1.000(5)
C4–C5	1.442(8)	C70–H70A	0.980(5)
C4–C11	1.480(8)	C70–H70B	0.980(6)
C5–C6	1.378(8)	C70–H70C	0.980(5)
C5–H5	0.950(5)	C71–H71A	0.980(6)
C6–C7	1.519(7)	C71–H71B	0.980(5)
C7–C8	1.543(8)	C71–H71C	0.980(5)
C7–C9	1.526(8)	C72–C73	1.507(8)
C7–C10	1.530(8)	C72–H72A	0.980(5)
C8–H8A	0.980(5)	C72–H72B	0.980(6)

C8–H8B	0.980(5)	C72–H72C	0.980(6)
C8–H8C	0.980(5)	C73–C74	1.383(8)
C9–H9A	0.980(6)	C74–C75	1.390(8)
C9–H9B	0.980(7)	C74–H74	0.950(5)
C9–H9C	0.980(7)	C75–C76	1.476(7)
C10–H10A	0.980(6)	C76–C77	1.395(7)
C10–H10B	0.980(6)	C76–C81	1.397(7)
C10–H10C	0.980(5)	C77–C78	1.398(8)
C11–C12	1.401(8)	C77–H77	0.950(5)
C11–C16	1.402(8)	C78–C79	1.374(8)
C12–C13	1.365(9)	C78–H78	0.950(5)
C12–H12	0.950(6)	C79–C80	1.398(7)
C13–C14	1.402(9)	C79–C82	1.509(7)
C13–C27	1.484(9)	C80–C81	1.373(7)
C14–C15	1.416(7)	C80–H80	0.950(5)
C14–H14	0.950(5)	C81–H81	0.950(5)
C15–C16	1.376(8)	C82–C83	1.536(8)
C15–C17	1.489(8)	C82–C84	1.505(8)
C16–H16	0.950(5)	C82–H82	1.000(5)
C17–C18	1.372(7)	C83–H83A	0.980(6)
C17–C22	1.433(8)	C83–H83B	0.980(5)
C18–C19	1.401(7)	C83–H83C	0.980(6)
C18–H18	0.950(5)	C84–H84A	0.980(5)
C19–C20	1.462(7)	C84–H84B	0.980(6)
C20–C21	1.434(7)	C84–H84C	0.980(6)
C21–C22	1.372(8)	C85–C86	1.483(8)
C21–C23	1.533(7)	C85–H85A	0.980(5)
C22–H22	0.950(5)	C85–H85B	0.980(5)
C23–C24	1.542(7)	C85–H85C	0.980(5)
C23–C25	1.526(8)	C86–C87	1.377(8)
C23–C26	1.541(8)	C87–C88	1.393(8)
C24–H24A	0.980(6)	C87–H87	0.950(5)
C24–H24B	0.980(7)	C88–C89	1.471(8)
C24–H24C	0.980(6)	C89–C90	1.382(8)
C25–H25A	0.980(5)	C89–C94	1.395(8)
C25–H25B	0.980(5)	C90–C91	1.394(8)
C25–H25C	0.980(6)	C90–H90	0.950(5)
C26–H26A	0.980(6)	C91–C92	1.411(10)
C26–H26B	0.980(5)	C91–H91	0.950(6)
C26–H26C	0.980(6)	C92–C93	1.360(11)
C27–C28	1.367(15)	C92–C95	1.501(10)
C27–C32	1.335(16)	C93–C94	1.342(10)
C28–C29	1.425(13)	C93–H93	0.950(6)
C28–H28	0.950(11)	C94–H94	0.950(6)
C29–C30	1.37(2)	C95–C96	1.450(14)
C29–H29	0.950(12)	C95–C97	1.566(13)
C30–C31	1.33(3)	C95–H95	1.000(7)
C30–H30	0.950(11)	C96–H96A	0.980(9)
C31–C32	1.427(13)	C96–H96B	0.980(9)
C31–H31	0.950(15)	C96–H96C	0.980(12)
C32–H32	0.950(11)	C97–H97A	0.980(12)
C33–C34	1.502(8)	C97–H97B	0.980(10)
C33–H33A	0.980(5)	C97–H97C	0.980(8)
C33–H33B	0.980(5)	C98–C99	1.483(8)
C33–H33C	0.980(5)	C98–H98A	0.980(6)
C34–C35	1.377(8)	C98–H98B	0.980(5)
C35–C36	1.389(8)	C98–H98C	0.980(5)

C35-H35	0.950(5)	C99-C100	1.364(9)
C36-C37	1.461(8)	C100-C101	1.395(8)
C37-C38	1.381(8)	C100-H100	0.950(5)
C37-C42	1.390(8)	C101-C102	1.463(9)
C38-C39	1.370(9)	C102-C103	1.407(8)
C38-H38	0.950(5)	C102-C107	1.396(9)
C39-C40	1.391(10)	C103-C104	1.375(11)
C39-H39	0.950(6)	C103-H103	0.950(6)
C40-C41	1.389(12)	C104-C105	1.383(12)
C40-C43	1.508(10)	C104-H104	0.950(6)
C41-C42	1.347(10)	C105-C106	1.386(10)
C41-H41	0.950(6)	C105-C108	1.469(11)
C42-H42	0.950(6)	C106-C107	1.376(9)
C43-C44	1.311(19)	C106-H106	0.950(6)
C43-C45	1.522(15)	C107-H107	0.950(6)
C43-H43	1.000(8)	C108-C109	1.451(20)
C44-H44A	0.980(10)	C108-C110	1.468(15)
C44-H44B	0.980(18)	C108-H108	1.000(9)
C44-H44C	0.980(12)	C109-H109A	0.980(13)
C45-H45A	0.980(9)	C109-H109B	0.980(16)
C45-H45B	0.980(10)	C109-H109C	0.98(2)
C45-H45C	0.980(8)	C110-H110A	0.980(10)
C46-C47	1.488(8)	C110-H110B	0.980(17)
C46-H46A	0.980(6)	C110-H110C	0.980(17)
C46-H46B	0.980(5)		

O1-ZN1-O2	79.88(13)	H46A-C46-H46C	109.5(5)
O1-ZN1-N1	168.49(14)	H46B-C46-H46C	109.5(5)
O1-ZN1-N3	94.77(14)	N4-C47-C46	122.5(5)
O1-ZN1-N5	98.22(14)	N4-C47-C48	107.9(4)
O2-ZN1-N1	93.90(14)	C46-C47-C48	129.6(4)
O2-ZN1-N3	142.29(14)	C47-C48-C49	105.8(4)
O2-ZN1-N5	120.00(13)	N3-C49-C48	109.5(5)
N1-ZN1-N3	84.19(15)	N3-C49-C50	122.9(5)
N1-ZN1-N5	93.28(15)	C48-C49-C50	127.4(5)
N3-ZN1-N5	97.69(15)	C49-C50-C51	119.6(5)
O3-ZN2-O4	79.48(13)	C49-C50-C55	122.9(5)
O3-ZN2-N7	97.36(14)	C51-C50-C55	117.3(5)
O3-ZN2-N9	169.92(14)	C50-C51-C52	119.7(5)
O3-ZN2-N11	95.26(14)	C50-C51-H51	119.7(6)
O4-ZN2-N7	121.30(14)	C52-C51-H51	120.5(6)
O4-ZN2-N9	94.68(14)	C51-C52-C53	122.5(5)
O4-ZN2-N11	140.97(15)	C51-C52-H52	118.5(7)
N7-ZN2-N9	92.69(15)	C53-C52-H52	119.0(7)
N7-ZN2-N11	97.70(16)	C52-C53-C54	116.8(6)
N9-ZN2-N11	84.09(15)	C52-C53-C56	121.5(6)
ZN1-O1-C1	111.4(3)	C54-C53-C56	121.7(6)
ZN1-O2-C2	114.6(3)	C53-C54-C55	121.0(6)
ZN2-O3-C20	111.7(3)	C53-C54-H54	119.3(7)
ZN2-O4-C19	114.7(3)	C55-C54-H54	119.7(6)
N2-B1-N4	107.3(4)	C50-C55-C54	122.6(5)
N2-B1-N6	109.6(4)	C50-C55-H55	118.8(6)
N2-B1-H1	110.8(4)	C54-C55-H55	118.6(6)
N4-B1-N6	108.1(4)	C53-C56-C57	113.7(7)
N4-B1-H1	110.5(4)	C53-C56-C58	109.2(7)

N6-B1-H1	110.5(5)	C53-C56-H56	103.3(6)
ZN1-N1-N2	109.4(3)	C57-C56-C58	124.6(8)
ZN1-N1-C36	141.5(3)	C57-C56-H56	100.9(9)
N2-N1-C36	106.3(4)	C58-C56-H56	101.6(7)
B1-N2-N1	119.9(4)	C56-C57-H57A	111.0(11)
B1-N2-C34	129.1(4)	C56-C57-H57B	110.4(10)
N1-N2-C34	110.3(4)	C56-C57-H57C	106.9(11)
ZN1-N3-N4	113.0(3)	H57A-C57-H57B	109.5(13)
ZN1-N3-C49	139.7(4)	H57A-C57-H57C	109.5(11)
N4-N3-C49	107.1(4)	H57B-C57-H57C	109.5(12)
B1-N4-N3	121.2(4)	C56-C58-H58A	110.0(8)
B1-N4-C47	129.1(4)	C56-C58-H58B	110.7(11)
N3-N4-C47	109.7(4)	C56-C58-H58C	107.7(9)
ZN1-N5-N6	111.4(3)	H58A-C58-H58B	109.5(10)
ZN1-N5-C62	136.8(3)	H58A-C58-H58C	109.5(12)
N6-N5-C62	105.6(4)	H58B-C58-H58C	109.5(9)
B1-N6-N5	120.0(4)	C60-C59-H59A	109.2(4)
B1-N6-C60	129.4(4)	C60-C59-H59B	109.8(5)
N5-N6-C60	110.5(4)	C60-C59-H59C	109.4(4)
N8-B2-N10	109.3(4)	H59A-C59-H59B	109.5(5)
N8-B2-N12	108.5(4)	H59A-C59-H59C	109.5(5)
N8-B2-H2	110.1(5)	H59B-C59-H59C	109.5(5)
N10-B2-N12	108.4(4)	N6-C60-C59	122.7(4)
N10-B2-H2	110.2(4)	N6-C60-C61	107.7(4)
N12-B2-H2	110.2(5)	C59-C60-C61	129.5(5)
ZN2-N7-N8	111.6(3)	C60-C61-C62	105.7(4)
ZN2-N7-C75	136.8(3)	C60-C61-H61	127.2(5)
N8-N7-C75	106.0(4)	C62-C61-H61	127.1(5)
B2-N8-N7	119.9(4)	N5-C62-C61	110.4(4)
B2-N8-C73	130.3(4)	N5-C62-C63	120.4(4)
N7-N8-C73	109.9(4)	C61-C62-C63	129.2(4)
ZN2-N9-N10	109.2(3)	C62-C63-C64	121.8(4)
ZN2-N9-C88	140.8(3)	C62-C63-C68	120.9(4)
N10-N9-C88	107.1(4)	C64-C63-C68	117.3(4)
B2-N10-N9	120.1(4)	C63-C64-C65	122.2(4)
B2-N10-C86	129.4(4)	C63-C64-H64	118.9(5)
N9-N10-C86	109.8(4)	C65-C64-H64	118.8(5)
ZN2-N11-N12	112.9(3)	C64-C65-C66	119.6(4)
ZN2-N11-C101	139.5(4)	C65-C66-C67	118.8(4)
N12-N11-C101	107.5(4)	C65-C66-C69	120.5(4)
B2-N12-N11	121.0(4)	C67-C66-C69	120.6(4)
B2-N12-C99	129.4(5)	C66-C67-C68	121.1(4)
N11-N12-C99	109.6(4)	C66-C67-H67	119.5(5)
O1-C1-C2	117.0(4)	C68-C67-H67	119.4(5)
O1-C1-C6	124.0(5)	C63-C68-C67	120.9(4)
C2-C1-C6	119.0(5)	C63-C68-H68	119.4(5)
O2-C2-C1	117.0(4)	C67-C68-H68	119.7(5)
O2-C2-C3	122.3(4)	C66-C69-C70	111.5(4)
C1-C2-C3	120.7(4)	C66-C69-C71	111.5(4)
C2-C3-C4	120.1(5)	C66-C69-H69	108.1(4)
C2-C3-H3	120.0(5)	C70-C69-C71	110.1(4)
C4-C3-H3	119.9(5)	C70-C69-H69	107.7(4)
C3-C4-C5	119.3(5)	C71-C69-H69	107.8(4)
C3-C4-C11	120.3(5)	C69-C70-H70A	109.4(5)
C5-C4-C11	120.2(5)	C69-C70-H70B	109.6(5)
C4-C5-C6	124.2(4)	C69-C70-H70C	109.4(5)
C4-C5-H5	117.9(6)	H70A-C70-H70B	109.5(5)

C6–C5–H5	117.9(6)	H70A–C70–H70C	109.5(5)
C1–C6–C5	116.7(5)	H70B–C70–H70C	109.5(5)
C1–C6–C7	120.6(5)	C69–C71–H71A	109.2(5)
C5–C6–C7	122.7(5)	C69–C71–H71B	109.8(5)
C6–C7–C8	108.7(4)	C69–C71–H71C	109.4(5)
C6–C7–C9	112.3(5)	H71A–C71–H71B	109.5(5)
C6–C7–C10	109.5(4)	H71A–C71–H71C	109.5(5)
C8–C7–C9	108.0(4)	H71B–C71–H71C	109.5(5)
C8–C7–C10	110.0(5)	C73–C72–H72A	109.2(5)
C9–C7–C10	108.3(5)	C73–C72–H72B	109.8(5)
C7–C8–H8A	109.4(4)	C73–C72–H72C	109.4(5)
C7–C8–H8B	109.7(5)	H72A–C72–H72B	109.5(5)
C7–C8–H8C	109.3(5)	H72A–C72–H72C	109.5(6)
H8A–C8–H8B	109.5(5)	H72B–C72–H72C	109.5(5)
H8A–C8–H8C	109.5(5)	N8–C73–C72	122.6(5)
H8B–C8–H8C	109.5(5)	N8–C73–C74	108.3(5)
C7–C9–H9A	109.3(6)	C72–C73–C74	129.1(5)
C7–C9–H9B	109.9(5)	C73–C74–C75	105.8(5)
C7–C9–H9C	109.2(5)	C73–C74–H74	127.2(6)
H9A–C9–H9B	109.5(6)	C75–C74–H74	126.9(6)
H9A–C9–H9C	109.5(6)	N7–C75–C74	110.0(4)
H9B–C9–H9C	109.5(6)	N7–C75–C76	120.6(5)
C7–C10–H10A	109.1(5)	C74–C75–C76	129.3(5)
C7–C10–H10B	109.6(5)	C75–C76–C77	119.4(5)
C7–C10–H10C	109.7(5)	C75–C76–C81	122.6(5)
H10A–C10–H10B	109.5(5)	C77–C76–C81	118.0(5)
H10A–C10–H10C	109.5(6)	C76–C77–C78	120.4(5)
H10B–C10–H10C	109.5(5)	C76–C77–H77	119.7(5)
C4–C11–C12	119.9(5)	C78–C77–H77	119.9(5)
C4–C11–C16	122.2(4)	C77–C78–C79	121.8(5)
C12–C11–C16	117.9(5)	C77–C78–H78	119.2(5)
C11–C12–C13	122.6(5)	C79–C78–H78	119.0(5)
C11–C12–H12	118.8(6)	C78–C79–C80	117.0(5)
C13–C12–H12	118.6(6)	C78–C79–C82	120.9(4)
C12–C13–C14	118.6(5)	C80–C79–C82	122.0(5)
C12–C13–C27	120.8(6)	C79–C80–C81	122.4(5)
C14–C13–C27	120.6(6)	C79–C80–H80	118.7(5)
C13–C14–C15	120.6(5)	C81–C80–H80	118.9(5)
C13–C14–H14	119.4(5)	C76–C81–C80	120.4(4)
C15–C14–H14	120.0(6)	C76–C81–H81	119.7(5)
C14–C15–C16	118.9(5)	C80–C81–H81	120.0(5)
C14–C15–C17	118.6(5)	C79–C82–C83	113.0(4)
C16–C15–C17	122.6(4)	C79–C82–C84	111.0(4)
C11–C16–C15	121.4(5)	C79–C82–H82	107.5(4)
C11–C16–H16	119.1(5)	C83–C82–C84	110.4(5)
C15–C16–H16	119.4(5)	C83–C82–H82	107.2(5)
C15–C17–C18	121.2(5)	C84–C82–H82	107.4(5)
C15–C17–C22	119.4(4)	C82–C83–H83A	109.5(5)
C18–C17–C22	119.4(5)	C82–C83–H83B	109.6(5)
C17–C18–C19	120.8(5)	C82–C83–H83C	109.3(5)
C17–C18–H18	119.8(5)	H83A–C83–H83B	109.5(6)
C19–C18–H18	119.5(5)	H83A–C83–H83C	109.5(5)
O4–C19–C18	122.9(4)	H83B–C83–H83C	109.5(6)
O4–C19–C20	118.4(4)	C82–C84–H84A	109.8(5)
C18–C19–C20	118.7(4)	C82–C84–H84B	109.1(5)
O3–C20–C19	115.7(4)	C82–C84–H84C	109.5(5)
O3–C20–C21	123.4(5)	H84A–C84–H84B	109.5(6)

C19-C20-C21	120.9(5)	H84A-C84-H84C	109.5(6)
C20-C21-C22	116.2(5)	H84B-C84-H84C	109.5(6)
C20-C21-C23	119.8(5)	C86-C85-H85A	109.1(4)
C22-C21-C23	124.0(4)	C86-C85-H85B	109.6(5)
C17-C22-C21	123.9(4)	C86-C85-H85C	109.7(5)
C17-C22-H22	118.2(6)	H85A-C85-H85B	109.5(5)
C21-C22-H22	117.9(5)	H85A-C85-H85C	109.5(5)
C21-C23-C24	111.6(5)	H85B-C85-H85C	109.5(5)
C21-C23-C25	110.2(4)	N10-C86-C85	123.2(5)
C21-C23-C26	109.8(4)	N10-C86-C87	106.4(4)
C24-C23-C25	107.5(4)	C85-C86-C87	130.4(5)
C24-C23-C26	107.8(4)	C86-C87-C88	107.2(4)
C25-C23-C26	109.9(5)	C86-C87-H87	126.6(6)
C23-C24-H24A	110.0(5)	C88-C87-H87	126.2(6)
C23-C24-H24B	108.8(5)	N9-C88-C87	109.5(5)
C23-C24-H24C	109.6(5)	N9-C88-C89	121.8(5)
H24A-C24-H24B	109.5(6)	C87-C88-C89	128.5(5)
H24A-C24-H24C	109.5(6)	C88-C89-C90	121.9(5)
H24B-C24-H24C	109.5(5)	C88-C89-C94	121.1(5)
C23-C25-H25A	109.6(5)	C90-C89-C94	117.0(5)
C23-C25-H25B	109.7(5)	C89-C90-C91	120.9(5)
C23-C25-H25C	109.2(5)	C89-C90-H90	119.5(5)
H25A-C25-H25B	109.5(5)	C91-C90-H90	119.6(6)
H25A-C25-H25C	109.5(5)	C90-C91-C92	119.8(6)
H25B-C25-H25C	109.5(5)	C90-C91-H91	119.8(7)
C23-C26-H26A	109.8(5)	C92-C91-H91	120.5(6)
C23-C26-H26B	109.2(5)	C91-C92-C93	117.9(6)
C23-C26-H26C	109.4(5)	C91-C92-C95	122.1(7)
H26A-C26-H26B	109.5(5)	C93-C92-C95	119.9(6)
H26A-C26-H26C	109.5(5)	C92-C93-C94	121.9(6)
H26B-C26-H26C	109.5(6)	C92-C93-H93	118.8(7)
C13-C27-C28	120.1(9)	C94-C93-H93	119.3(8)
C13-C27-C32	122.0(9)	C89-C94-C93	122.2(6)
C28-C27-C32	117.8(8)	C89-C94-H94	118.9(6)
C27-C28-C29	120.6(10)	C93-C94-H94	118.9(6)
C27-C28-H28	119.4(8)	C92-C95-C96	114.2(7)
C29-C28-H28	120.0(11)	C92-C95-C97	109.8(6)
C28-C29-C30	119.7(11)	C92-C95-H95	107.6(7)
C28-C29-H29	120.4(14)	C96-C95-C97	109.7(8)
C30-C29-H29	120.0(11)	C96-C95-H95	108.2(8)
C29-C30-C31	120.2(10)	C97-C95-H95	107.2(8)
C29-C30-H30	120.5(18)	C95-C96-H96A	109.7(9)
C31-C30-H30	119.4(18)	C95-C96-H96B	109.9(9)
C30-C31-C32	119.0(13)	C95-C96-H96C	108.8(8)
C30-C31-H31	120.1(11)	H96A-C96-H96B	109.5(9)
C32-C31-H31	120.9(14)	H96A-C96-H96C	109.5(10)
C27-C32-C31	122.8(11)	H96B-C96-H96C	109.5(10)
C27-C32-H32	118.9(8)	C95-C97-H97A	109.1(7)
C31-C32-H32	118.3(12)	C95-C97-H97B	109.0(10)
C34-C33-H33A	109.4(4)	C95-C97-H97C	110.2(8)
C34-C33-H33B	109.5(4)	H97A-C97-H97B	109.5(9)
C34-C33-H33C	109.5(5)	H97A-C97-H97C	109.5(11)
H33A-C33-H33B	109.5(5)	H97B-C97-H97C	109.5(9)
H33A-C33-H33C	109.5(5)	C99-C98-H98A	109.4(5)
H33B-C33-H33C	109.5(5)	C99-C98-H98B	109.5(5)
N2-C34-C33	122.7(5)	C99-C98-H98C	109.5(5)
N2-C34-C35	106.8(5)	H98A-C98-H98B	109.5(5)

C33-C34-C35	130.5(5)	H98A-C98-H98C	109.5(6)
C34-C35-C36	107.2(5)	H98B-C98-H98C	109.5(5)
C34-C35-H35	126.4(6)	N12-C99-C98	122.9(5)
C36-C35-H35	126.4(6)	N12-C99-C100	107.3(5)
N1-C36-C35	109.5(5)	C98-C99-C100	129.7(5)
N1-C36-C37	122.1(5)	C99-C100-C101	107.6(5)
C35-C36-C37	128.3(5)	C99-C100-H100	126.3(6)
C36-C37-C38	121.7(5)	C101-C100-H100	126.1(6)
C36-C37-C42	121.5(5)	N11-C101-C100	108.0(5)
C38-C37-C42	116.8(5)	N11-C101-C102	123.1(5)
C37-C38-C39	122.0(5)	C100-C101-C102	128.8(5)
C37-C38-H38	119.2(6)	C101-C102-C103	120.1(5)
C39-C38-H38	118.8(6)	C101-C102-C107	123.0(5)
C38-C39-C40	120.6(6)	C103-C102-C107	116.7(6)
C38-C39-H39	120.0(6)	C102-C103-C104	120.6(6)
C40-C39-H39	119.4(6)	C102-C103-H103	119.5(7)
C39-C40-C41	116.9(6)	C104-C103-H103	119.9(6)
C39-C40-C43	122.8(7)	C103-C104-C105	122.1(6)
C41-C40-C43	120.3(7)	C103-C104-H104	118.6(8)
C40-C41-C42	122.1(6)	C105-C104-H104	119.4(8)
C40-C41-H41	118.7(7)	C104-C105-C106	117.8(6)
C42-C41-H41	119.1(8)	C104-C105-C108	120.2(6)
C37-C42-C41	121.4(6)	C106-C105-C108	122.0(7)
C37-C42-H42	119.3(6)	C105-C106-C107	120.7(6)
C41-C42-H42	119.2(6)	C105-C106-H106	119.6(7)
C40-C43-C44	119.6(9)	C107-C106-H106	119.7(6)
C40-C43-C45	110.6(8)	C102-C107-C106	122.1(5)
C40-C43-H43	103.6(8)	C102-C107-H107	118.9(6)
C44-C43-C45	115.5(9)	C106-C107-H107	119.0(6)
C44-C43-H43	102.0(11)	C105-C108-C109	111.0(9)
C45-C43-H43	102.8(9)	C105-C108-C110	112.0(7)
C43-C44-H44A	111.5(14)	C105-C108-H108	97.8(7)
C43-C44-H44B	107.9(9)	C109-C108-C110	132.8(9)
C43-C44-H44C	109.1(13)	C109-C108-H108	94.9(11)
H44A-C44-H44B	109.5(14)	C110-C108-H108	97.7(10)
H44A-C44-H44C	109.5(10)	C108-C109-H109A	108.9(11)
H44B-C44-H44C	109.5(15)	C108-C109-H109B	113(2)
C43-C45-H45A	109.1(7)	C108-C109-H109C	105.8(12)
C43-C45-H45B	109.0(8)	H109A-C109-H109B	109.5(14)
C43-C45-H45C	110.3(9)	H109A-C109-H109C	109(2)
H45A-C45-H45B	109.5(10)	H109B-C109-H109C	109.5(12)
H45A-C45-H45C	109.5(9)	C108-C110-H110A	111.3(12)
H45B-C45-H45C	109.5(7)	C108-C110-H110B	109.4(10)
C47-C46-H46A	109.8(4)	C108-C110-H110C	107.7(13)
C47-C46-H46B	109.6(5)	H110A-C110-H110B	109.5(16)
C47-C46-H46C	109.0(5)	H110A-C110-H110C	109.5(12)
H46A-C46-H46B	109.5(5)	H110B-C110-H110C	109.5(13)

Table A.4 Table of u(i,j) or U values *100.
E.S.Ds. refer to the last digit printed

Atom	u11(U)	u22	u33	u12	u13	u23
ZN1	2.49(3)	3.49(4)	5.50(4)	-0.36(3)	-0.81(3)	-1.19(3)
ZN2	2.84(3)	5.58(4)	3.34(4)	0.27(3)	-0.78(3)	-0.56(3)
O1	3.13(20)	3.7 (2)	6.3 (2)	-0.01(16)	-0.93(18)	-1.68(18)
O2	2.89(19)	3.55(19)	5.4 (2)	0.14(15)	-0.56(16)	-2.05(18)
O3	3.13(20)	6.4 (2)	3.5 (2)	0.46(18)	-0.28(16)	-0.61(18)
O4	3.47(19)	5.5 (2)	2.8 (2)	0.55(17)	-0.41(15)	-0.94(17)
B1	4.1 (4)	3.5 (4)	5.3 (4)	-0.3 (3)	-1.7 (3)	-0.8 (3)
N1	2.5 (2)	4.1 (3)	4.6 (3)	-0.6 (2)	-0.57(20)	-1.3 (2)
N2	2.9 (2)	2.9 (3)	5.8 (3)	-0.4 (2)	-1.0 (2)	-0.7 (2)
N3	2.2 (2)	3.5 (2)	5.6 (3)	-0.08(19)	-0.7 (2)	-0.7 (2)
N4	2.9 (3)	3.7 (2)	5.8 (3)	-0.24(20)	-1.2 (2)	-1.3 (2)
N5	3.0 (2)	3.5 (3)	5.0 (3)	-0.3 (2)	-1.2 (2)	-1.1 (2)
N6	3.0 (2)	3.8 (3)	5.7 (3)	-0.3 (2)	-1.0 (2)	-0.9 (2)
B2	4.5 (4)	5.3 (4)	3.3 (4)	-0.6 (3)	-1.0 (3)	-0.6 (3)
N7	3.2 (2)	4.9 (3)	3.6 (3)	-0.2 (2)	-0.7 (2)	-0.5 (2)
N8	3.7 (3)	5.1 (3)	3.9 (3)	-0.3 (2)	-0.7 (2)	-0.6 (2)
N9	2.8 (2)	4.9 (3)	3.5 (3)	0.3 (2)	-0.99(20)	-0.6 (2)
N10	3.1 (2)	5.2 (3)	3.5 (3)	-0.1 (2)	-0.7 (2)	-0.7 (2)
N11	2.9 (3)	6.0 (3)	3.7 (3)	0.1 (2)	-0.7 (2)	-0.6 (2)
N12	2.5 (3)	6.3 (3)	4.0 (3)	-0.5 (2)	-1.08(20)	-0.9 (2)
C1	3.1 (3)	2.9 (3)	5.0 (4)	-0.8 (3)	0.8 (3)	-1.2 (3)
C2	3.0 (3)	2.9 (3)	4.0 (3)	-0.6 (3)	0.0 (3)	-0.8 (3)
C3	4.0 (3)	2.8 (3)	4.9 (4)	-0.1 (2)	0.8 (3)	-1.2 (3)
C4	6.6 (4)	3.6 (3)	3.9 (4)	-0.7 (3)	0.7 (3)	-0.8 (3)
C5	6.9 (4)	3.0 (3)	5.0 (4)	-0.1 (3)	1.6 (3)	-1.6 (3)
C6	4.0 (3)	3.7 (3)	5.1 (4)	-0.2 (3)	0.5 (3)	-0.7 (3)
C7	4.7 (4)	3.0 (3)	8.2 (4)	0.6 (3)	-0.6 (3)	-2.2 (3)
C8	4.9 (4)	3.7 (3)	8.1 (4)	0.4 (3)	-1.2 (3)	0.1 (3)
C9	8.8 (5)	4.9 (4)	10.0 (5)	1.7 (4)	-0.7 (4)	-2.1 (4)
C10	4.0 (4)	4.7 (4)	12.5 (5)	1.2 (3)	0.0 (3)	-1.6 (4)
C11	8.3 (4)	3.4 (3)	3.5 (3)	0.4 (3)	0.3 (3)	-0.8 (3)
C12	13.5 (6)	4.1 (4)	3.6 (4)	-0.8 (4)	0.4 (4)	-1.5 (3)
C13	15.5 (7)	3.7 (4)	3.4 (4)	1.3 (4)	-0.7 (4)	-0.4 (3)
C14	12.1 (6)	4.6 (4)	3.1 (3)	0.6 (4)	-0.6 (3)	-0.8 (3)
C15	8.2 (4)	3.4 (3)	3.4 (4)	0.9 (3)	0.6 (3)	-0.5 (3)
C16	7.5 (4)	3.8 (3)	2.6 (3)	0.7 (3)	-0.5 (3)	-0.3 (3)
C17	6.2 (4)	4.6 (3)	2.6 (3)	1.6 (3)	-0.6 (3)	-0.1 (3)
C18	4.8 (3)	4.7 (3)	3.1 (3)	1.2 (3)	-0.4 (3)	-0.6 (3)
C19	3.4 (3)	5.2 (3)	2.2 (3)	0.7 (3)	-0.5 (2)	-0.6 (3)
C20	3.2 (3)	4.9 (3)	4.0 (4)	1.2 (3)	-1.1 (3)	-1.0 (3)
C21	4.4 (3)	6.3 (4)	2.5 (3)	2.1 (3)	-0.1 (3)	-0.8 (3)
C22	6.9 (4)	5.1 (4)	3.1 (3)	1.5 (3)	-0.7 (3)	-1.0 (3)
C23	4.7 (4)	6.8 (4)	3.8 (3)	1.1 (3)	-0.2 (3)	-0.6 (3)
C24	9.7 (5)	7.9 (4)	3.9 (4)	-0.4 (4)	1.3 (3)	-1.1 (3)
C25	5.6 (4)	6.8 (4)	4.5 (3)	-0.3 (3)	-0.3 (3)	0.4 (3)
C26	5.6 (4)	9.6 (5)	4.5 (4)	0.5 (4)	1.6 (3)	-0.1 (3)
C27	20.7 (10)	4.6 (5)	3.7 (4)	-0.2 (6)	0.0 (5)	-0.9 (4)
C28	26.1 (13)	5.3 (5)	6.3 (5)	-3.6 (7)	0.8 (6)	-0.3 (4)
C29	27.9 (16)	7.4 (7)	8.8 (7)	-4.9 (8)	1.7 (8)	-1.2 (6)
C30	36. (3)	7.2 (8)	6.6 (7)	4.1 (10)	-0.6 (10)	0.0 (6)
C31	35. (2)	7.2 (8)	6.8 (6)	4.9 (9)	2.7 (9)	0.2 (6)

C32	28.6 (14)	6.1 (6)	4.3 (5)	5.8 (7)	-1.3 (6)	-0.1 (4)
C33	4.2 (3)	5.2 (3)	6.3 (4)	0.1 (3)	-0.1 (3)	-2.6 (3)
C34	2.2 (3)	3.6 (3)	6.7 (4)	-0.6 (3)	0.4 (3)	-1.2 (3)
C35	2.7 (3)	3.6 (3)	6.2 (4)	-0.3 (2)	-0.8 (3)	-0.7 (3)
C36	1.6 (3)	2.9 (3)	5.4 (4)	-0.4 (2)	-0.7 (2)	-0.5 (3)
C37	2.3 (3)	3.2 (3)	6.0 (4)	-0.6 (3)	-0.5 (3)	-0.7 (3)
C38	4.8 (3)	4.2 (3)	5.2 (4)	-0.4 (3)	-2.1 (3)	-0.5 (3)
C39	7.1 (4)	5.7 (4)	5.9 (5)	0.3 (4)	-1.8 (3)	-0.5 (3)
C40	9.6 (6)	8.4 (5)	5.8 (5)	0.4 (5)	-4.0 (4)	0.3 (4)
C41	5.3 (4)	6.7 (4)	8.5 (6)	0.8 (3)	-1.6 (4)	1.2 (4)
C42	3.9 (3)	5.0 (4)	6.1 (4)	0.2 (3)	-0.6 (3)	0.7 (3)
C43	16.9 (10)	11.9 (7)	8.6 (7)	3.7 (7)	-6.3 (7)	-0.3 (6)
C44	28.8 (17)	33.7 (18)	4.8 (6)	-17.0 (14)	-2.4 (8)	5.0 (8)
C45	15.0 (8)	20.3 (10)	6.2 (5)	1.0 (8)	-3.3 (5)	-4.8 (6)
C46	3.4 (3)	6.0 (4)	8.4 (4)	-0.9 (3)	-2.6 (3)	-1.3 (3)
C47	2.8 (3)	3.7 (3)	6.6 (4)	-0.5 (3)	-2.1 (3)	-0.5 (3)
C48	3.8 (3)	3.6 (3)	6.1 (4)	-0.5 (3)	-1.6 (3)	0.1 (3)
C49	3.4 (3)	3.1 (3)	5.4 (4)	0.0 (3)	0.1 (3)	-0.3 (3)
C50	2.4 (3)	3.2 (3)	7.3 (4)	-0.3 (3)	-0.5 (3)	0.0 (3)
C51	3.8 (4)	4.7 (4)	7.8 (5)	-0.2 (3)	-0.1 (3)	-0.8 (3)
C52	4.1 (4)	4.7 (4)	8.8 (5)	0.4 (3)	0.1 (4)	-0.2 (4)
C53	6.9 (5)	4.4 (4)	6.2 (4)	0.1 (3)	1.6 (4)	-0.4 (3)
C54	5.9 (4)	5.1 (4)	7.4 (5)	0.4 (3)	-0.9 (4)	-0.3 (3)
C55	4.4 (3)	4.3 (3)	6.4 (4)	0.2 (3)	0.0 (3)	-0.9 (3)
C56	9.8 (6)	7.8 (5)	9.7 (6)	2.0 (5)	1.6 (5)	-0.7 (5)
C57	30.2 (16)	17.3 (11)	15.1 (9)	4.5 (11)	9.5 (10)	-7.7 (8)
C58	22.5 (12)	16.0 (9)	15.4 (9)	-1.8 (9)	13.1 (9)	-2.2 (7)
C59	4.5 (3)	4.6 (3)	5.8 (4)	-0.6 (3)	-1.5 (3)	0.2 (3)
C60	3.7 (3)	3.5 (3)	5.0 (4)	0.0 (3)	-0.7 (3)	0.0 (3)
C61	3.5 (3)	3.6 (3)	5.8 (4)	-0.6 (3)	-0.8 (3)	-0.2 (3)
C62	2.9 (3)	3.1 (3)	5.3 (4)	-0.2 (2)	-0.5 (3)	-0.8 (3)
C63	2.8 (3)	3.1 (3)	4.8 (3)	-0.2 (2)	-0.4 (3)	-0.7 (3)
C64	2.8 (3)	2.5 (3)	5.1 (3)	-0.3 (2)	-0.1 (3)	-0.4 (3)
C65	2.5 (3)	3.3 (3)	5.9 (3)	-0.3 (2)	0.6 (2)	-1.3 (3)
C66	2.0 (3)	3.5 (3)	5.4 (4)	-0.2 (2)	-0.4 (2)	-1.1 (3)
C67	3.7 (3)	3.0 (3)	5.5 (4)	-0.6 (2)	-1.1 (3)	-0.6 (3)
C68	3.5 (3)	4.3 (3)	4.5 (3)	-0.4 (3)	-0.5 (2)	-0.1 (3)
C69	4.1 (3)	3.3 (3)	6.3 (4)	-0.1 (3)	-1.6 (3)	-1.1 (3)
C70	7.5 (4)	5.3 (4)	6.3 (4)	-0.4 (3)	-1.9 (3)	-1.7 (3)
C71	4.9 (4)	4.3 (3)	8.8 (4)	-0.6 (3)	-2.5 (3)	-0.9 (3)
C72	6.3 (4)	5.3 (4)	7.3 (4)	-0.9 (3)	-2.3 (3)	-0.4 (3)
C73	4.2 (3)	5.2 (4)	5.6 (4)	0.1 (3)	-0.9 (3)	-0.9 (3)
C74	5.6 (4)	4.5 (4)	4.9 (4)	0.6 (3)	-1.5 (3)	-0.1 (3)
C75	3.6 (3)	5.4 (4)	3.7 (3)	0.6 (3)	-0.2 (3)	-0.7 (3)
C76	3.4 (3)	5.4 (4)	3.5 (3)	1.3 (3)	-0.8 (2)	-0.9 (3)
C77	4.3 (3)	5.2 (3)	4.4 (4)	0.9 (3)	-1.3 (3)	-0.5 (3)
C78	4.8 (3)	5.2 (4)	4.0 (3)	1.1 (3)	-1.1 (3)	0.2 (3)
C79	3.3 (3)	4.7 (3)	4.1 (3)	1.0 (3)	-0.8 (2)	-0.4 (3)
C80	3.2 (3)	5.0 (3)	4.1 (3)	0.8 (3)	-0.5 (3)	-0.6 (3)
C81	3.0 (3)	4.4 (3)	3.8 (3)	0.6 (3)	-0.6 (2)	0.1 (3)
C82	5.2 (4)	5.3 (4)	4.2 (3)	0.2 (3)	-1.5 (3)	-0.4 (3)
C83	4.7 (4)	12.1 (6)	5.5 (4)	-0.5 (4)	-1.6 (3)	-2.0 (4)
C84	7.2 (4)	7.9 (4)	6.5 (4)	0.6 (4)	-1.8 (3)	-2.7 (4)
C85	4.7 (3)	8.2 (4)	3.8 (3)	0.0 (3)	-0.5 (3)	-1.8 (3)
C86	2.4 (3)	6.4 (4)	3.4 (3)	0.4 (3)	-0.8 (2)	-0.9 (3)
C87	2.9 (3)	6.5 (4)	3.2 (3)	0.7 (3)	-0.8 (2)	0.1 (3)
C88	2.2 (3)	5.6 (4)	3.4 (3)	0.4 (3)	-1.3 (2)	-0.3 (3)

C89	3.2 (3)	6.0 (4)	3.6 (3)	0.0 (3)	-1.2 (3)	0.4 (3)
C90	5.9 (4)	5.7 (4)	3.6 (3)	-0.9 (3)	-1.2 (3)	-0.4 (3)
C91	11.8 (6)	6.0 (4)	4.5 (4)	-0.8 (4)	-1.1 (4)	-1.1 (3)
C92	10.3 (6)	4.2 (4)	6.4 (4)	-2.6 (4)	-1.8 (4)	0.7 (3)
C93	7.1 (5)	5.5 (5)	9.5 (5)	-0.5 (4)	0.0 (4)	0.1 (4)
C94	5.0 (4)	5.7 (4)	6.9 (4)	0.2 (3)	-0.5 (3)	1.0 (3)
C95	13.9 (8)	9.4 (6)	7.5 (5)	-3.2 (6)	0.1 (5)	-2.1 (4)
C96	14.7 (9)	8.1 (6)	21.6 (11)	-2.5 (6)	7.4 (8)	-3.8 (6)
C97	28.3 (14)	10.8 (7)	9.7 (7)	-6.4 (8)	-4.5 (8)	-2.0 (5)
C98	3.8 (3)	8.9 (5)	5.9 (4)	-1.9 (3)	-1.6 (3)	-0.3 (3)
C99	3.4 (3)	6.3 (4)	4.2 (3)	-1.2 (3)	-1.0 (3)	0.5 (3)
C100	2.6 (3)	7.1 (4)	5.2 (4)	-0.4 (3)	-0.9 (3)	0.3 (3)
C101	2.7 (3)	6.5 (4)	4.2 (3)	-0.1 (3)	-0.6 (3)	0.5 (3)
C102	3.3 (3)	7.2 (4)	4.0 (3)	1.3 (3)	-0.4 (3)	0.1 (3)
C103	4.4 (4)	8.8 (5)	4.6 (4)	0.8 (3)	-0.5 (3)	0.3 (3)
C104	6.0 (4)	8.8 (5)	5.6 (4)	2.7 (4)	0.6 (3)	0.2 (4)
C105	8.1 (5)	6.8 (5)	5.9 (4)	2.7 (4)	1.7 (4)	-0.3 (4)
C106	7.1 (5)	6.2 (4)	6.9 (4)	0.7 (4)	0.4 (4)	-1.1 (4)
C107	4.7 (4)	6.5 (4)	5.1 (4)	0.7 (3)	-1.0 (3)	0.6 (3)
C108	13.7 (8)	9.0 (6)	10.7 (7)	3.5 (6)	2.5 (6)	-0.7 (5)
C109	59. (3)	15.6 (11)	27.5 (17)	20.8 (17)	21.3 (19)	1.2 (11)
C110	43. (2)	21.4 (13)	14.3 (10)	11.1 (14)	10.8 (12)	-7.6 (9)

Table A.5. Hydrogen coordinates (10^4) and isotropic displacement parameters ($Å^3$).
E.S.Ds. refer to the last digit printed.

Atom	x	y	z	Biso
H1	0.792	0.418	0.595	4.2
H2	0.191	-0.144	0.021	4.2
H3	0.547	0.362	0.341	3.9
H5	0.681	0.162	0.333	4.7
H8A	0.760	0.127	0.477	5.2
H8B	0.809	0.049	0.471	5.2
H8C	0.681	0.073	0.458	5.2
H9A	0.853	0.027	0.391	7.0
H9B	0.833	0.090	0.346	7.0
H9C	0.724	0.052	0.379	7.0
H10A	0.935	0.189	0.426	6.3
H10B	0.962	0.174	0.375	6.3
H10C	0.979	0.109	0.420	6.3
H12	0.597	0.380	0.259	6.4
H14	0.430	0.294	0.168	6.0
H16	0.502	0.164	0.293	4.4
H18	0.464	0.178	0.148	4.1
H22	0.320	0.113	0.281	4.8
H24A	0.155	0.070	0.322	6.4
H24B	0.255	0.011	0.335	6.4
H24C	0.122	-0.014	0.346	6.4
H25A	0.219	-0.095	0.251	5.3
H25B	0.162	-0.113	0.304	5.3

H25C	0.294	-0.087	0.293	5.3
H26A	0.031	0.060	0.256	6.0
H26B	0.003	-0.023	0.283	6.0
H26C	0.054	-0.005	0.229	6.0
H28	0.690	0.442	0.182	10.7
H29	0.699	0.561	0.131	12.4
H30	0.534	0.610	0.095	14.0
H31	0.367	0.542	0.107	13.7
H32	0.362	0.423	0.158	11.0
H33A	0.680	0.499	0.610	4.9
H33B	0.565	0.546	0.599	4.9
H33C	0.689	0.586	0.587	4.9
H35	0.581	0.613	0.494	4.1
H38	0.755	0.482	0.393	4.6
H39	0.729	0.513	0.315	5.7
H41	0.491	0.662	0.338	6.2
H42	0.513	0.629	0.416	4.7
H43	0.553	0.663	0.262	10.6
H44A	0.645	0.635	0.203	18.5
H44B	0.712	0.574	0.239	18.5
H44C	0.722	0.659	0.240	18.5
H45A	0.421	0.565	0.282	11.7
H45B	0.506	0.519	0.254	11.7
H45C	0.449	0.594	0.227	11.7
H46A	0.956	0.439	0.603	5.5
H46B	1.067	0.481	0.573	5.5
H46C	1.078	0.398	0.602	5.5
H51	1.192	0.304	0.450	5.1
H52	1.255	0.286	0.376	5.4
H54	0.954	0.367	0.326	5.6
H55	0.893	0.387	0.397	4.8
H56	1.092	0.333	0.275	8.0
H57A	1.192	0.237	0.260	17.3
H57B	1.088	0.217	0.299	17.3
H57C	1.218	0.216	0.314	17.3
H58A	1.225	0.422	0.281	15.0
H58B	1.262	0.379	0.240	15.0
H58C	1.321	0.358	0.289	15.0
H59A	0.786	0.331	0.652	4.7
H59B	0.798	0.243	0.668	4.7
H59C	0.683	0.283	0.683	4.7
H61	0.599	0.175	0.629	4.2
H64	0.499	0.286	0.481	3.5
H67	0.438	0.033	0.533	4.0
H68	0.544	0.096	0.576	4.0
H69	0.356	0.023	0.464	4.4
H70A	0.369	0.062	0.382	5.8
H70B	0.490	0.074	0.402	5.8
H70C	0.407	0.143	0.386	5.8
H71A	0.185	0.089	0.479	5.5
H71B	0.184	0.066	0.430	5.5
H71C	0.214	0.149	0.432	5.5
H72A	0.183	-0.253	0.057	5.8
H72B	0.164	-0.307	0.108	5.8
H72C	0.279	-0.313	0.076	5.8
H74	0.365	-0.278	0.163	4.7
H77	0.413	-0.237	0.233	4.5

H78	0.516	-0.204	0.290	4.5
H80	0.587	-0.005	0.205	4.0
H81	0.491	-0.037	0.147	3.7
H82	0.623	-0.123	0.320	4.7
H83A	0.789	-0.092	0.267	6.7
H83B	0.783	-0.044	0.306	6.7
H83C	0.748	-0.008	0.254	6.7
H84A	0.594	-0.006	0.337	6.5
H84B	0.476	-0.039	0.324	6.5
H84C	0.547	0.024	0.286	6.5
H85A	0.309	-0.136	-0.037	5.2
H85B	0.429	-0.104	-0.064	5.2
H85C	0.309	-0.075	-0.085	5.2
H87	0.432	0.060	-0.070	4.1
H90	0.246	0.154	0.047	4.8
H91	0.287	0.273	0.055	6.7
H93	0.552	0.287	-0.043	6.6
H94	0.520	0.168	-0.048	5.4
H95	0.514	0.390	-0.015	8.9
H96A	0.394	0.463	0.022	12.5
H96B	0.314	0.392	0.045	12.5
H96C	0.325	0.423	-0.011	12.5
H97A	0.601	0.324	0.054	13.6
H97B	0.488	0.339	0.085	13.6
H97C	0.569	0.407	0.058	13.6
H98A	0.027	-0.150	0.008	5.7
H98B	-0.078	-0.095	-0.008	5.7
H98C	-0.098	-0.164	0.035	5.7
H100	-0.160	-0.032	0.074	4.7
H103	-0.200	0.016	0.148	5.5
H104	-0.254	0.109	0.186	6.2
H106	0.061	0.204	0.152	6.1
H107	0.115	0.113	0.113	5.1
H108	-0.067	0.254	0.191	9.6
H109A	-0.172	0.284	0.131	27.7
H109B	-0.190	0.334	0.168	27.7
H109C	-0.283	0.271	0.167	27.7
H110A	-0.175	0.243	0.261	21.6
H110B	-0.075	0.185	0.256	21.6
H110C	-0.207	0.162	0.255	21.6

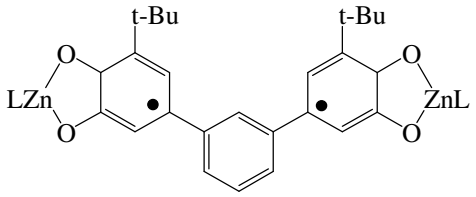

Table A.6. 4-H Atomic coordinates (x 10^4) and equivalent isotropic displacement parameters (A^2 x 10^3). U(eq) is defined as one third of the trace of the orthogonalized Uij tensor.

	x	y	z	U(eq)
Zn(1)	1543(1)	3910(1)	8757(1)	41(1)
Zn(2)	5877(1)	2539(1)	5648(1)	43(1)
O(1)	2256(4)	3294(2)	8503(1)	48(1)
O(2)	941(3)	4240(2)	8312(1)	39(1)
O(3)	5222(3)	2142(2)	6002(1)	42(1)
O(4)	6266(3)	3222(2)	5986(1)	44(1)
N(1)	-112(4)	3935(2)	8931(1)	41(1)
N(2)	-77(4)	4251(2)	9203(1)	42(1)
N(3)	2288(4)	3513(2)	9183(1)	44(1)
N(4)	1872(4)	3810(2)	9429(1)	45(1)
N(5)	2209(4)	4720(2)	8922(1)	37(1)
N(6)	1862(4)	4871(2)	9204(1)	39(1)
N(7)	7553(4)	2419(2)	5503(1)	46(1)
N(8)	7565(4)	2379(2)	5190(1)	46(1)
N(9)	5191(4)	1806(2)	5357(1)	44(1)
N(10)	5607(4)	1835(2)	5070(1)	44(1)
N(11)	5200(4)	3110(2)	5308(1)	51(1)
N(12)	5686(4)	2996(2)	5035(1)	48(1)
B(1)	1156(6)	4405(3)	9381(1)	43(2)
B(2)	6367(6)	2397(4)	4988(2)	53(2)
C(1)	2120(4)	3400(2)	8213(1)	34(1)
C(2)	2659(4)	3023(2)	8002(1)	34(1)
C(3)	2507(4)	3159(2)	7696(1)	33(1)
C(4)	1802(4)	3672(2)	7596(1)	31(1)
C(5)	1208(4)	4047(2)	7783(1)	32(1)
C(6)	1392(4)	3921(2)	8108(1)	32(1)
C(7)	2986(5)	2732(2)	7475(1)	34(1)
C(8)	2898(5)	2109(2)	7529(1)	44(2)
C(9)	3298(6)	1683(3)	7326(1)	50(2)
C(10)	3850(5)	1894(3)	7071(1)	46(2)
C(11)	3969(5)	2519(2)	7012(1)	35(1)
C(12)	3518(4)	2934(2)	7217(1)	33(1)
C(13)	4580(5)	2708(2)	6740(1)	35(1)
C(14)	4568(4)	2327(2)	6490(1)	33(1)
C(15)	5188(4)	2499(2)	6238(1)	36(1)
C(16)	5791(5)	3092(2)	6233(1)	37(1)
C(17)	5827(5)	3472(3)	6499(1)	39(2)
C(18)	5207(5)	3277(2)	6733(1)	37(1)
C(19)	358(4)	4552(2)	7669(1)	35(1)

C(20)	273(5)	4601(3)	7320(1)	52(2)
C(21)	-909(5)	4413(3)	7762(1)	54(2)
C(22)	770(5)	5178(2)	7800(1)	41(2)
C(23)	6540(5)	4068(2)	6503(1)	46(2)
C(24)	6032(6)	4500(3)	6256(1)	58(2)
C(25)	7880(5)	3925(3)	6457(2)	64(2)
C(26)	6541(6)	4396(3)	6812(1)	58(2)
C(27)	-1484(5)	4671(3)	9566(1)	62(2)
C(28)	-1223(5)	4327(3)	9284(1)	48(2)
C(29)	-1977(5)	4041(3)	9061(1)	58(2)
C(30)	-1262(5)	3812(3)	8846(1)	47(2)
C(31)	-1659(6)	3491(3)	8562(1)	56(2)
C(32)	-892(7)	3103(3)	8420(1)	62(2)
C(33)	-1290(8)	2808(3)	8149(1)	82(3)
C(34)	-2460(9)	2870(4)	8023(2)	99(3)
C(35)	-3230(8)	3238(4)	8172(2)	94(3)
C(36)	-2836(6)	3552(3)	8439(1)	71(2)
C(37)	-2957(13)	2559(3)	7732(2)	168(6)
C(38)	-3171(8)	2951(4)	7470(1)	111(3)
C(39)	-2868(12)	1904(3)	7727(2)	201(6)
C(40)	2047(5)	5743(3)	9579(1)	50(2)
C(41)	2256(5)	5447(3)	9281(1)	42(2)
C(42)	2868(5)	5660(2)	9046(1)	38(1)
C(43)	2816(4)	5203(3)	8825(1)	38(1)
C(44)	3350(4)	5195(3)	8529(1)	38(1)
C(45)	3418(5)	5732(3)	8360(1)	45(2)
C(46)	3876(5)	5726(3)	8080(1)	60(2)
C(47)	4291(5)	5202(3)	7958(1)	61(2)
C(48)	4266(5)	4656(3)	8129(1)	67(2)
C(49)	3796(5)	4664(3)	8412(1)	49(2)
C(50)	4785(5)	5191(3)	7640(1)	98(3)
C(51)	3842(5)	5038(4)	7399(1)	78(2)
C(52)	5878(6)	4819(5)	7630(2)	182(6)
C(53)	1666(5)	3660(3)	9985(1)	56(2)
C(54)	2047(5)	3463(3)	9682(1)	48(2)
C(55)	2620(5)	2931(3)	9603(1)	50(2)
C(56)	2759(5)	2979(3)	9293(1)	43(2)
C(57)	3352(5)	2546(3)	9100(1)	46(2)
C(58)	4194(5)	2735(3)	8904(1)	50(2)
C(59)	4757(6)	2315(3)	8724(1)	62(2)
C(60)	4509(7)	1689(3)	8741(2)	71(2)
C(61)	3671(7)	1510(3)	8935(2)	80(2)
C(62)	3129(6)	1926(3)	9116(2)	67(2)
C(63)	5074(6)	1239(4)	8530(2)	110(3)
C(64)	4533(7)	1261(4)	8214(2)	109(3)
C(65)	6385(6)	1250(5)	8568(2)	162(4)
C(66)	8994(6)	2278(3)	4785(1)	63(2)
C(67)	8708(5)	2335(3)	5115(1)	51(2)
C(68)	9458(5)	2332(3)	5376(1)	54(2)
C(69)	8707(5)	2386(3)	5616(1)	44(2)
C(70)	9074(5)	2399(3)	5945(1)	45(2)
C(71)	10223(5)	2592(3)	6054(1)	59(2)
C(72)	10607(6)	2560(3)	6360(1)	58(2)
C(73)	9856(5)	2345(3)	6570(1)	45(2)
C(74)	8695(5)	2177(3)	6464(1)	44(2)
C(75)	8325(5)	2190(3)	6160(1)	48(2)
C(76)	10253(5)	2329(2)	6913(1)	52(2)

C(77)	9951(6)	1742(2)	7055(1)	59(2)
C(78)	9792(6)	2866(2)	7064(1)	75(2)
C(79)	5553(6)	1226(3)	4589(1)	61(2)
C(80)	5285(5)	1327(3)	4912(1)	44(2)
C(81)	4690(5)	947(3)	5101(1)	44(2)
C(82)	4629(5)	1273(3)	5370(1)	38(2)
C(83)	3951(5)	1103(3)	5636(1)	41(2)
C(84)	4145(5)	569(3)	5788(1)	59(2)
C(85)	3500(6)	417(4)	6036(2)	94(3)
C(86)	2601(6)	795(5)	6121(1)	98(3)
C(87)	2400(5)	1337(4)	5966(1)	74(2)
C(88)	3064(5)	1497(3)	5729(1)	50(2)
C(89)	1842(5)	655(6)	6360(1)	141(4)
C(90)	530(4)	599(4)	6300(1)	73(2)
C(91)	2360(6)	576(5)	6670(1)	104(3)
C(92)	5875(6)	3499(3)	4533(1)	71(2)
C(93)	5436(6)	3471(3)	4844(1)	53(2)
C(94)	4758(6)	3893(3)	4989(1)	65(2)
C(95)	4626(6)	3647(3)	5275(1)	54(2)
C(96)	3965(5)	3894(3)	5528(1)	54(2)
C(97)	3737(6)	4520(3)	5552(2)	61(2)
C(98)	3111(5)	4752(3)	5787(2)	60(2)
C(99)	2685(5)	4359(3)	6001(2)	57(2)
C(100)	2918(5)	3735(3)	5984(1)	53(2)
C(101)	3518(5)	3509(3)	5740(1)	52(2)
C(102)	2034(6)	4612(3)	6273(2)	73(2)
C(103)	743(8)	4432(5)	6238(3)	232(6)
C(104)	2634(10)	4447(5)	6574(2)	155(4)

Table A.7 4-H Bond lengths [Å] and angles [deg].

Zn(1)-O(1)	1.958(4)
Zn(1)-N(5)	2.027(4)
Zn(1)-N(1)	2.055(4)
Zn(1)-O(2)	2.140(3)
Zn(1)-N(3)	2.169(4)
Zn(2)-O(3)	1.975(3)
Zn(2)-N(7)	2.037(4)
Zn(2)-N(11)	2.041(5)
Zn(2)-O(4)	2.125(4)
Zn(2)-N(9)	2.149(5)
O(1)-C(1)	1.294(6)
O(2)-C(6)	1.272(6)
O(3)-C(15)	1.302(6)
O(4)-C(16)	1.279(6)
N(1)-C(30)	1.328(7)
N(1)-N(2)	1.377(6)
N(2)-C(28)	1.362(7)
N(2)-B(1)	1.558(8)
N(3)-C(56)	1.350(7)
N(3)-N(4)	1.375(6)
N(4)-C(54)	1.348(7)
N(4)-B(1)	1.527(8)
N(5)-C(43)	1.342(7)
N(5)-N(6)	1.372(5)
N(6)-C(41)	1.365(7)
N(6)-B(1)	1.536(8)
N(7)-C(69)	1.339(7)
N(7)-N(8)	1.385(6)
N(8)-C(67)	1.343(7)
N(8)-B(2)	1.539(8)
N(9)-C(82)	1.324(7)
N(9)-N(10)	1.384(6)
N(10)-C(80)	1.343(7)
N(10)-B(2)	1.548(9)
N(11)-C(95)	1.337(8)
N(11)-N(12)	1.384(6)
N(12)-C(93)	1.347(7)
N(12)-B(2)	1.534(9)
C(1)-C(2)	1.411(7)
C(1)-C(6)	1.449(7)
C(2)-C(3)	1.377(7)
C(3)-C(4)	1.415(7)
C(3)-C(7)	1.481(7)
C(4)-C(5)	1.369(7)
C(5)-C(6)	1.454(7)
C(5)-C(19)	1.509(7)
C(7)-C(8)	1.386(7)
C(7)-C(12)	1.395(7)
C(8)-C(9)	1.389(7)
C(9)-C(10)	1.399(8)
C(10)-C(11)	1.397(8)
C(11)-C(12)	1.403(7)
C(11)-C(13)	1.486(7)
C(13)-C(14)	1.379(7)

C(13)-C(18)	1.425(7)
C(14)-C(15)	1.404(7)
C(15)-C(16)	1.459(7)
C(16)-C(17)	1.434(7)
C(17)-C(18)	1.354(7)
C(17)-C(23)	1.524(8)
C(19)-C(21)	1.531(7)
C(19)-C(22)	1.537(7)
C(19)-C(20)	1.534(7)
C(23)-C(24)	1.512(8)
C(23)-C(26)	1.539(8)
C(23)-C(25)	1.552(8)
C(27)-C(28)	1.505(7)
C(28)-C(29)	1.385(8)
C(29)-C(30)	1.378(8)
C(30)-C(31)	1.471(8)
C(31)-C(36)	1.378(9)
C(31)-C(32)	1.387(9)
C(32)-C(33)	1.394(8)
C(33)-C(34)	1.378(12)
C(34)-C(35)	1.380(12)
C(34)-C(37)	1.510(10)
C(35)-C(36)	1.401(9)
C(37)-C(39)	1.433(7)
C(37)-C(38)	1.441(7)
C(40)-C(41)	1.498(7)
C(41)-C(42)	1.368(7)
C(42)-C(43)	1.391(7)
C(43)-C(44)	1.479(7)
C(44)-C(49)	1.377(8)
C(44)-C(45)	1.393(8)
C(45)-C(46)	1.375(8)
C(46)-C(47)	1.361(9)
C(47)-C(48)	1.409(10)
C(47)-C(50)	1.549(8)
C(48)-C(49)	1.395(8)
C(50)-C(51)	1.464(6)
C(50)-C(52)	1.467(7)
C(53)-C(54)	1.495(8)
C(54)-C(55)	1.384(8)
C(55)-C(56)	1.391(7)
C(56)-C(57)	1.465(8)
C(57)-C(62)	1.378(9)
C(57)-C(58)	1.388(8)
C(58)-C(59)	1.394(8)
C(59)-C(60)	1.395(9)
C(60)-C(61)	1.375(10)
C(60)-C(63)	1.524(10)
C(61)-C(62)	1.380(10)
C(63)-C(65)	1.453(7)
C(63)-C(64)	1.468(7)
C(66)-C(67)	1.518(8)
C(67)-C(68)	1.362(8)
C(68)-C(69)	1.407(8)
C(69)-C(70)	1.470(7)
C(70)-C(75)	1.388(8)
C(70)-C(71)	1.390(8)

C(71)-C(72)	1.384(8)
C(72)-C(73)	1.379(8)
C(73)-C(74)	1.384(8)
C(73)-C(76)	1.537(7)
C(74)-C(75)	1.371(7)
C(76)-C(78)	1.462(5)
C(76)-C(77)	1.477(5)
C(79)-C(80)	1.493(7)
C(80)-C(81)	1.383(8)
C(81)-C(82)	1.392(7)
C(82)-C(83)	1.491(7)
C(83)-C(84)	1.352(8)
C(83)-C(88)	1.397(8)
C(84)-C(85)	1.401(9)
C(85)-C(86)	1.372(12)
C(86)-C(87)	1.375(12)
C(86)-C(89)	1.439(9)
C(87)-C(88)	1.372(8)
C(89)-C(91)	1.445(5)
C(89)-C(90)	1.466(5)
C(92)-C(93)	1.495(8)
C(93)-C(94)	1.380(9)
C(94)-C(95)	1.389(8)
C(95)-C(96)	1.485(8)
C(96)-C(101)	1.382(8)
C(96)-C(97)	1.394(9)
C(97)-C(98)	1.391(9)
C(98)-C(99)	1.386(9)
C(99)-C(100)	1.389(8)
C(99)-C(102)	1.554(9)
C(100)-C(101)	1.402(8)
C(102)-C(104)	1.479(11)
C(102)-C(103)	1.484(10)

O(1)-Zn(1)-N(5)	130.56(17)
O(1)-Zn(1)-N(1)	130.58(18)
N(5)-Zn(1)-N(1)	98.85(17)
O(1)-Zn(1)-O(2)	79.55(14)
N(5)-Zn(1)-O(2)	96.50(15)
N(1)-Zn(1)-O(2)	96.51(15)
O(1)-Zn(1)-N(3)	94.37(16)
N(5)-Zn(1)-N(3)	86.31(17)
N(1)-Zn(1)-N(3)	88.56(17)
O(2)-Zn(1)-N(3)	173.74(15)
O(3)-Zn(2)-N(7)	126.82(17)
O(3)-Zn(2)-N(11)	135.09(17)
N(7)-Zn(2)-N(11)	97.98(19)
O(3)-Zn(2)-O(4)	79.67(14)
N(7)-Zn(2)-O(4)	99.96(16)
N(11)-Zn(2)-O(4)	97.31(17)
O(3)-Zn(2)-N(9)	90.48(15)
N(7)-Zn(2)-N(9)	90.31(17)
N(11)-Zn(2)-N(9)	85.75(18)
O(4)-Zn(2)-N(9)	168.73(15)
C(1)-O(1)-Zn(1)	115.0(3)
C(6)-O(2)-Zn(1)	110.6(3)
C(15)-O(3)-Zn(2)	114.0(3)

C(16)-O(4)-Zn(2)	111.5(3)
C(30)-N(1)-N(2)	107.5(4)
C(30)-N(1)-Zn(1)	139.5(3)
N(2)-N(1)-Zn(1)	112.2(3)
C(28)-N(2)-N(1)	109.3(4)
C(28)-N(2)-B(1)	130.1(4)
N(1)-N(2)-B(1)	120.3(4)
C(56)-N(3)-N(4)	105.8(4)
C(56)-N(3)-Zn(1)	139.8(4)
N(4)-N(3)-Zn(1)	111.3(3)
C(54)-N(4)-N(3)	110.6(5)
C(54)-N(4)-B(1)	128.9(5)
N(3)-N(4)-B(1)	119.9(4)
C(43)-N(5)-N(6)	106.8(4)
C(43)-N(5)-Zn(1)	138.4(3)
N(6)-N(5)-Zn(1)	114.4(3)
C(41)-N(6)-N(5)	109.7(4)
C(41)-N(6)-B(1)	130.7(4)
N(5)-N(6)-B(1)	119.7(4)
C(69)-N(7)-N(8)	106.1(4)
C(69)-N(7)-Zn(2)	139.8(4)
N(8)-N(7)-Zn(2)	114.0(3)
C(67)-N(8)-N(7)	109.8(4)
C(67)-N(8)-B(2)	130.6(5)
N(7)-N(8)-B(2)	119.6(4)
C(82)-N(9)-N(10)	106.1(4)
C(82)-N(9)-Zn(2)	140.6(3)
N(10)-N(9)-Zn(2)	112.4(3)
C(80)-N(10)-N(9)	109.9(5)
C(80)-N(10)-B(2)	131.2(5)
N(9)-N(10)-B(2)	118.8(4)
C(95)-N(11)-N(12)	106.3(5)
C(95)-N(11)-Zn(2)	139.3(4)
N(12)-N(11)-Zn(2)	112.4(3)
C(93)-N(12)-N(11)	109.2(5)
C(93)-N(12)-B(2)	130.5(5)
N(11)-N(12)-B(2)	120.3(5)
N(4)-B(1)-N(6)	110.5(5)
N(4)-B(1)-N(2)	108.2(5)
N(6)-B(1)-N(2)	110.7(4)
N(12)-B(2)-N(8)	110.9(5)
N(12)-B(2)-N(10)	110.9(5)
N(8)-B(2)-N(10)	107.9(5)
O(1)-C(1)-C(2)	121.7(5)
O(1)-C(1)-C(6)	118.0(4)
C(2)-C(1)-C(6)	120.3(4)
C(3)-C(2)-C(1)	119.6(5)
C(2)-C(3)-C(4)	119.6(4)
C(2)-C(3)-C(7)	119.2(5)
C(4)-C(3)-C(7)	120.9(4)
C(5)-C(4)-C(3)	124.6(5)
C(4)-C(5)-C(6)	116.3(4)
C(4)-C(5)-C(19)	123.8(4)
C(6)-C(5)-C(19)	119.8(4)
O(2)-C(6)-C(1)	116.6(4)
O(2)-C(6)-C(5)	124.1(5)
C(1)-C(6)-C(5)	119.4(4)

C(8)-C(7)-C(12)	119.3(5)
C(8)-C(7)-C(3)	118.1(5)
C(12)-C(7)-C(3)	122.5(5)
C(7)-C(8)-C(9)	121.1(5)
C(8)-C(9)-C(10)	118.7(5)
C(11)-C(10)-C(9)	121.8(5)
C(10)-C(11)-C(12)	117.7(5)
C(10)-C(11)-C(13)	118.7(5)
C(12)-C(11)-C(13)	123.6(5)
C(7)-C(12)-C(11)	121.3(5)
C(14)-C(13)-C(18)	118.7(5)
C(14)-C(13)-C(11)	120.1(5)
C(18)-C(13)-C(11)	121.2(4)
C(13)-C(14)-C(15)	119.7(5)
O(3)-C(15)-C(14)	121.4(5)
O(3)-C(15)-C(16)	118.2(4)
C(14)-C(15)-C(16)	120.5(4)
O(4)-C(16)-C(17)	125.5(5)
O(4)-C(16)-C(15)	115.7(4)
C(17)-C(16)-C(15)	118.7(5)
C(18)-C(17)-C(16)	117.3(5)
C(18)-C(17)-C(23)	123.9(5)
C(16)-C(17)-C(23)	118.8(5)
C(17)-C(18)-C(13)	124.8(5)
C(5)-C(19)-C(21)	109.3(4)
C(5)-C(19)-C(22)	111.4(4)
C(21)-C(19)-C(22)	109.2(4)
C(5)-C(19)-C(20)	111.6(4)
C(21)-C(19)-C(20)	107.5(4)
C(22)-C(19)-C(20)	107.7(4)
C(24)-C(23)-C(17)	111.2(5)
C(24)-C(23)-C(26)	108.6(5)
C(17)-C(23)-C(26)	111.6(4)
C(24)-C(23)-C(25)	109.6(5)
C(17)-C(23)-C(25)	109.3(5)
C(26)-C(23)-C(25)	106.3(5)
N(2)-C(28)-C(29)	106.4(5)
N(2)-C(28)-C(27)	121.9(5)
C(29)-C(28)-C(27)	131.6(5)
C(30)-C(29)-C(28)	107.4(5)
N(1)-C(30)-C(29)	109.4(5)
N(1)-C(30)-C(31)	123.2(5)
C(29)-C(30)-C(31)	127.4(5)
C(36)-C(31)-C(32)	118.9(6)
C(36)-C(31)-C(30)	119.6(6)
C(32)-C(31)-C(30)	121.4(6)
C(31)-C(32)-C(33)	120.2(7)
C(34)-C(33)-C(32)	121.4(7)
C(35)-C(34)-C(33)	117.8(7)
C(35)-C(34)-C(37)	117.9(9)
C(33)-C(34)-C(37)	124.3(9)
C(34)-C(35)-C(36)	121.5(8)
C(31)-C(36)-C(35)	120.0(7)
C(39)-C(37)-C(38)	125.8(6)
C(39)-C(37)-C(34)	116.3(7)
C(38)-C(37)-C(34)	115.8(6)
N(6)-C(41)-C(42)	107.1(5)

N(6)-C(41)-C(40)	123.0(5)
C(42)-C(41)-C(40)	129.9(5)
C(41)-C(42)-C(43)	107.0(5)
N(5)-C(43)-C(42)	109.4(5)
N(5)-C(43)-C(44)	121.5(5)
C(42)-C(43)-C(44)	129.1(5)
C(49)-C(44)-C(45)	118.2(5)
C(49)-C(44)-C(43)	121.5(5)
C(45)-C(44)-C(43)	120.2(5)
C(46)-C(45)-C(44)	120.7(6)
C(47)-C(46)-C(45)	121.8(6)
C(46)-C(47)-C(48)	118.5(6)
C(46)-C(47)-C(50)	121.9(6)
C(48)-C(47)-C(50)	119.7(6)
C(49)-C(48)-C(47)	119.6(6)
C(44)-C(49)-C(48)	121.2(6)
C(51)-C(50)-C(52)	113.3(6)
C(51)-C(50)-C(47)	111.8(5)
C(52)-C(50)-C(47)	113.2(6)
N(4)-C(54)-C(55)	107.5(5)
N(4)-C(54)-C(53)	123.0(6)
C(55)-C(54)-C(53)	129.6(5)
C(54)-C(55)-C(56)	106.0(5)
N(3)-C(56)-C(55)	110.2(5)
N(3)-C(56)-C(57)	121.9(5)
C(55)-C(56)-C(57)	127.9(6)
C(62)-C(57)-C(58)	117.2(6)
C(62)-C(57)-C(56)	120.7(6)
C(58)-C(57)-C(56)	122.0(5)
C(57)-C(58)-C(59)	121.1(6)
C(58)-C(59)-C(60)	120.9(6)
C(61)-C(60)-C(59)	117.3(6)
C(61)-C(60)-C(63)	122.1(7)
C(59)-C(60)-C(63)	120.4(7)
C(60)-C(61)-C(62)	121.6(7)
C(61)-C(62)-C(57)	121.9(7)
C(65)-C(63)-C(64)	115.8(6)
C(65)-C(63)-C(60)	112.3(7)
C(64)-C(63)-C(60)	113.6(6)
N(8)-C(67)-C(68)	108.5(5)
N(8)-C(67)-C(66)	121.4(5)
C(68)-C(67)-C(66)	130.1(5)
C(67)-C(68)-C(69)	105.9(5)
N(7)-C(69)-C(68)	109.6(5)
N(7)-C(69)-C(70)	122.8(5)
C(68)-C(69)-C(70)	127.5(5)
C(75)-C(70)-C(71)	116.9(5)
C(75)-C(70)-C(69)	122.1(5)
C(71)-C(70)-C(69)	120.9(5)
C(72)-C(71)-C(70)	121.3(6)
C(73)-C(72)-C(71)	121.1(6)
C(72)-C(73)-C(74)	117.8(5)
C(72)-C(73)-C(76)	121.7(5)
C(74)-C(73)-C(76)	120.4(5)
C(75)-C(74)-C(73)	121.1(5)
C(74)-C(75)-C(70)	121.8(5)
C(78)-C(76)-C(77)	113.7(4)

C(78)-C(76)-C(73)	110.2(4)
C(77)-C(76)-C(73)	112.2(4)
N(10)-C(80)-C(81)	107.7(5)
N(10)-C(80)-C(79)	123.4(5)
C(81)-C(80)-C(79)	129.0(6)
C(80)-C(81)-C(82)	105.4(5)
N(9)-C(82)-C(81)	110.8(5)
N(9)-C(82)-C(83)	121.7(5)
C(81)-C(82)-C(83)	127.3(5)
C(84)-C(83)-C(88)	118.1(5)
C(84)-C(83)-C(82)	122.2(5)
C(88)-C(83)-C(82)	119.6(5)
C(83)-C(84)-C(85)	121.4(7)
C(86)-C(85)-C(84)	120.2(8)
C(85)-C(86)-C(87)	118.3(6)
C(85)-C(86)-C(89)	123.8(9)
C(87)-C(86)-C(89)	117.9(8)
C(88)-C(87)-C(86)	121.4(7)
C(87)-C(88)-C(83)	120.4(6)
C(86)-C(89)-C(91)	120.4(5)
C(86)-C(89)-C(90)	121.5(5)
C(91)-C(89)-C(90)	118.1(5)
N(12)-C(93)-C(94)	108.5(5)
N(12)-C(93)-C(92)	122.5(6)
C(94)-C(93)-C(92)	129.0(6)
C(93)-C(94)-C(95)	105.4(6)
N(11)-C(95)-C(94)	110.5(5)
N(11)-C(95)-C(96)	119.9(5)
C(94)-C(95)-C(96)	129.6(6)
C(101)-C(96)-C(97)	117.8(6)
C(101)-C(96)-C(95)	121.0(6)
C(97)-C(96)-C(95)	121.2(6)
C(98)-C(97)-C(96)	121.3(6)
C(99)-C(98)-C(97)	120.2(6)
C(98)-C(99)-C(100)	119.5(6)
C(98)-C(99)-C(102)	120.9(6)
C(100)-C(99)-C(102)	119.4(6)
C(99)-C(100)-C(101)	119.3(6)
C(96)-C(101)-C(100)	121.7(6)
C(104)-C(102)-C(103)	112.8(9)
C(104)-C(102)-C(99)	113.7(6)
C(103)-C(102)-C(99)	109.6(7)

Table A.8 Symmetry transformations used to generate equivalent atoms: Anisotropic displacement parameters (A^2 x 10^3) for 4-H. The anisotropic displacement factor exponent takes the form: -2 pi^2 [h^2 a*^2 U11 + ... + 2 h k a* b* U12]

	U11	U22	U33	U23	U13	U12
Zn(1)	50(1)	50(1)	24(1)	-11(1)	10(1)	0(1)
Zn(2)	47(1)	54(1)	29(1)	-8(1)	13(1)	-1(1)
O(1)	71(3)	54(2)	20(2)	-5(2)	5(2)	14(2)
O(2)	39(2)	46(2)	33(2)	-12(2)	12(2)	4(2)
O(3)	52(2)	50(2)	24(2)	-16(2)	9(2)	-11(2)
O(4)	49(2)	49(2)	38(2)	-5(2)	18(2)	-5(2)
N(1)	48(3)	58(3)	18(2)	-14(2)	6(2)	-10(2)
N(2)	49(3)	54(3)	23(2)	-11(2)	8(2)	-6(2)
N(3)	55(3)	49(3)	29(2)	-8(2)	9(2)	4(2)
N(4)	54(3)	61(3)	21(2)	-10(2)	5(2)	-4(3)
N(5)	40(2)	50(3)	23(2)	-15(2)	5(2)	8(2)
N(6)	37(2)	55(3)	25(2)	-11(2)	5(2)	0(2)
N(7)	47(3)	63(3)	30(2)	-8(2)	14(2)	1(3)
N(8)	40(3)	73(3)	25(2)	-3(2)	11(2)	3(2)
N(9)	44(3)	69(3)	20(2)	-9(2)	11(2)	-3(2)
N(10)	44(3)	68(3)	20(2)	-2(2)	6(2)	8(2)
N(11)	58(3)	58(3)	38(3)	-1(2)	15(2)	1(3)
N(12)	57(3)	54(3)	35(3)	-4(2)	16(2)	2(3)
B(1)	57(4)	51(4)	21(3)	-14(3)	6(3)	-5(4)
B(2)	59(4)	75(5)	27(3)	1(3)	15(3)	1(4)
C(1)	31(3)	50(3)	23(3)	-10(2)	7(2)	0(3)
C(2)	34(3)	33(3)	34(3)	-2(2)	3(2)	0(2)
C(3)	35(3)	41(3)	23(3)	-9(2)	9(2)	-4(3)
C(4)	40(3)	32(3)	22(3)	-5(2)	4(2)	-6(2)
C(5)	33(3)	33(3)	30(3)	-4(2)	10(2)	-3(2)
C(6)	24(3)	39(3)	33(3)	-10(3)	7(2)	1(2)
C(7)	42(3)	35(3)	26(3)	-9(2)	7(2)	1(2)
C(8)	68(4)	41(3)	27(3)	-5(3)	22(3)	1(3)
C(9)	80(4)	29(3)	44(3)	-2(3)	20(3)	2(3)
C(10)	55(3)	46(4)	39(3)	-11(3)	23(3)	7(3)
C(11)	41(3)	36(3)	28(3)	-4(2)	4(2)	1(3)
C(12)	39(3)	33(3)	29(3)	-8(2)	8(2)	3(2)
C(13)	39(3)	40(3)	25(3)	-3(2)	6(2)	7(3)
C(14)	33(3)	39(3)	29(3)	-8(2)	8(2)	-2(2)
C(15)	37(3)	37(3)	34(3)	-7(3)	8(2)	-1(3)
C(16)	39(3)	45(3)	30(3)	-13(3)	14(2)	-4(3)
C(17)	41(3)	50(3)	28(3)	-5(3)	9(2)	1(3)
C(18)	46(3)	37(3)	28(3)	-7(2)	11(2)	2(3)
C(19)	34(3)	39(3)	33(3)	-8(2)	5(2)	4(3)
C(20)	60(4)	52(4)	42(3)	-12(3)	-10(3)	13(3)
C(21)	36(3)	58(4)	68(4)	-8(3)	2(3)	6(3)
C(22)	53(3)	37(3)	33(3)	-7(3)	1(3)	9(3)
C(23)	58(4)	35(3)	49(3)	-12(3)	22(3)	-8(3)
C(24)	77(4)	43(4)	54(4)	-2(3)	15(3)	0(3)
C(25)	48(4)	67(4)	81(5)	-30(4)	21(3)	-23(3)
C(26)	80(4)	39(3)	60(4)	-20(3)	28(3)	-21(3)
C(27)	44(3)	107(5)	36(3)	-28(3)	15(3)	-7(4)
C(28)	52(3)	69(4)	25(3)	-8(3)	21(3)	-12(3)
C(29)	46(3)	95(5)	32(3)	-16(3)	7(3)	-21(4)

C(30)	52(4)	59(4)	32(3)	-6(3)	11(3)	-16(3)
C(31)	71(4)	76(4)	22(3)	-14(3)	11(3)	-36(4)
C(32)	90(5)	66(4)	31(3)	-10(3)	11(3)	-15(4)
C(33)	155(7)	57(4)	35(4)	-21(3)	20(4)	-30(5)
C(34)	172(8)	77(5)	44(4)	-7(4)	-22(5)	-49(6)
C(35)	125(7)	104(6)	48(4)	3(4)	-22(4)	-48(5)
C(36)	74(5)	98(5)	40(4)	-7(4)	0(3)	-37(4)
C(37)	359(16)	82(6)	49(5)	-19(5)	-69(7)	-27(9)
C(38)	97(6)	194(10)	41(4)	-37(5)	-5(4)	-22(6)
C(39)	341(15)	195(10)	63(6)	-51(6)	-14(8)	-166(11)
C(40)	56(4)	61(4)	35(3)	-24(3)	7(3)	-3(3)
C(41)	36(3)	50(4)	39(3)	-13(3)	3(3)	3(3)
C(42)	36(3)	38(3)	40(3)	-10(3)	3(3)	0(3)
C(43)	29(3)	48(3)	36(3)	-3(3)	0(2)	3(3)
C(44)	28(3)	48(3)	38(3)	-17(3)	5(2)	1(3)
C(45)	34(3)	52(4)	51(4)	-13(3)	9(3)	-6(3)
C(46)	49(4)	88(5)	45(4)	-1(4)	12(3)	-18(4)
C(47)	35(3)	95(5)	56(4)	-26(4)	16(3)	-29(3)
C(48)	42(3)	91(5)	70(4)	-55(4)	24(3)	-17(3)
C(49)	38(3)	54(4)	55(4)	-21(3)	9(3)	-6(3)
C(50)	69(4)	160(7)	73(5)	-57(5)	44(4)	-66(5)
C(51)	89(5)	112(6)	36(4)	1(4)	19(4)	-14(5)
C(52)	57(5)	438(19)	51(5)	-69(8)	10(4)	63(8)
C(53)	53(4)	89(5)	27(3)	3(3)	1(3)	-2(4)
C(54)	41(3)	74(4)	28(3)	-6(3)	7(3)	-6(3)
C(55)	45(3)	71(4)	35(3)	11(3)	2(3)	-7(3)
C(56)	37(3)	58(4)	34(3)	-17(3)	2(3)	-10(3)
C(57)	53(3)	44(4)	41(3)	-4(3)	0(3)	-4(3)
C(58)	60(4)	48(4)	42(3)	-5(3)	-2(3)	14(3)
C(59)	70(4)	75(5)	42(4)	11(3)	10(3)	14(4)
C(60)	99(5)	45(4)	69(5)	-12(4)	1(4)	13(4)
C(61)	99(6)	53(4)	89(5)	-2(4)	14(5)	0(4)
C(62)	73(5)	60(4)	68(4)	-6(4)	12(4)	9(4)
C(63)	163(8)	78(6)	97(6)	-6(5)	48(6)	43(6)
C(64)	138(7)	94(6)	98(6)	-55(5)	33(6)	5(6)
C(65)	168(8)	200(10)	120(8)	-12(7)	33(7)	134(8)
C(66)	57(4)	97(5)	38(3)	5(3)	26(3)	1(4)
C(67)	47(3)	59(4)	49(4)	0(3)	16(3)	2(3)
C(68)	41(3)	80(5)	41(3)	-11(3)	12(3)	-4(3)
C(69)	43(3)	54(4)	35(3)	-11(3)	11(3)	-8(3)
C(70)	42(3)	50(4)	45(3)	-8(3)	11(3)	-8(3)
C(71)	50(4)	88(5)	42(3)	-5(3)	16(3)	-18(4)
C(72)	54(4)	74(4)	45(4)	-6(3)	3(3)	-24(3)
C(73)	55(4)	41(3)	40(3)	-4(3)	1(3)	-18(3)
C(74)	55(4)	47(3)	31(3)	-6(3)	7(3)	-10(3)
C(75)	42(3)	57(4)	43(3)	-8(3)	4(3)	-4(3)
C(76)	60(4)	45(4)	51(4)	-7(3)	6(3)	-20(3)
C(77)	77(4)	57(4)	42(4)	0(3)	-4(3)	-16(4)
C(78)	112(6)	61(4)	48(4)	-21(3)	-16(4)	-4(4)
C(79)	58(4)	92(5)	33(3)	-18(3)	5(3)	16(4)
C(80)	41(3)	61(4)	28(3)	-9(3)	2(3)	12(3)
C(81)	41(3)	48(3)	43(3)	-18(3)	-1(3)	2(3)
C(82)	36(3)	51(4)	27(3)	-7(3)	3(2)	6(3)
C(83)	45(3)	52(3)	24(3)	1(3)	-6(2)	-13(3)
C(84)	43(4)	71(4)	63(4)	-5(4)	1(3)	-22(3)
C(85)	47(4)	151(7)	78(5)	52(5)	-25(4)	-47(5)
C(86)	27(3)	229(10)	35(4)	39(5)	-11(3)	-33(5)

C(87)	35(3)	158(7)	28(3)	-18(4)	-3(3)	-6(4)
C(88)	42(3)	77(4)	32(3)	-12(3)	10(3)	0(3)
C(89)	86(5)	221(8)	118(6)	36(6)	11(5)	-27(6)
C(90)	42(4)	128(6)	52(4)	-13(4)	14(3)	-33(4)
C(91)	67(5)	191(10)	54(5)	-8(5)	13(4)	1(6)
C(92)	84(5)	89(5)	41(4)	9(4)	18(3)	-11(4)
C(93)	62(4)	59(4)	38(3)	6(3)	6(3)	2(3)
C(94)	78(5)	63(4)	55(4)	4(4)	14(4)	-4(4)
C(95)	57(4)	55(4)	50(4)	3(3)	18(3)	4(3)
C(96)	53(4)	61(4)	51(4)	1(3)	16(3)	0(3)
C(97)	69(4)	48(4)	67(4)	9(3)	21(4)	2(3)
C(98)	54(4)	37(3)	91(5)	-5(3)	16(4)	2(3)
C(99)	36(3)	45(4)	92(5)	-11(4)	15(3)	8(3)
C(100)	42(3)	55(4)	64(4)	-8(3)	17(3)	-3(3)
C(101)	45(3)	48(4)	64(4)	-13(3)	16(3)	1(3)
C(102)	51(4)	51(4)	123(6)	-24(4)	34(4)	-4(3)
C(103)	93(5)	223(10)	405(14)	-209(10)	162(7)	-86(6)
C(104)	207(9)	188(10)	83(6)	22(6)	87(6)	99(8)

Table A.9. Hydrogen coordinates (10^4) and isotropic displacement parameters ($Å^3$).

	x	y	z	U(eq)
H(1)	1008	4581	9584	51
H(2)	6541	2365	4769	63
H(2A)	3125	2678	8071	41
H(4A)	1735	3763	7385	37
H(8A)	2559	1970	7707	53
H(9A)	3199	1256	7358	60
H(10A)	4153	1605	6936	55
H(12A)	3577	3362	7180	40
H(14A)	4141	1950	6487	40
H(18A)	5187	3539	6904	44
H(20A)	1072	4692	7254	79
H(20B)	−289	4931	7254	79
H(20C)	−21	4213	7230	79
H(21A)	−884	4379	7984	81
H(21B)	−1196	4026	7669	81
H(21C)	−1459	4745	7692	81
H(22A)	823	5162	8023	62
H(22B)	187	5493	7727	62
H(22C)	1565	5278	7732	62
H(24A)	5190	4594	6287	86
H(24B)	6074	4307	6056	86
H(24C)	6504	4880	6264	86
H(25A)	7928	3714	6262	96
H(25B)	8219	3662	6623	96
H(25C)	8339	4308	6457	96
H(26A)	5710	4499	6852	87
H(26B)	7021	4772	6809	87
H(26C)	6892	4125	6974	87
H(27A)	−1112	4457	9746	93
H(27B)	−2359	4695	9579	93
H(27C)	−1152	5086	9559	93
H(29A)	−2830	4008	9056	69
H(32A)	−92	3037	8508	74
H(33A)	−744	2558	8050	98
H(35A)	−4047	3280	8091	113
H(36A)	−3379	3808	8536	85
H(38A)	−3494	2707	7295	166
H(38B)	−2411	3143	7424	166
H(38C)	−3753	3270	7513	166
H(39A)	−3386	1743	7554	302
H(39B)	−3126	1736	7917	302
H(39C)	−2029	1786	7705	302
H(40A)	1580	5466	9699	75
H(40B)	1599	6126	9541	75
H(40C)	2825	5832	9692	75
H(42A)	3256	6046	9036	46
H(45A)	3145	6107	8440	54
H(46A)	3903	6098	7969	73
H(48A)	4567	4286	8051	80
H(49A)	3785	4296	8528	58
H(50A)	5032	5622	7599	118

H(51A)	4180	5049	7201	117
H(51B)	3183	5337	7401	117
H(51C)	3531	4627	7435	117
H(52A)	6151	4833	7424	273
H(52B)	5701	4394	7682	273
H(52C)	6514	4980	7776	273
H(53A)	2086	4040	10048	85
H(53B)	1871	3339	10136	85
H(53C)	793	3731	9968	85
H(55A)	2867	2600	9734	60
H(58A)	4390	3157	8892	61
H(59A)	5318	2456	8589	74
H(61A)	3460	1089	8945	96
H(62A)	2586	1782	9255	80
H(63A)	4850	826	8605	132
H(64A)	4921	955	8092	163
H(64B)	4650	1670	8129	163
H(64C)	3668	1173	8210	163
H(65A)	6655	1208	8785	243
H(65B)	6677	1639	8491	243
H(65C)	6706	910	8454	243
H(66A)	8242	2291	4652	94
H(66B)	9407	1888	4757	94
H(66C)	9517	2618	4734	94
H(68A)	10313	2299	5393	64
H(71A)	10754	2748	5914	71
H(72A)	11402	2688	6428	69
H(74A)	8145	2050	6606	53
H(75A)	7535	2053	6093	57
H(76A)	11154	2362	6933	62
H(77A)	10301	1403	6946	89
H(77B)	9072	1694	7044	89
H(77C)	10279	1738	7269	89
H(78A)	10034	3239	6961	113
H(78B)	10125	2875	7277	113
H(78C)	8910	2845	7055	113
H(79A)	5147	1541	4459	91
H(79B)	5261	820	4522	91
H(79C)	6426	1250	4574	91
H(81A)	4386	547	5056	53
H(84A)	4732	291	5724	71
H(85A)	3684	50	6147	112
H(87A)	1787	1606	6023	89
H(88A)	2919	1878	5628	60
H(89A)	1938	206	6322	170
H(90A)	194	405	6475	110
H(90B)	343	347	6118	110
H(90C)	175	1007	6267	110
H(91A)	1767	382	6791	155
H(91B)	2584	978	6758	155
H(91C)	3080	317	6671	155
H(92A)	6351	3131	4498	106
H(92B)	6379	3864	4517	106
H(92C)	5182	3519	4380	106
H(94A)	4447	4271	4909	78
H(97A)	4014	4793	5405	73
H(98A)	2975	5180	5801	72

H(10B)	2674	3465	6136	63
H(10C)	3619	3079	5720	62
H(10D)	2058	5069	6259	88
H(10E)	389	4553	6035	349
H(10F)	311	4637	6394	349
H(10G)	675	3987	6261	349
H(10H)	2183	4623	6735	232
H(10I)	3460	4608	6593	232
H(10J)	2657	4000	6595	232